THE UNIVERSITY OF CHICAGO

# NEUROMECHANICS OF THE PRIMATE TONGUE DURING FEEDING

A DISSERTATION SUBMITTED TO

THE FACULTY OF THE DIVISION OF THE BIOLOGICAL SCIENCES

AND THE PRITZKER SCHOOL OF MEDICINE

IN CANDIDACY FOR THE DEGREE OF

DOCTOR OF PHILOSOPHY

GRADUATE PROGRAM IN INTEGRATIVE BIOLOGY

BY

JEFFREY DAVID LAURENCE-CHASEN

CHICAGO, ILLINOIS

AUGUST 2021

For Mom and Dad

# TABLE OF CONTENTS

# ACKNOWLEDGEMENTS

This dissertation was influenced and enabled by many people. First and foremost, my advisor Callum Ross gave me unequivocal support over these four years. The impact of his mentorship on my growth as a scientistic and as a teacher has been profound, and I feel incredibly fortunate to call the Ross Lab my home.

My dissertation committee—Nicho Hatsopoulos, Fritzie Arce-McShane, Sliman Bensmaia, and Matt Kaufman—put unwavering trust in me and provided guidance at every turn that made my work (and my confidence in it) progressively stronger. Nicho introduced me to neuroscience even before I matriculated at UChicago, Fritzie enabled my entire PhD through the authorship and leadership of the NIH grant upon which it is based, and Sliman and Matt provided crucial feedback and suggestions that led to my initial use of DeepLabCut and exploration of various analytical approaches.

To Beth Brainerd, I without a doubt owe my entire scientific career. It was Beth who welcomed me into science as a college sophomore, taught me the ins and outs of XROMM, and told me I could be good at it. I am constantly returning to her many lessons.

Outside of my committee and previous professors, the two people who most influenced my growth as a scientist are Aaron Olsen and Courtney Orsbon. Before stepping foot into the Ross Lab, Aaron introduced me to the mindset that no analysis or piece of software needs to be off-limits—that taking the time to go under-the-hood and understand things deeply results in better science. Courtney (in large part also inspired by Aaron), showed me that same philosophy applied to monkey-tongue XROMM. It’s not an overstatement to say that this dissertation would’ve taken twice as long were it not for Courtney’s methodological standard-setting. Without Aaron and

Courtney, I certainly wouldn't have had the confidence to pursue the methods development and coding that have come to constitute the core of my scientific identity. So, to them, I'm deeply grateful.

Speaking of methods…I would be nowhere without the work of the wonderful folks at the Brown University Morphology Group. Through the development of XROMM, this PhD and many others were made possible. In particular, I want to thank Ben Knörlein for XMALab and Steve Gatesy, Dave Baier, and Armita Manafzadeh for their various Maya scripts—all of which were foundational to my work. I'll not soon forget my summer at Friday Harbor with Ben, and my many XROMM-critical conversations with Armita.

I'm truly grateful to everyone in the Ross, Hatsopoulos, and McShane Labs, past and present, who helped me along the way. So, to Kelsey Stilson, Katie Whitlow, Sam Gartner, Kara Feilich, Michael Granatosky, Myra Laird, Amanda Smith, Carrie Balcer, Karthikeyan Balasubramanian, Rebecca Junod, Hernando Fereira, Patrick Byrne, Derrick Tang, Victoria Hosack, and many more, thank you.

I am in perpetual awe of the staff of the UChicago Animal Resources Center, specifically, Alyssa Brown, Marquis Bucanan, Joanne Hernandez, Pierre Latalladi, Marek Niekrasz, Darya Mailhiot, Jennifer McGrath, Cara Mitchell, Nicole Patch, and Jenna Schoenberger. Their constant care and support for the animals means everything to me. Those folks are the true heroes of this story. Relatedly, I want to acknowledge the animals—Rocky, Yosemite, and Bright Angel—upon whom the entirety of this work is based. They had little choice in the matter—a fact I am not interested in forgetting.

Finally, I’m grateful to my partner Madison, and to my family, whose support made all the difference.

# LIST OF TABLES

# LIST OF FIGURES

# ABSTRACT

The tongue plays a key motor role in eating, drinking, and speaking. Through dynamic movements and deformations, the tongue manipulates food within the mouth, transports it during swallowing, and forms the many vowels and consonants upon which spoken language is built. But relatively little is known about the neuromechanics of tongue movement, since the tongue is hidden inside the mouth and difficult to visualize in 3D. In this dissertation, I use X-ray Reconstruction of Moving Morphology (XROMM) to precisely quantify 3D tongue kinematics during feeding in Rhesus macaque monkeys (*Macaca mulatta*), a well-developed model for mastication and motor control. In Chapter 1 I provide an introduction to the neuromechanics of primate feeding, with particular emphasis on the role of the tongue, the sensory innervation of the oral cavity, and the role of the orofacial sensorimotor cortex. In Chapter 2 I describe a novel, high-throughput pipeline for processing XROMM data. My workflow integrates DeepLabCut, a recent machine learning software for animal pose estimation, and XMALab, the go-to program for XROMM data processing. In Chapter 3 I employ a temporary oral nerve block to examine the role of oral tactile feedback on 3D tongue movement and tongue-jaw coordination during feeding. I find that loss of oral tactile feedback impairs feeding performance via alterations to the pattern of tongue-jaw coordination. In Chapter 4 I endeavor to decode 3D tongue kinematics from the activity of neural populations in the sensorimotor cortex. I find that a Long Short-Term Memory network can accurately predict various dimensions of tongue posture and movement from the neural responses of both the primary motor and somatosensory cortex. In Chapter 5, I offer a summary of my work, comment on the implications of my results, outline plans for additional development of the XROMM-DeepLabCut pipeline, and propose various potential directions for future research in primate tongue neuromechanics. Overall, this dissertation provides novel insight into the

neuromechanics of tongue function during feeding, and in doing so illuminates potential avenues of advancement for the treatment of the numerous sensorimotor disorders that impact eating, drinking, and speaking.

# CHAPTER 1 - GENERAL INTRODUCTION

*Tongue posture is difficult to estimate,*
*and the results obtained so far have been disappointing.*

-Alan A. Lowe, The Neural Regulation of Tongue Movements, 1980

Most of us pay relatively little attention to the squishy muscular thing in our mouth called the tongue. Except, perhaps, in the unfortunate case when it gets in the way of our teeth. Or when we're asked if we can curl it (I can) or if we can turn it into a clover (I can't). In those infrequent moments we become acutely aware of the strange organ that fills the oral cavity—and the remarkable dexterity it commands. The reality is that our tongue is in virtually constant motion during several vital behaviors: eating, drinking, and, of course, speech (Hiiemae & Palmer, 2003). And much like our legs as we walk down the street, or our hand as we reach for a cup of coffee, our tongue goes about performing its coordinated[1] motor functions without penetrating our consciousness. But unlike our hands and legs, the tongue has no rigid internal structure (bones) to support its movement; it twists and curls and deforms in complex ways. *What sort of ways, exactly?* The question is straightforward in nature and simple enough to pose. But as researcher Alan Lowe noted 40 years ago (Lowe, 1980), it is not so easy to answer.

The inconvenient fact—for the study of lingual biomechanics—is that the tongue is hidden inside the mouth, obscured from view by lips, cheeks, and teeth. As a consequence, we have been fundamentally constrained in our ability to visualize the various postures and movements the tongue makes during routine behaviors. It is perhaps unsurprising, then, that our

[1] The concept of 'coordination' will be deployed frequently in this dissertation. I define coordination, following (Ram & Ross, 2019), as the "the modulation (adjustment or maintenance) of relative muscle activity (amplitude and/or timing) to achieve goal-specific force production and kinematics."

understanding of the tongue's neuromechanical function in chewing—the subject of this dissertation—is relatively basic; the general tasks the tongue performs (e.g., food handling and transport) are well documented, but quantitative measurements of tongue kinematics in three dimensions (3D) have only recently entered the feeding biomechanics 'scene' (Feilich et al., 2021; Montuelle, Olson, Curtis, & Williams, 2020; Orsbon et al., 2018, 2020).

In this chapter I will begin with a general introduction to tongue anatomy and kinematics during mastication. I will summarize our current understanding of the role of peripheral feedback and the sensorimotor cortex in mastication, and follow by detailing of the methods used to see inside of the mouth to quantify tongue motions, several outstanding questions in lingual neuromechanics, why those questions matter, and, finally, the aims of this dissertation.

## TONGUE ANATOMY AND BIOMECHANICS, BRIEFLY

### MUSCLES

The primate tongue is, essentially, a bag of muscles[2]. Some muscles are contained exclusively within the bag and are capable of deforming it, but not of moving it. Others originate from skeleton (the cranium, mandible, or hyoid bone, specifically), and weave their way into the tongue and are capable of generating external torques, and thus of deforming *and* moving it. After

[2] And a lot of nerves and vessels—the latter I do not explore in this dissertation.

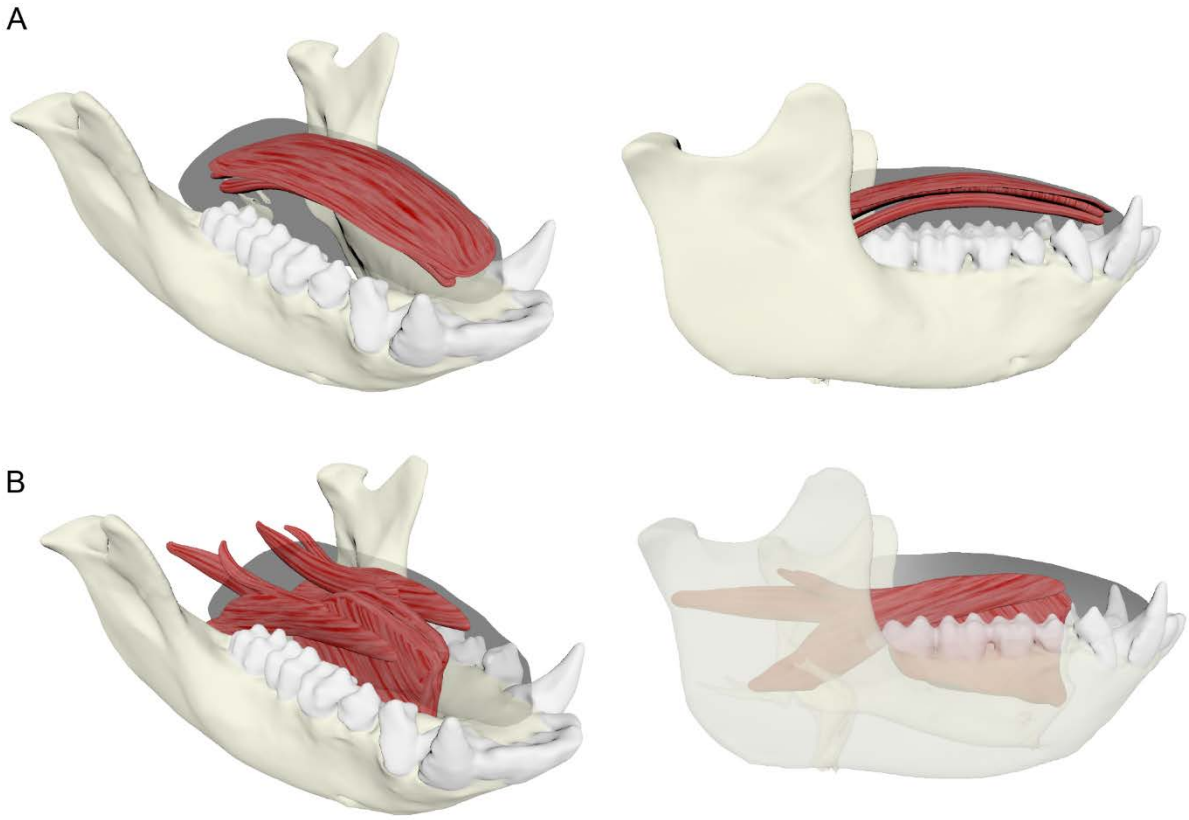


**Figure 1.1. 3D model of *Macaca mulatta* tongue muscles**. (A) Intrinsic muscles. (B) Extrinsic muscles. Models were sculpted from scratch in Autodesk Maya based on reference diceCT scans and published anatomy (Orsbon et al., 2018).

the anatomical difference, we term the former the 'intrinsic' tongue muscles (Fig. 1.1 A) and the latter the 'extrinsic' tongue muscles (Fig. 1.1 B). Importantly, the four intrinsic tongue muscles contain fibers oriented in all three anatomical directions: superior-inferior, anterior-

posterior, and medial-lateral. This 3D organization allows for complex shape change and gives rise to biomechanical properties that are more hydraulic than lever-like (Bailey et al., 2006; Kier & Smith, 1985). Consequently, the tongue is termed a 'muscular hydrostat'—a biomechanical model that describes a muscular structure's motion and deformation in terms of regional volume changes (i.e., muscle contraction) with total volume held constant (Kier & Smith, 1985). Whether

or not the tongue actually adheres to the assumption of constant overall volume remains empirically unconfirmed, but the data that exist do support the hydrostat model (Cheng et al., 2008; Z. J. Liu et al., 2009; Olson et al., 2021). Measuring the activity and action of specific tongue muscles is beyond the scope of this dissertation; thus, for simplicity's sake it can be assumed that the lingual motions described throughout are the result of some combination of intrinsic and extrinsic tongue muscle activity[3].

## Regions

The tongue comprises two main regions: the oral (anterior two-thirds) and pharyngeal (posterior one-third; Fig. 1.2 A). The basis for the distinction is both a difference in innervation (due to distinct developmental origins) and in location. The oral tongue receives innervation principally from the trigeminal and hypoglossal nerves (cranial nerves V and XII, respectively), whereas the pharyngeal tongue is exclusively innervated by the glossopharyngeal nerve (cranial nerve IX). Moreover, the anterior 2/3 of the tongue fills the oral cavity (hence 'oral'), whereas the

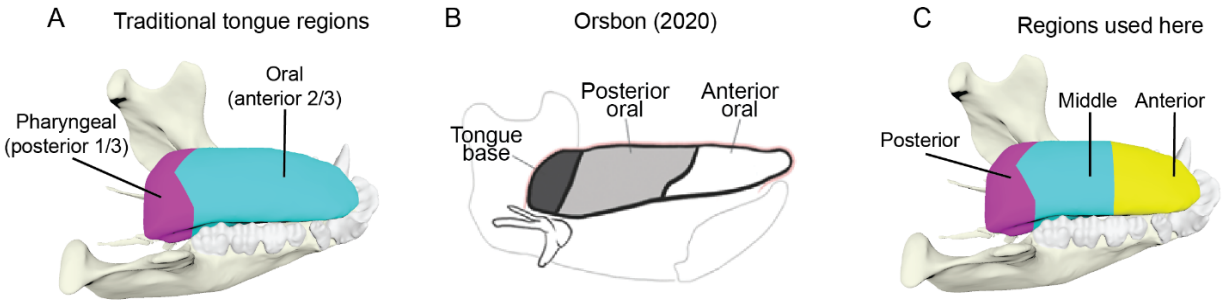


**Figure 1.2. Regions of the tongue.** (A) Traditional anatomical regions. (B) Regions defined by Orsbon et al. (2020). (C) Regions used in this dissertation.

[3] For an introduction to the anatomy and theoretical functions of all tongue muscles, see Sanders & Mu (2013)

posterior 1/3 constitutes much of the anterior border of the oropharynx (hence ‘pharyngeal’). In the context of feeding kinematics this distinction has insufficient resolution, as the oral tongue exhibits a high degree of regional kinematic variance during chewing (Feilich et al., 2021; Olson et al., 2021; Pouderoux & Kahrilas, 1995). Thus, I follow Orsbon et al. (2020) and sub-divide the oral tongue into two regions; I use ‘anterior’ tongue to refer to the anterior *one*-third of the tongue, and ‘middle’ tongue to refer to the middle *one*-third (Fig. 1.2 B).

### MOTIONS

The formal definition of tongue motions is complicated by the fact that we are only just beginning to visualize the tongue with high resolution and dimensionality. Moreover, after

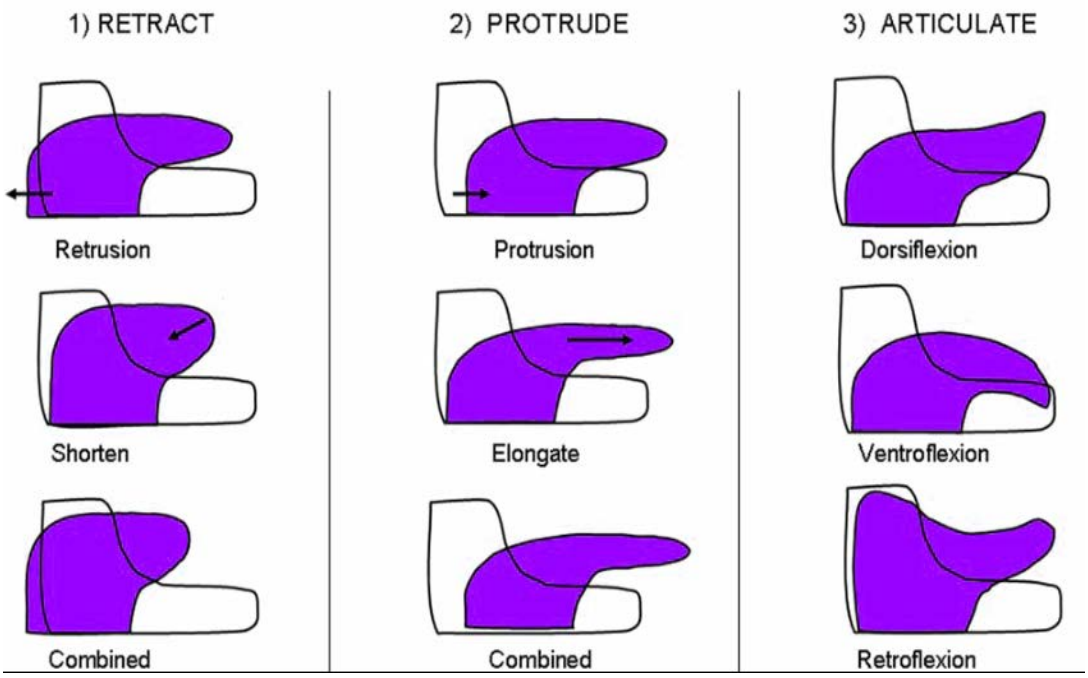


**Figure 1.3. A speech-centric characterization of tongue motions (is incomplete).** Modified from Sanders & Mu (2013), these kinematic definitions are useful for understanding tongue motions in speech, but ignore the crucial motion of the posterior tongue during swallowing, and the mediolateral motions of the middle and anterior tongue during manipulation and chewing.

visualization, there are quantitative challenges that emerge from the inherent non-linearity of tongue deformation (Davidson, 2006; Z. J. Liu et al., 2009). One can define tongue motions using specific terminology typically applied to the musculoskeletal system (e.g. flexion, extension, etc.), but the limitations of these terms become apparent as soon as quantitative measurement of their values is attempted. Namely, they oversimplify complex, compound motions and deformations; is tongue protrusion the result of hyoid (tongue-base) protraction, or the elongation of the tongue body, or both?

A common schema for characterizing tongue motions in speech can be seen in Fig. 1.3. Unfortunately, not only do these definitions exclude mediolateral motions, but they also ignore the crucial movement of the posterior tongue during swallowing (Hiiemae & Crompton, 1985; Orsbon et al., 2020). Feilich et al. (2021) proposed new terminology for characterizing mediolateral motions that are core to the chewing kinematic pattern. Specifically, anterior tongue roll is defined as rotation about the long-axis (anterior-posterior) of the tongue, where positive roll is rotation of the superior surface of the tongue to the right tooth row. Anterior tongue yaw is defined as rotation about a vertically oriented axis.

I prefer this Tait-Bryan nomenclature, as it highlights a conceptual distinction between movement and deformation. Movement involves a repositioning and/or reorientation of an object in space—it is a translation and/or rotation within a coordinate system (Brannon, 2018). Deformation is an internal shape change that occurs independent of any coordinate system (Zelditch et al., 2012). Most tongue ‘motions’ (i.e., those shown in Fig. 1.3) seem to be a combination of movement and deformation. Thus, I consider a given tongue *posture* to be the net result of some combination of movement and deformation, in either a cranial or mandibular

coordinate system. Through the application of pseudo-rigid body modeling (see Chapter 4), the specific contribution of the different types of motions can be attributed to a given posture. As will be described in a subsequent section of this chapter, this approach has only recently been enabled by XROMM.

## Action During Feeding

During feeding, the tongue has two principal motor roles: food bolus transport and food bolus formation. The former can between separated into two stages: stage 1 transport (S1T) and stage 2 transport (ST2; Hiiemae et al., 1995). In S1T, the tongue retracts to bring food from the front of the mouth (usually in between the incisors) to the post-canine molars so chewing can begin. There is a large-magnitude tongue roll (*a la* Abd-El-Malek, 1955) at the end of S1T to deposit the food onto the tooth row. S1T can take one to several jaw (gape) cycles if the food item is large or otherwise stubborn. As chewing begins the tongue performs its second role: continuous positioning of the food on the tooth row and aggregation of newly created food particles into a swallow-safe bolus (Lucas et al., 2002). The exact motions that characterize this step have only recently been described in 3D (Feilich et al., 2021). At the most basic level, the tongue seems to 'cycle' rhythmically with the vertical jaw motions that characterize chewing (Hiiemae & Palmer, 2001; Nakamura et al., 2017). During late jaw opening and early closing, the tongue rolls to the working side (dorsum to working side), likely repositioning and/or holding the food on the tooth row (Feilich et al., 2021). As breakdown progresses and the food becomes swallow ready, the tongue transports the reduced particles from the teeth to the valleculae in ST2. In the case of wet foods (e.g. grapes), this ST2 maybe be immediately followed by a mid-sequence swallow.

Otherwise, food may accumulate in the valleculae, until a terminal swallow is performed by dynamic action of the tongue and hyoid (Orsbon et al., 2018, 2020).

## Mechanosensory Sources of Peripheral Feedback

The mouth is richly innervated with chemoreceptors, thermoreceptors, and, most relevant for tongue-jaw kinematics, mechanoreceptors. The term 'mechanoreceptor' is often used to refer specifically to subset of tactile receptors found in the skin (Johansson & Vallbo, 1979), but it also includes other mechanically sensitive structures like stretch-sensitive spindles in muscles (Granit, 1975), baroreceptors (pressure sensors) in the carotid sinus (Seagard et al., 1990), and force sensors in the periodontal ligament (Trulsson, 2006). In the context of feeding, mechanoreceptors provide the feedback that forms the basis of oral stereognosis—the 3D perception[4] of the food and its properties (Haggard & de Boer, 2014). Oral mechanoreceptors can be classified by their location, structural anatomy, innervation, or firing characteristics (Table 1.1), all of which are useful for understanding the nature of the sensory information being integrated during feeding. By location, the three main sources of mechanosensory feedback from the mouth are the oral mucosa, the teeth (via periodontal ligament), and muscle spindles in lingual[5] and masticatory muscles. In the following sections I will briefly characterize the anatomical path and information carried by afferents from each of those locations.

---

[4] Perhaps not perception *sensu stricto*, as we only notice the food when we focus on it.
[5] There is some debate about the presence of spindles in specific tongue muscles. Several early histological studies in humans and monkeys documented their existence (Fitzgerald & Sachithanandan, 1979; Kubota et al., 1975), but no recent studies have replicated these findings.

## MUSCLE SPINDLES

The distribution and functional role of jaw closer (mainly masseter) muscle spindles has been well studied (Appenteng et al., 1985; Hidaka et al., 1999; Rowlerson et al., 1988; Scutter & Türker, 1999). Overall, masseteric spindles convey proprioceptive information about the jaw that informs real-time modifications (gape magnitude, bite force) to the masticatory motor pattern (Komuro et al., 2001). Muscles spindle afferents travel along the masseteric nerve, a branch of the mandibular nerve (of cranial nerve V) and enter the brainstem at the pons.

The presence of muscle spindles in the tongue was noted in a few early studies. Specifically, in both humans and rhesus macaques, spindles were found in all of the intrinsic tongue muscles, and several of the extrinsic tongue muscles (Bowman, 1968; Fitzgerald & Sachithanandan, 1979; Kubota et al., 1975). Importantly, the exact role of the information conveyed by lingual muscle spindles is difficult to pinpoint, since the tongue (and spindles within it) can be deformed by the internal activity of muscles, or forces imposed by the external objects (food, other oral structures) with which the tongue interacting. In principle, lingual muscles spindles convey information about the location of the tongue within the mouth (Kubota et al., 1975). I conjecture that they may also convey information about the location and internal properties of the food. From their termination in the tongue, afferents of lingual muscle spindles initially travel along the hypoglossal nerve (XII)—the efferent motor pathway of most tongue muscles—then appear to take multiple paths[6] back to the central nervous system: some travel along ansa cervicalis to enter the spinal cord through C2 and C3 spinal nerves (Fitzgerald &

[6] This is so terribly confusing.

Sachithanandan, 1979), whereas others find their way to the vagus (X), glossopharyngeal (IX), and trigeminal (V) nerves (Nazruddin et al., 1989).

### Periodontal Afferents

Mechanoreceptors in the periodontal ligament, the tissue that surrounds the tooth roots, convey information about forces the teeth are experiencing (Trulsson, 2006). Specifically, periodontal afferents convey information about which teeth are being loaded, the direction of the force, and the magnitude of the force (Trulsson, 2006; Trulsson et al., 1992; Trulsson & Essick, 2010). Thus far, only slowly adapting periodontal afferents have been found (Table. 1.1). Periodontal afferents innervating mandibular teeth travel along the inferior alveolar nerve, a branch of the mandibular nerve. Afferents innervating the maxillary teeth travel along the superior alveolar nerves, branches of the maxillary nerve (also a branch of cranial nerve V).

Table 1.1. Mechanoreceptors in the mouth

| Receptor | Adaptation | PDL[†] | Mucosa |
|---|---|---|---|
| Meissner corpuscles | Rapid (RA1) | No | Yes |
| Pacinian corpuscles | Rapid (RA2) | No | No |
| Merkel cells | Slow (SA1) | N/A | Yes |
| Ruffini (like) endings | Slow (SA2) | Yes | Yes |

[†]Periodontal ligament
Data from Haggard & de Boer, 2014; Jacobs et al., 2002; Trulsson & Essick, 2010.

### Mucosal Afferents

The oral mucosa is the membranous inner lining of the mouth. In some regions it exhibits specialization, such as the presence of taste cells on the tongue, or tight adherence to underlying

tissues on the gingivae (gums) and hard palate. In virtually all regions it is densely innervated with both rapidly and slowly adapting tactile mechanoreceptors (Table 1.1; Haggard & de Boer, 2014; Trulsson & Essick, 1997; Trulsson & Johansson, 2002). This innervation conveys copious amounts of information about the state and contents of the mouth. Though mucosal receptors are often considered 'tactile' (they are indeed the same sensory structures found in the glabrous skin), I conjecture that sensation from the oral mucosa also contributes to proprioception through the encoding of information related to tongue and jaw position. The role of this sensation in modulating tongue and jaw kinematics is not well known and will be discussed at length in Chapter 3. All oral mucosal mechanoreceptor afferents (except for the posterior 1/3 of the tongue) travel on branches of the trigeminal nerve. Afferents from the palate, upper gingivae, and upper lip travel to the CNS on branches of the maxillary nerve, and those from the cheeks, anterior 2/3 of the tongue, floor of the mouth, mandibular gingiva, and lower lip travel on the mandibular nerve.

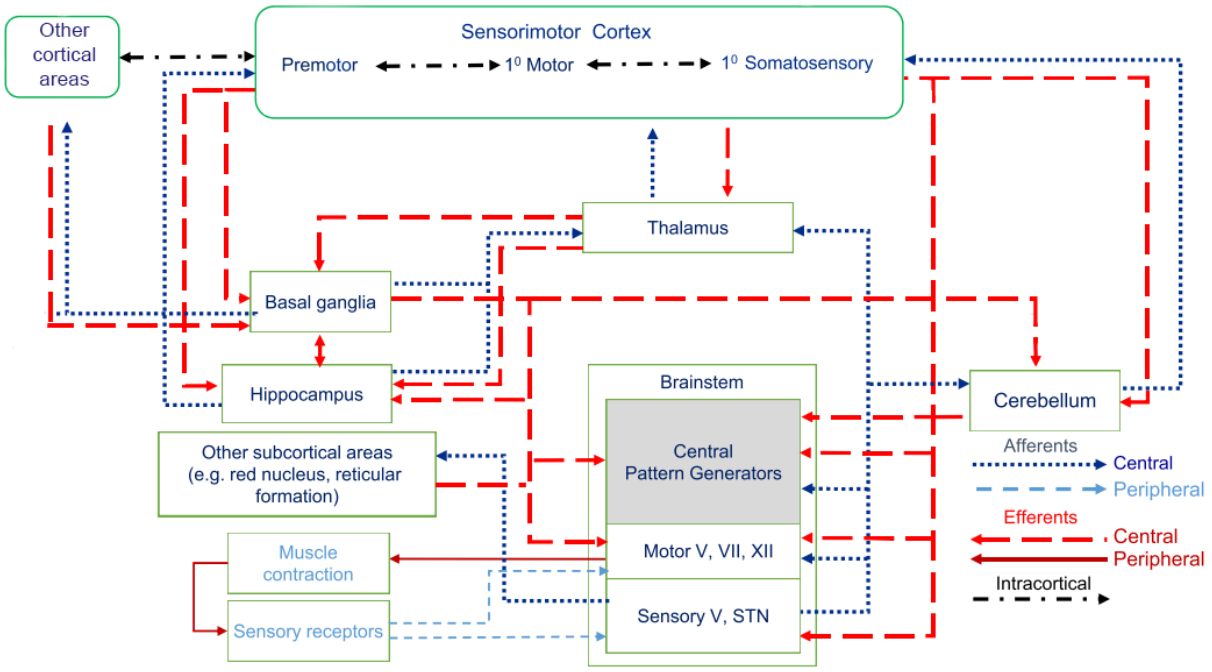


**Figure 1.4. Major connections between the cortex and orofacial muscles.** Modified from Avivi-Arber and Sessle (2017).

## The Role of the Sensorimotor Cortex

The orofacial sensorimotor cortex (oSMcx) communicates with many other brain regions in a dense web of connections that leads—with varying directness—to the masticatory central pattern generators (CPGs) and sensorimotor nuclei in the brainstem (Fig. 1.4; Avivi-Arber & Sessle, 2018; Morquette et al., 2012; Sessle, 2011). A full review of the functional neuroanatomy of the oSMcx and its associated areas is well beyond the scope of this introductory chapter. Broadly, the sensorimotor cortex is involved in motor control and learning (Arce-McShane et al., 2014; Kaas, 2013; Kawai et al., 2015; Larson et al., 1980; Molina-Luna et al., 2009; Omrani et al., 2017). For the purpose of contextualizing the work in this dissertation, I will highlight two general

findings: 1) damage to the oSMcx has catastrophic consequences for routine orofacial behaviors, and 2) artificial electrical stimulation of oSMcx evokes chewing-like rhythmic jaw and tongue movements.

## Damage to the Orofacial Cortex

Early experiments showed that bilateral ablation of the oSMcx dramatically impaired monkey's ability to consume food and vocalize (Green & Walker, 1938). Immediately after the loss of the oSMcx, animals were unable to move the lower facial muscles and the anterior tongue. After several weeks, basic movement ability was regained, but food still fell from the mouth; coordinated chewing never returned. Forty years later, a similar experiment was conducted with both unilateral and bilateral oSMcx ablation (Larson et al., 1980). It was found that bilateral—but not unilateral—ablation induced permanent changes to feeding. Importantly, Larson and colleagues found that, though coordination was lost, the basic chewing frequency was unaffected, even in the bilateral ablation condition. The data were interpreted as implicating the oSMcx in the coordination and control of complex orofacial motor behaviors, and also as constituting evidence for the existence of a brainstem masticatory CPG (see Lund, 1991; Morquette et al., 2012).

Alternatively, the role of oSMcx in oral behaviors is highlighted by consequences of pathological damage to the brain (i.e., stroke, Parkinson's disease, Alzheimer's disease, etc.). Difficulty swallowing (dysphagia), speaking, and even breathing are among the potential—and tragically common—symptoms (Schimmel et al., 2017; Takizawa et al., 2016).

### ‘Fictive’ Mastication

One hundred years ago,  Bremer (1923) discovered that various ‘chewing’ patterns could be evoked by electrical stimulation of the oSMcx and related cortical masticatory area (CMA) of the cat and rabbit. Since then, intracortical microstimulation studies have shown that rhythmic jaw and tongue movements that resemble chewing can be artificially evoked in many more mammals (Goldberg et al., 1982; Huang et al., 1989; James P. Lund et al., 1984; Sasamoto et al., 1990). Importantly, the existence of a ‘kinesiotopic map’ has been repeatedly reported; stimulating different regions of the cortex evokes different patterns of tongue-jaw movement that, in many cases, correspond to patterns that emerge during natural feeding (Huang et al., 1989; James P. Lund et al., 1984). These results may lead one to imagine the oSMcx as a conductor or orchestrator, listening closely (integrating sensory feedback) calling on the various sections of the orchestra to play certain motifs (entraining the CPGs and motor programs that exist in the circuitry between the cortex and orofacial muscles) to create a full score (the ultimate behavior). Regardless of one’s opinion of the utility or explanatory power of that metaphor, the fact remains that a wealth of behaviorally relevant information is present in the activity of the oSMcx (Arce-McShane et al., 2013; S. Liu et al., 2019), as will be demonstrated in Chapter 4.

## Seeing Inside the Mouth

With the principal neuromechanical foundation for this dissertation laid, the last topic to address is that of methodology. Following the epigraph that began this chapter, quantifying tongue

kinematics is a non-trivial challenge. Here, I will give a brief history[7] of attempts to do so, and then detail the current 'state-of-the-art'.

Over fifty years ago, Abd-El-Malek (1955) published a series of seminal illustrations that depict the posture of the human tongue at different stages of the feeding sequence. How did he visualize the tongue? He only selected subjects who were missing several teeth, and then retracted their lips with forceps to see inside the mouth as they chewed. He then manually illustrated his observations, which, for all intents and purposes, appear to be exactly right (Feilich et al., 2021). Unfortunately, though clever, the Abd-El-Malek approach did not allow quantitative analysis of either tongue shape itself or its timing relative to jaw movements.

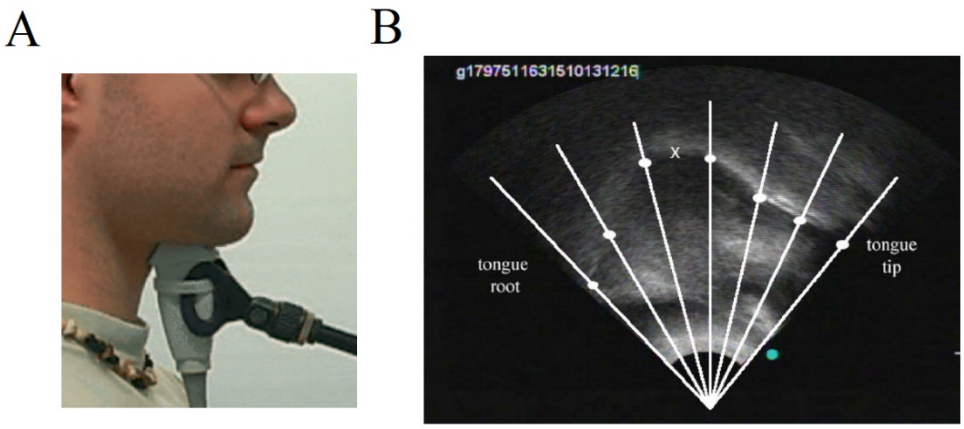


**Figure 1.5. Ultrasound approach to tongue visualization.** Modified from Davidson (2006) and Menard et al. (2012).

The vast majority of effort toward quantitative measurement of tongue posture has been in the context of speech, rather than feeding (Hiiemae & Palmer, 2003). This is consequential insofar as it relates to the (lack of) emphasis placed on quantifying asymmetrical aspects of tongue posture;

[7] See Hiiemae and Palmer (2003) for a comprehensive review.

most vowel and consonant sounds are produced with bilateral symmetry; thus, speech researchers are principally interested in tongue posture in sagittal planes. Moreover, as humans—as far as we can tell—are the only speaking animals, there is an added constraint of non-invasiveness in any methodology to be used for measuring human tongue posture. That criterion is (in a sense) met through lateral view videoradiography and videofluoroscopy. The former came to prominence in the 1950s and 60s (Perkell, 1969), but was quickly halted due to concerns of radiation exposure. The latter, requiring far less radiation, became a staple of diagnostic radiology from the 1980s onward (Splaingard et al., 1988). The use of lateral view videofluoroscopy paired with surgically implanted metal beads yielded a landmark dataset of tongue and jaw movements during feeding in monkeys (Hiiemae et al., 1995). This methodology is still used in modern experiments (Nakamura et al., 2017). Sensor based approaches such electropalatograpy and electromagnetic articulometry were developed in the late twentieth century (Badin et al., 2010; Stone & Lundberg, 1996), but did not receive wide adoption.

Today, the most common technique for measuring tongue posture in humans is ultrasound (Fig. 1.5; (Davidson, 2006; Ménard et al., 2012; Stone & Lundberg, 1996). Ultrasound is relatively easy to perform, and yields images from which mathematical representations of tongue shape (shape of the dorsum, specifically) can be generated. Unfortunately, ultrasound simply does not allow for the high resolution, 3D visualization that is required to accurately characterize tongue motions during feeding.

In a landmark study in pigs, sonomicrometry was used to precisely quantify internal deformation of the tongue during feeding (Z. J. Liu et al., 2009). The downside to this approach is that deformation occurs independent of a biologically meaningful coordinate system; so, one can

tell the tongue is changing change, but not how that shape change relates to its posture relative to the mandible and cranium.

Over the last few years, X-ray Reconstruction of Moving Morphology (XROMM; Brainerd et al., 2010) has provided a novel means of quantifying both tongue deformation and tongue movement (Feilich et al., 2021; Montuelle, Olson, Curtis, & Williams, 2020; Olson et al., 2021; Orsbon et al., 2018, 2020). XROMM involves biplanar videoradiography paired with mesh models of bones created from CT scans. In reconstructing the 3D positions of both a lattice of tongue markers and the cranium and mandible, one can measure the internal deformation of the tongue as well as positional changes relative to the skull. XROMM has unlocked new avenues of biomechanics research, especially in common model systems such as pigs and rhesus macaque monkeys (*Macaca mulatta*). This dissertation will focus solely on the latter, in large part due to their high degree of anatomical similarity with humans (Orsbon & Nabavizadeh, 2015). A detailed description of XROMM used in the context of the primate feeding apparatus has been expertly provided by Orsbon and colleagues (2018). The methodology they describe is virtually identical to that used in this dissertation, so I will omit any further description here, and direct the reader to their work, or to the individual methods sections of the chapters that follow.[8]

[8] Recently, deep learning algorithms have been used to measure extra-oral tongue volume and position (Bollu et al., 2021). This is a powerful approach, but it is constrained in that it can only measure the part of the tongue that is visible outside of the mouth. I imagine its utility in measuring lingual kinematics during feeding is limited.

## Outstanding Questions

By this point I hope to have convinced you that the neuromechanics of the feeding system, and the tongue in particular, are complex and poorly understood. For an organ that plays a vital role in some of the most ubiquitous motor behaviors, we know surprisingly little about the tongue's 3D kinematics—especially those during feeding. Here, I will set the stage for the aims of this dissertation by outlining some specific questions that, up to this point, have been unanswered.

### Methodology

At the end of the previous section I introduced XROMM, which has opened new avenues for lingual biomechanics visualization and research. But as aptly noted by Orsbon (2018), there are major bottlenecks in the XROMM workflow that constrain the feasibility of large datasets. This is particularly troubling for two reasons. First, there is substantial variation in feeding kinematics—the sources of which are still under investigation (Iriarte-Díaz et al., 2011; Montuelle, Olson, Curtis, Beery, et al., 2020; Ross et al., 2010). Thus, having sufficiently large sample sizes (across and within individuals) for feeding studies is essential. Second, the relatively low signal-to-noise ratio inherent to neural data often necessitates larger datasets than required in kinematics studies (Schultz, 2007). In short: we need more data—much more.

Q: Can the existing XROMM workflow be augmented to enable the throughput that feeding neuromechanics studies demand?

## Role of Sensory Feedback

The sensory innervation of the oral cavity is dense and rich. There have been some excellent attempts to quantify the effect of the loss of (aspects of) that feedback on feeding kinematics (Inoue et al., 1989; Montuelle et al., 2019; Montuelle, Olson, Curtis, & Williams, 2020). These studies were conducted in non-primates, which is consequential simply for the fact that pig and rabbit tongues are different in size and shape than primate tongues. This anatomical difference can manifest in different biomechanics and kinematics of routine behaviors (German et al., 1992). Thus, as a model for human speech and swallowing, the importance of using non-human primates cannot be overstated. Additionally, the most comprehensive oral deafferentation study to-date, that performed by Inoue and colleagues on rabbits, measured changes to jaw kinematics, not 3D tongue kinematics. In short: we know a lot about the influence of sensory feedback on the jaw; we know little about the tongue.

Q: To what extent does loss of oral tactile feedback impact 3D tongue kinematics in a non-human primate?

## Cortical Representation of Tongue Posture

The orofacial sensorimotor cortex plays a crucial role in the regulation of complex tongue and jaw movements (Avivi-Arber & Sessle, 2018; Sessle, 2011). But any study of the cortical representation of 3D tongue posture during feeding has previously been precluded by our inability to visualize the tongue with adequate resolution and dimensionality. With that methodological barrier now lifted and the successful development of the primate orofacial cortex as a model system in motor neuroscience (Arce-McShane, 2021; Arce-McShane et al., 2014), we can ask and answer questions about the tongue and jaw that have previously been explored only in the arm and hand.

In short: the methodology now exists to deploy the full motor systems neuroscience toolkit on the feeding system.

Q: Can we decode 3D tongue posture and movement from the orofacial sensorimotor cortex in the same way we can arm and hand kinematics?

## AIMS

This dissertation has three aims related to the neuromechanics of the primate tongue during feeding. The aims correspond to Chapters 2-4.

**Aim 1: Improve the XROMM data processing pipeline to enable larger datasets.**

*Significance*: XROMM, while innovative, is markedly constrained by an arduous data processing bottleneck. This bottleneck has resulted in studies being limited in sample size and, in some cases, under-powered. Alleviation of this bottleneck would improve the quality of the science and feasibility of larger-scale XROMM studies.

**Aim 2: Quantify the role of oral tactile feedback in tongue kinematics and tongue-jaw coordination during feeding.**

*Significance*: Oral tactile feedback is known to be important for healthy orofacial function, but there has been little quantitative study of its role in the generation and/or modification of 3D tongue movements crucial to mastication. Characterizing the role of information from mucosal afferents (versus muscle spindles) to the performance of feeding will deepen our understanding of the neuromechanics of the behavior on the whole, as well as inform clinical approaches to the various neuropathies of the tongue and jaw.

**Aim 3: Evaluate the extent to which the orofacial sensorimotor cortex carries information about 3D tongue posture and movement.**

*Significance*: The decoding of arm and hand movements from the motor cortex has ushered in a new era of brain-computer interface approaches to movement restoration. The extent to which 3D tongue movements and deformations are represented in the activity of orofacial sensorimotor cortex populations is not known. Successful decoding 3D tongue posture from the cortex would lay the groundwork for a similar revolution in the treatment of serious orofacial motor disability.

# CHAPTER 2 - INTEGRATING XMALAB AND DEEPLABCUT FOR HIGH-THROUGHPUT XROMM[9]

## INTRODUCTION

Data processing in kinematics workflows can be a time-consuming and laborious task, especially when three-dimensional (3D) reconstruction requires the integration of data from multiple cameras. In marker-based XROMM (X-ray reconstruction of moving morphology; Brainerd et al., 2010), every radiopaque marker in every frame of two X-ray videos must be accurately tracked. This step has been streamlined by the open-source program XMALab (Knörlein et al., 2016), which offers a suite of features for marker detection, visualization, and tracking. Marker tracking remains a major bottleneck in the XROMM workflow, however, limiting the feasibility of studies that require large sample sizes across multiple individuals or species (Gintof et al., 2010; Granatosky et al., 2019; Iriarte-Díaz et al., 2011; Martinez et al., 2018). In the past several years, deep learning, a type of machine learning, has emerged as a powerful tool for automating pose estimation in kinematics workflows (Graving et al., 2019; Insafutdinov et al., 2016; M. W. Mathis & Mathis, 2019; Pereira et al., 2019). In particular, the open-source deep learning toolbox DeepLabCut (A. Mathis et al., 2018; Nath et al., 2018) has been rapidly and widely adopted in the scientific community. DeepLabCut was designed for markerless, automatic tracking of body parts in RGB/monochrome camera videos and has been used in a disparate range of study systems with impressive performance and robustness (Labuguen et al., 2019; Owen et al.,

[9] See Laurence-Chasen et al. (2020) for the publication associated with this work. Author list: JD Laurence-Chasen, AR Manafzadeh, NG Hatsopoulos, CF Ross, FI Arce-McShane. Author contributions (following CRediT Taxonomy): Conceptualization, Methodology, J.D.L-C and F.I.A-M.; Analysis & Software, J.D.L-C; Investigation, J.D.L-C and A.R.M.; Writing – Original Draft, J.D.L-C; Writing – Review & Editing, All; Funding Acquisition, F.I.A-M. (PI), N.G.H., and C.F.R.; Supervision, F.I.A-M. and C.F.R.

2019; Parmiani et al., 2019; Stringer et al., 2019); and many others). The degree to which DeepLabCut's utility in digitizing visible-light videos can be transferred to the biplanar videoradiographic data at the core of XROMM is not known. Whereas in visible light video different body parts are immediately distinguishable by their shape and appearance alone, in X-ray videos the markers are often identical in appearance (small black spheres), and thus only identifiable in their broader spatiotemporal context. Moreover, as many XROMM studies aim to quantify subtle motions, the desired error threshold in marker tracking is extremely small (i.e. reprojection error ≤1 pixel; (Brainerd et al., 2010). The graphical user interface (GUI) and reconstruction features of XMALab are specifically designed for the accurate identification and tracking of markers under these challenging conditions. Additionally, XMALab and DeepLabCut utilize fundamentally different mechanisms for marker tracking. XMALab uses a point's velocity to make a prediction about where it will be in the following frame, then searches for the point using a template. It also uses camera calibration information such as reprojection error and rigid body error for user visualization as well as to establish thresholds at which to stop tracking. In contrast, DeepLabCut uses neither camera calibration information nor velocity when tracking. DeepLabCut evaluates each frame of video in isolation, essentially pattern- matching the appearance of the frame at-hand with frames from the training dataset.

The purpose of this chapter is to present a workflow that integrates DeepLabCut into the existing XROMM data processing pipeline, retaining the XMALab labeling GUI and reconstruction tools while offloading initial batch tracking to DeepLabCut. We compare the performance of my pipeline to the standard XMALab workflow on three different datasets, each with different behaviors and marker sets. Strengths and weakness of the two different pipelines are

discussed, and instructions and recommendations for the full implementation of my pipeline are provided.

## METHODS

Open-source Python code under the name XROMM_DLCTools and Jupyter Notebooks for the full implementation of my integrated workflow are available at github.com/jdlaurence/XROMM_ DLCTools. DeepLabCut is available at github.com/AlexEMG/ DeepLabCut.

### DATA FLOW

The flow of data through my pipeline is cyclic (Fig. 2.1). A training dataset – a relatively small subset of paired camera 1 and camera 2 frames – is tracked as accurately as possible in

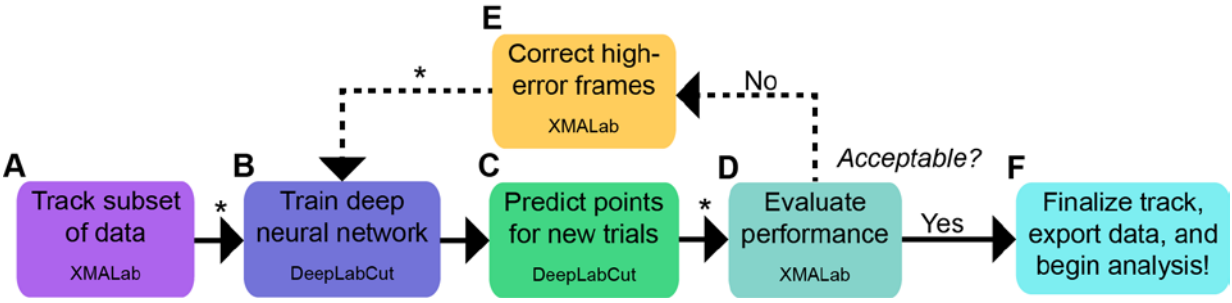


**Figure 2.1. Integrated XMALab and DeepLabCut workflow for marker tracking.** (A) The user begins by tracking approximately 200–500 frames from the dataset in XMALab. (B) Those frames serve as the training dataset for a deep neural network trained with DeepLabCut. (C) This network can then predict 2D points for new trials. (D) The predicted points are imported back into XMALab and measures of tracking quality (e.g. reprojection and rigid body error) are used to determine whether the project-specific performance criteria are met. (E) If errors are too high, selected frames can be corrected, added to the training dataset, and steps B–D repeated. (F) Once performance is acceptable, the user corrects any remaining errors in XMALab, and can export the data (3D points and rigid body transformations) for analysis. Asterisks indicate that the step is performed by an XROMM_DLCTools function.

XMALab. Then those tracked data, in the form of 2D points and their corresponding images, are migrated to DeepLabCut where they are used to train an artificial neural network. Different videos can then be directly input to DeepLabCut for automated tracking. After the network predicts the marker locations in the new videos, the predicted 2D points are brought back into XMALab for error correction, performance evaluation, and 3D reconstruction. If the network's performance is sub-optimal then areas of high error/poor performance can be manually corrected in XMALab, those corrected frames added to the training dataset, and the process repeated until the desired performance is achieved.

### TRAINING DATASET GENERATION

The composition of the training dataset is perhaps the single most important factor in DeepLabCut's performance. The network will generalize, i.e., perform well on new trials, when frames in the training dataset completely capture the variation in the full dataset. Thus, for each test case, we tracked 250–500 consecutive frames from 3–6trials (approximately 800–2000 frames in total). We intentionally selected regions that contained the most variation in posture and/or stages of the behavior of interest. Once all frames were tracked and 2D points exported from XMALab, we created a DeepLabCut project using standard DeepLabCut practice. The project configuration file was edited to match the specifics of the dataset (i.e. marker names, file location paths, etc.). After the project was successfully created, we used the DLCTools Python function `xma_to_dlc` to create a DeepLabCut-ready training dataset. The user specifies the location of the data and the desired size of the training dataset, and the function reads XMALab 2Dpoints files and extracts point positions from frames with tracked data. It also extracts the corresponding video

frames, either from avi files or from jpg stacks, and converts them to png images. The output of the function is identical to the output of the native DeepLabCut labeling GUI; thus, after this step the user proceeds to the established DeepLabCut workflow, starting with the function `create_training_dataset`. Given the redundancy of postures inherent in consecutive frames of high-speed video, as well as the added computational cost of a larger training dataset, we uniformly subsampled the tracked frames by setting the 'nframes' argument to either 500 or 750. This meant the training dataset was composed of every other initially tracked frame. The choice to create an initial training dataset with more frames than the recommended number for a DeepLabCut study (~200) was made based on the inherent visual complexity and challenge of identifying multiple, visually homogeneous markers in X-ray videos. The impact of smaller and larger initial training datasets on performance is discussed in the Results section.

### NETWORK TRAINING AND ANALYSIS

Once the training dataset is generated, the standard DeepLabCut workflow is followed. The functions `create_training_dataset` and `train_network` were used to train a single neural network whose weights were optimized for both camera 1 and camera 2 videos. In all cases, I used ResNet-101. I allowed training to run until DeepLabCut's native cross-entropy loss function plateaued, typically between 200,000 and 500,000 iterations. DLCTools supports the use of separate neural networks foreach camera plane, if the user chooses. This would double the amount of training but may improve performance. If the user wishes to analyze visible light videos alongside the x-ray videos, a separate network should be used. The DLCTools function `analyze_xromm_videos` calls the native `analyze_videos` function to predict points for

new trials. It automatically detects the camera 1 and camera 2 videos and combines DeepLabCut's predicted points output into a single 2D file in XMALab format. The predicted 2D points files can then be imported into a XMALab file with the corresponding calibration.

### Performance evaluation

I evaluated the trained neural network's tracking performance in two ways. The first method, which I do not recommend to be used exclusively, consists of DeepLabCut's `evaluate_network` function, which measures the mean 2D distance between the predicted points and the user-provided (via XMALab) 'ground-truth' points for the test fraction of the training dataset. In my experience, this native function is not a sufficient measure of tracking quality for XROMM data for several reasons: (1) camera calibration information is not used to measure 3D error (see Discussion), (2) the function can be affected by over-fitting of the network to the training dataset, and (3) the function cannot, by definition, assess the performance of a network's tracking of a novel trial. In other words, the error values provided by `evaluate_network` may not indicate that the network is ready to generalize and perform adequately on novel trials. The second means of evaluating the network's tracking performance, which I recommend, is the suite of error measurement tools in XMALab. I use individual marker reprojection error (see Knörlein et al., 2016) as an overall heuristic for tracking performance. As the goal of marker tracking with DeepLabCut is to accelerate the process while maintaining accuracy, I determined the reprojection error value at which the measured kinematic variables did not meaningfully differ by tracking mode. These variables were joint coordinate system (JCS; (Grood & Suntay, 1983) data and, in the case of the tongue data set, 3D marker positions. For each

network iteration (see following section), I tested a novel trial that had also been tracked in XMALab alone. Thus, there were two sets of data for that trial: data tracked with DeepLabCut, and data tracked with XMALab. I took the tracked data through the XROMM pipeline and then calculated the mean difference between corresponding variables across all test frames. I deemed the tracking acceptable if this value is smaller than the precision threshold for that variable (*sensu* Menegaz et al., 2015). When this threshold was reached, the reprojection error values for all points were recorded, as was the time spent for post-DeepLabCut corrections in XMALab. This approach necessitates meticulous tracking in XMALab for the training dataset and for the comparison dataset. When evaluating DeepLabCut output, single frames or regions of frames that exhibit critically poor tracking may not be captured by the mean reprojection or rigid body error. Thus, it is essential that the predicted points data are migrated into XMALab and the reprojection error, 2D position and rigid body error plots are visually inspected for large outliers.

### TRAINING DATASET AUGMENTATION

When DeepLabCut's tracking quality is not satisfactory, areas of poor performance can be manually corrected and added to the training dataset for the network to 'learn'—a form of boosting (Schwenk & Bengio, 2000). The user identifies high-error frames by visual inspection of the reprojection error and rigid body error traces, as well as the gestalt appearance of the tracking in the main window; i.e. are the crosshairs on the markers? The exact numbers that constitute poor performance depend on the specific study, but typically involve reprojection errors over 2 pixels, and rigid body errors over 0.5 mm. Once the user corrects all markers in a frame, they add the frame number to a frame index spreadsheet that contains the trial name and frames corrected from

that trial. The DLCTools function `add_frames` reads this file, extracts the corrected frame images and their new 2D point data, and appends them to the training dataset. The user can then repeat network training and re-analyze the same videos with improved marker prediction. Exact file format and folder structure for the use of this function are detailed in the online package instructions.

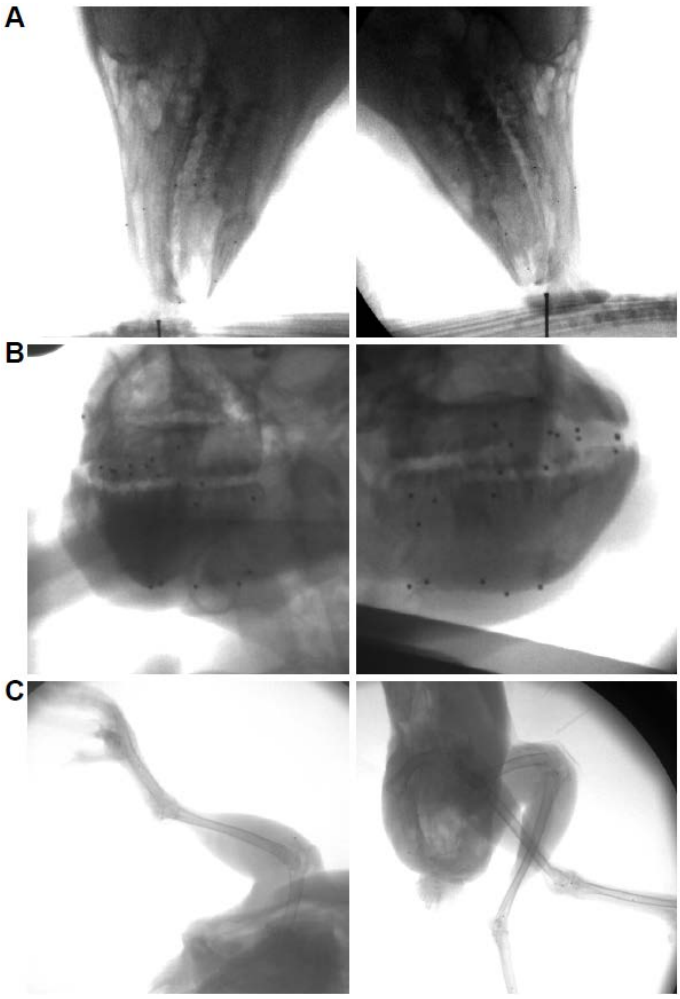


**Figure 2.2. Example bi-planar X-ray images from each test dataset.** (A) Pig feeding; (B) Monkey feeding; (C) Bird range of motion. Note differences in marker number, size, and general appearance.

## TEST CASES

In order to assess the accuracy and limitations of my new workflow, I tested it on three previously collected datasets: pig feeding, monkey feeding and bird leg range of motion (ROM). Importantly, the datasets share few similarities; they were collected on three different biplanar radiography systems and differ in species, number of markers, marker size and marker locations. Example images from each dataset are provided (Fig. 2.2). While these case studies are certainly not exhaustive in terms of taxa or behaviors, their differences provide a basis for evaluating the degree to which this workflow can be generalized to future XROMM studies. For each case study, I report the training parameters, reprojection error values, and time spent digitizing to achieve reconstructions that are statistically indistinguishable from those made from data tracked in XMALab alone (following the methods described above). As correction in XMALab is the final step in both workflows, and subject to user bias, I did not perform additional inferential statistics across conditions (e.g. mean reprojection error). The variables used to make this comparison are detailed in the following sections. All experiments were performed in compliance with Brown University and The University of Chicago's Institutional Animal Care and Use Committee protocols.

## TECHNICAL DETAILS

All network training and analyses for the test cases were performed with DeepLabCut 2.1 (installed via Anaconda environment) on Windows 10 and a NVIDIA GeForce 1080 Ti GPU. ResNet-101 was used and training was stopped when the cross-entropy loss plateaued or fell below 0.005, typically at 200,000–500,000 iterations. The 'global_scale' parameter was set to 1, and 'pos_dist_threshold' was left at the default 17. The native DeepLabCut filter (arima or median)

was not used; I filtered the predicted points in XMALab only. It is possible that a combination of the two filters could improve performance, and the user can choose which they wish to use. The two factors that have the largest impact on training and analysis speed are resolution and batch size, but speed is also influenced by training dataset size, number of network layers, and whether image augmentation is used ('imgaug' setting; strongly recommend, but not used here). The pig dataset took approximately 10 h of training to reach a loss plateau, whereas the monkey dataset took closer to 30 h. I recommend exploring and tuning the many DeepLabCut training parameters (e.g. 'pos_dist_threshold' or 'dataset_type') to find the settings that maximize performance for their specific dataset.

### STUDY 1: MINIPIG FEEDING

These publicly available minipig (*Sus scrofa*) feeding data were collected with C-arm videofluoroscopes (image resolution: 1024×1024 pixels) and have been used in XROMM tutorials and software testing for the last decade (Brainerd et al., 2010; Knörlein et al., 2016). Ten 1 mm tantalum markers – five in the cranium and five in the mandible – exhibit typical difficult-to-track characteristics; as the pig feeds unconstrained, the markers occasionally cross and occlude one another or enter areas of low contrast. The first iteration of the training dataset comprised a total of 500 frames from three trials of SusD feeding (dataset 2006-12-29). The network was then tested on a novel trial, specifically, the 435-frame trial from the same date that has been used for previous teaching and validation studies. I used the six degrees of freedom from the temporomandibular JCS as the output variables for performance comparisons.

### STUDY 2: MACAQUE FEEDING[10]

In this study, performed at The University of Chicago XROMM Facility, a male rhesus macaque (*Macaca mulatta*) fed on grapes and gummy bears while head-fixed. The data were collected at 200 Hz (image resolution: 900×900 pixels) with an X-ray technique of 100–105 kilovolt peak (kVp) and 10–12.5 milliamperes (mA). A total of 24 tantalum markers, all 1 mm in diameter, were located as follows: 4 in the cranium, 4 in the mandible, 1 in the hyoid and 15 in the tongue. The tongue markers, being in a soft body, moved in complex ways, frequently crossing and occluding one another. The combination of numerous bone and soft tissue markers makes these data extremely difficult to track; an expert XMALab user[11] took approximately 8 h to track a 10 s, 2000 frame trial. The first iteration of the training dataset comprised 750 frames sampled from six trials. Following sub-optimal performance on the test trial, the training dataset was augmented twice, such that the final training dataset comprised 1250 frames. Final manual corrections of output involved setting a reprojection error threshold at 2–2.5 pixels and correcting all frames that exceeded that threshold. I used the temporomandibular joint rotation values and tongue point 3D positions as the output variables for performance comparisons.

### STUDY 3: GUINEAFOWL RANGE OF MOTION

In this study, performed at the W.M. Keck Foundation XROMM Facility at Brown University, the hindlimb of a helmeted guineafowl (*Numida meleagris*) was physically

[10] This test dataset consists of a subset of the core dataset presented in the subsequent chapters of this dissertation. Specifically, the data here come from Monkey R.
[11] Me

manipulated *post mortem* to assess the ROM of the bird's hip, knee, and ankle joints. The data were collected at 50 Hz (image resolution: 1760×1760 pixels) with an X-ray technique of 70–85 kVp and 200 mA. A total of 12 0.8 mm zirconium oxide markers were placed in the pelvis, femur, tibiotarsus and tarsometatarsus – 3 in each element. Unlike the previous two studies, these data do not involve a cyclic behavior; in fact, the aim of the study was to explore each joint's full ROM through intentionally non-cyclic, non-repeated movements (Kambic et al., 2017; Manafzadeh & Padian, 2018). An expert XMALab user[12] took approximately 10 h to track an 1800 frame trial. The first iteration of the training dataset comprised 750 frames from four trials. The training dataset was augmented twice, and the final training dataset comprised 1500 frames. I used the rotations at the three joints as the output variables for performance comparisons.

## RESULTS

### STUDY 1: MINIPIG FEEDING

When applied to the pig feeding dataset, DeepLabCut rapidly reached XMALab-level performance. DeepLabCut's raw (i.e. pre-XMALab correction) marker predictions for a novel trial exhibited rigid body errors and JCS rotation values that fell within the precision threshold of the study (Fig. 2.3 A,C). Mean reprojection error of individual points, however, was higher in the trial tracked with DeepLabCut (0.51± 0.25 s.d. pixels) as compared with XMALab (0.16±0.02 pixels).

[12] Armita R. Manafzadeh

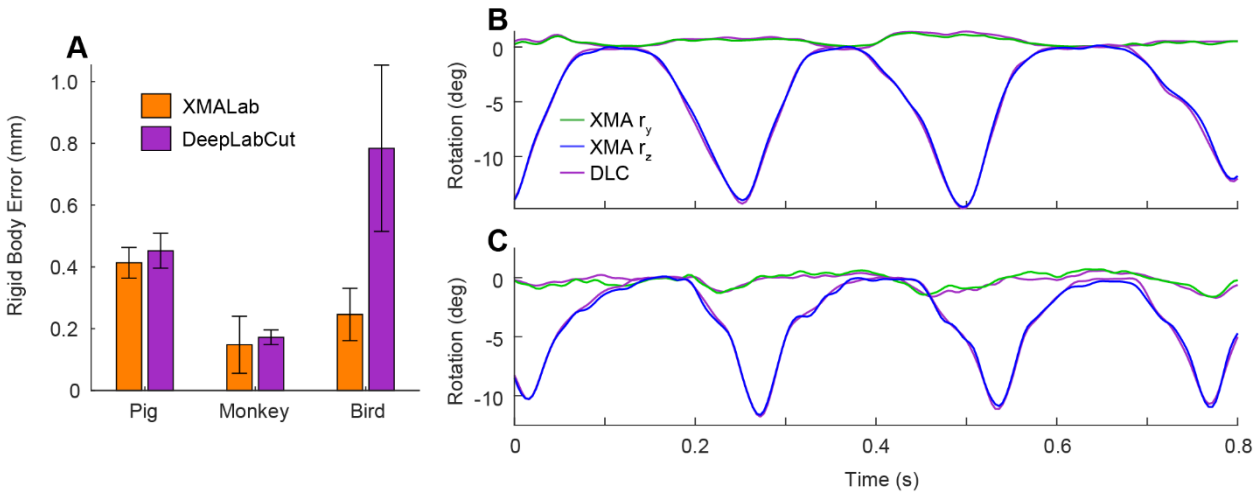


**Figure 2.3. Comparison of XMALab and DeepLabCut rigid body tracking performance.** (A) Mean (±s.d.) rigid body error (filtered at 30 Hz) from XMALab for the test trial of each case study where markers were tracked either with XMALab (orange) or with DeepLabCut (DLC; purple). Pig and monkey errors comprise the rigid body transformations of the cranium and mandible, and the bird errors comprise the transformations of all leg bones for their respective test trials. (B) Monkey and (C) pig temporomandibular joint rotation data derived from the two sets of rigid body transformations described in A. Green lines (XMA ry)are y-axis rotation, or yaw; blue lines (XMA rz)are z-axis rotation, or pitch; brown lines (DLC) are the same degrees of freedom, from DeepLabCut-tracked data. Note that despite differing mean reprojection errors (see main text), mean rigid body error and the resultant rotation values for the pig and monkey were comparable to those of the same trial tracked in XMALab. Here, the DeepLabCut marker predictions were not corrected in XMALab, and the joint coordinate systems were oriented following Menegaz et al. (2015) and Orsbon et al. (2018). The rx (x-axis rotation, roll) trace was omitted because it failed to exceed the established noise threshold in both tracking methods.

This difference in mean reprojection error persisted after manual correction of select, high error frames in XMALab. Nevertheless, the difference in measured JCS variables never fell outside of the error threshold. DeepLabCut was immediately robust to the cyclic crossing of select markers that consistently required manual intervention when tracking in XMALab. After training the neural network on the initial training dataset, time to fully track 1000 frames decreased from approximately 30 min with XMALab alone to 5 min with the integrated workflow, constituting a six-fold increase in throughput when tracking cranial and mandibular markers.

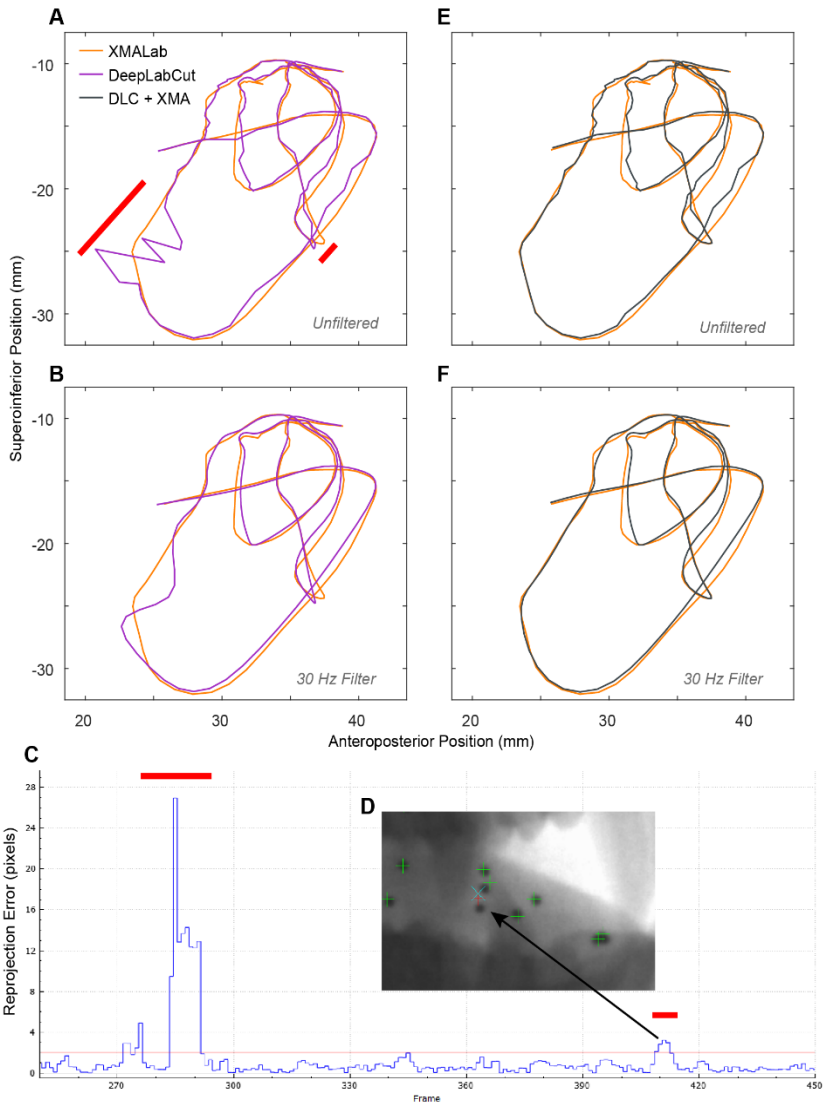


**Figure 2.4. Comparison of tracking methods for an example tongue marker trajectory.** (A–D) DeepLabCut predicted positions (purple) for the anterior right tongue marker were at times erroneous (red bars). After importing the predicted 2D points into XMALab, those regions of poor tracking were easily identified with the reprojection error trace (C). All frames with reprojection errors higher than the established threshold (2 pixels for this study) were corrected in both cameras (D). (E,F) The resulting DeepLabCut+XMALab marker trajectory (gray) is accurate – similar to the same marker tracked in XMALab alone (orange) – and 8–13× faster to generate. The trajectories are the X and Yvalues taken from the marker's X–Y–Z coordinates that have been exported from XMALab, and transformed into an anatomical coordinate system with its origin at the posterior nasal spine (Orsbon et al., 2018). Unfiltered trajectories (A,E) and trajectories filtered with a 30 Hz low-pass Butterworth filter (B,F) are shown.

## STUDY 2: MACAQUE FEEDING

DeepLabCut quick achieved XMALab-level performance when tracking the markers in the two rigid bodies – the cranium and mandible. Before any manual correction, mean rigid body error was comparable to that of the trial tracked using XMALab only. Likewise, the temporomandibular JCS y-and z-axis rotations fell within the respective variable's precision thresholds (Fig. 2.3 A,B). As in the pig dataset, DeepLabCut- predicted marker locations exhibited higher mean reprojection errors, both before and after manual correction, compared with the XMALab trial. For every iteration of the network, the uncorrected X-Y-Z positions of the tongue markers did not meet the threshold for successful performance (Fig. 2.4 A–D). The first iteration of the network produced predictions that required approximately 2 h of manual correction per 2000 frame trial to reach the error threshold. Satisfactory performance was achieved through the correction of all frames in which a marker's reprojection error exceeded 2–2.5 pixels (Fig. 2.4 E,F). In order to reduce the amount of manual correction needed, new frames were tracked and added to the training dataset two separate times, and each iteration resulted in progressively lower reprojection errors (Fig. 2.5). The output of the second iteration of the network required 1 h of manual correction, and the third iteration of the network required 20–30 min, an approximately 13-fold increase in throughput, including training dataset generation time.

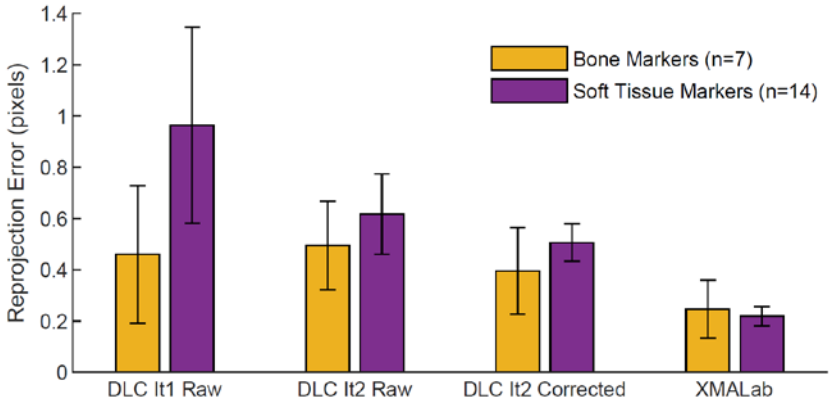


**Figure 2.5. Comparison of mean marker reprojection errors across DeepLabCut network iterations for monkey dataset.** It0 is not shown. Note that both the mean reprojection error and difference between bone and soft tissue markers is greatest in an early iteration (It1). All values are the mean of reprojection error across all frames of the same test trial for each marker. Error bars represent standard deviation.

### STUDY 3: GUINEAFOWL RANGE OF MOTION

This case study was unique in that the 'behavior' being studied, post-mortem specimen manipulation, was acyclic and designed to document the range of possible poses. In short, I was unable to achieve successful marker tracking results with DeepLabCut. After three iterative augmentations of the training dataset, reprojection and rigid body errors were still so high that it took longer to correct the output of DeepLabCut than to track the test trial from scratch in XMALab (Fig. 2.3 A). As each trial contained novel postures, I found it was virtually impossible to generate a training dataset that sufficiently captured the variation in the data without tracking a majority of every trial in XMALab, defeating the purpose of the new workflow.

# DISCUSSION

## COMPARISON WITH XMALAB

In two of the three case studies, my integrated workflow dramatically outperformed XMALab alone, in terms of overall processing time. After network optimization, per-trial marker tracking time was reduced 6-fold in the pig dataset and 13-fold in the monkey dataset. This high-throughput performance was robust to marker placement and number; the monkey dataset involved >20 markers in both rigid bodies (cranium and mandible) and soft tissue (tongue) structures. At the individual point level, DeepLabCut converged on, but never surpassed, XMALab quality. I found that mean reprojection errors of individual points were lowest when tracked in XMALab alone, but, crucially, this difference was not reflected in measured kinematic variables. After correction in XMALab, both JCS data and X-Y-Z marker positions did not differ meaningfully between the two tracking modes. In general, I found that what was difficult in XMALab was also more difficult for DeepLabCut; whereas DeepLabCut excelled at tracking markers in rigid bodies that followed cyclic trajectories, it had more difficulty (i.e. required more training frames) with dense and overlapping markers in soft tissue.

## ESTABLISHING AN ERROR TOLERANCE

Here, I set the error tolerance for marker tracking in DeepLabCut as the reprojection error and rigid body error values that corresponded to the point at which the measured variable (JCS data, or tongue marker positions) did not differ meaningfully from the same variable when tracked in XMALab alone. Depending on the nature of the study at hand, different performance criteria may be desired. For example, if a study is constrained to a small number of trials, noise inherent

to DeepLabCut's predictions can have a magnified impact and thus more stringent error tolerances are appropriate. Likewise, in a study that seeks to quantify subtle motions (e.g. hemimandible wiggle; (Bhullar et al., 2019), extra care must be taken when establishing the error tolerance.

### TRAINING DATASET

Algorithmic selection of training data based on visual dissimilarity can greatly improve performance for a given training dataset size (Brust et al., 2019). DeepLabCut offers a k-means method for extracting frames from videos that show maximum visual differences. In theory, this approach could be used on XROMM data, however, in practice this is generally not feasible as it can be virtually impossible to accurately identify markers in single frames of XROMM data out of their temporal context. For this reason, the workflow involves tracking sub-sequences of trials and it is up to the user to identify the regions that contain different postures. In the future, an algorithmic approach to identify ideal training frames could reduce time spent augmenting the training dataset.

### OTHER FACTORS INFLUENCING THROUGHPUT

Image resolution has a dramatic impact on DeepLabCut processing time (A. Mathis et al., 2018). As such, best practice is to down-sample large images before processing. I chose to omit any image down-sampling due to the small size of XROMM markers (5–10 pixels diameter) and our desire to maximize precision. For studies where markers are larger or processing time is of greater concern, down-sampling the raw X-ray data may yield better results. The hardware on which a user runs DeepLabCut should also be considered. Without a dedicated GPU, processing

full-sized XROMM images becomes practically infeasible. Here, we performed data analysis on a single individual from each case study as different individuals had different marker locations and marker numbers. Whether or not a single network can be generalized across multiple days of data collection probably depends on the variation in the day-to-day setup, as well as the marker locations.

### Areas for improvement

XMALab utilizes 3D camera information and marker velocity, whereas DeepLabCut—analyzing single frames in isolation—does neither. The lack of communication between the two camera views means that DeepLabCut might make a highly erroneous prediction when, to a user looking at both camera views simultaneously, it is obvious that marker correspondence is incorrect. If DeepLabCut employed a filter based on reprojection error (see open-source software DLTdv8; Hedrick, 2008) and used a marker's velocity, tracking performance might improve.

### Concluding Remarks

I showed that a marker tracking workflow that integrates deep learning can dramatically outperform the existing XROMM workflow in terms of throughput. Importantly, the throughput increase occurred when the behavior at hand was cyclic and when ROM was constrained experimentally. For this reason, I believe it is best to think about the present workflow as one that enables large scale studies, the likes of which were previously impossible, when such experimental design criteria are met. This workflow is not, however, a panacea for digitizing XROMM data. In cases where the sample size is small or the behavior is acyclic, the established XMALab only

marker tracking workflow is still more efficient. As deep learning algorithms improve, however, and when DeepLabCut incorporates camera calibration into its marker prediction, this balance will likely shift.[13]

[13] DeepLabCut is undergoing active development and several open-sourced software packages that augment DLC's base functionality have been released in the time since the writing of this chapter. I highly encourage any potential user to explore Anipose and Deep Graph Pose. See Chapter 5.

# CHAPTER 3 - LOSS OF TACTILE FEEDBACK IMPAIRS FEEDING PERFORMANCE AND CONSISTENCY OF TONGUE-JAW COORDINATION[14]

## INTRODUCTION

Mammalian feeding involves complex sequences of jaw and tongue movements. Cyclic jaw motions bring the teeth together to reduce the food item into smaller particles while the tongue positions the food between the teeth, forms it into a bolus, and transports it into the pharynx during swallows (Franks et al., 1984; Hiiemae et al., 1995; Palmer et al., 1997; Thexton, 1992). Effective coordination of these jaw and tongue movements depends on the sensorimotor integration of a diverse set of sensory receptors and musculoskeletal effectors. While the basic response properties of the oral cavity's rich array of mechanoreceptors are well documented (Haggard & de Boer, 2014), little is known about their role in generating, modifying, and coordinating jaw and tongue movements during normal feeding. Even less is known about how 3D jaw and tongue movements are affected by loss of that sensation.

As in other cyclic behaviors, the basic pattern of tongue-jaw coordination during chewing—rhythmic vertical and lateral jaw movements and semi-synchronous anteroposterior tongue 'cycles' (Hiiemae & Palmer, 2001; Nakamura et al., 2017)—emerges from a central pattern generator (CPG; Lund & Kolta, 2006; Marder & Bucher, 2001). The output of this masticatory CPG is modified by sensory feedback from mechanoreceptors in the tongue (Montuelle et al.,

[14] Author list: JD Laurence-Chasen, AR Manafzadeh, NG Hatsopoulos, CF Ross, FI Arce-McShane. Author contributions (following CRediT Taxonomy): Conceptualization, F.I.A-M., N.G.H., C.F.R.; Methodology, All; Analysis & Software, F.I.A-M., J.D.L-C and C.F.R.; Investigation, F.I.A-M., J.D.L-C. and C.F.R.; Writing – Original Draft, J.D.L-C.; Writing – Review & Editing, All; Project Administration, F.I.A-M.; Funding Acquisition, F.I.A-M. (PI), N.G.H., and C.F.R.; Supervision, F.I.A-M. and C.F.R

2019), teeth (Komuro et al., 2001), temporomandibular joint (Akito Tsuboi et al., 2009), and jaw muscles (Komuro et al., 2001; Yoshida et al., 2017). However, the basic function of chewing—reduction of the food item to a swallow-safe bolus—means that the tongue kinematics must by frequently modified to dexterously sense and control the changing bolus (Hiiemae & Palmer, 2003). Such manipulation must be carefully executed within the context of the gape cycle, lest the tongue be bitten or chewing otherwise disrupted. Few studies have evaluated the influence of tactile feedback specifically on this lingual kinematic flexibility and its coordination with the jaw (Wainwright et al., 2008).

The crucial role of cutaneous (tactile) feedback in coordinating the musculoskeletal elements of the limbs during grasping—a classic dexterous behavior—has been studied using injectable anesthetics (Augurelle et al., 2003; Robles-De-La-Torre, 2006). However, because tactile and proprioceptive afferents travel from the limbs on common nerves, this approach necessarily anesthetizes proprioceptive afferents as well (Ebied et al., 2004). Selective anesthesia of cutaneous mechanoreceptors on the plantar surface of the foot, achieved through cooling (Hohne et al., 2012), suggests that plantar sensation is more important for posture and balance than for the control of limb kinematics during cyclic locomotion (Höhne et al., 2009; Wang & Lin, 2008), which instead seem to rely more on feedback from proprioceptive mechanoreceptors (Akay et al., 2014). Whether and how these results might be extrapolated to feeding is not clear, given fundamental differences in the systems' biomechanics and functional roles (Granatosky et al., 2019; Granatosky & Ross, 2020). Indeed, given that one cannot see into one's own mouth, it is

likely that oral stereognosis arises from feedback from both tactile and proprioceptive somatosensory receptors (Haggard & de Boer, 2014; Macefield, 2021).

The anatomy of the mouth offers a unique opportunity to isolate the roles of tactile and proprioceptive feedback in the coordination of the jaw and tongue movements driving feeding performance: afferent axons from proprioceptive and tactile mechanoreceptors of the tongue enter the CNS on different nerves. Specifically, tongue muscle efferents and spindle afferents leave and enter the CNS on the hypoglossal nerve (Fitzgerald & Sachithanandan, 1979; Kubota et al., 1975), while afferents of superficial tactile mechanoreceptors in the oral mucosa (gums, cheeks, palate, and anterior 2/3 of the tongue) travel along sensory branches of the trigeminal nerve (Biedenbach & Chan, 1971; Trulsson & Essick, 1997). This anatomical organization means that oral tactile sensation can be perturbed by an injection-based nerve block with no impact on the efferent motor or proprioceptive signals from the tongue. Moreover, trigeminal nerve blocks, such as those deployed in the dentist's office, are minimally invasive and rapidly acting, minimizing the impact of surgery and long-term compensation strategies on results (Adachi et al., 2007; Montuelle et al., 2019).

Here, we employ an oral nerve block to temporarily silence oral tactile signals during feeding in macaque monkeys (*Macaca mulatta*), leaving motor and proprioceptive signals unaffected (Arce-McShane, 2021). Most studies of tongue movement during feeding have been limited to measurements in sagittal planes (Hiiemae et al., 1995; Mioche et al., 2002; Nakamura et al., 2017; Palmer et al., 1997), but it has long been known that the tongue deforms along mediolateral axes to position food onto the post-canine teeth (Abd-El-Malek, 1955; Feilich et al., 2021; Hiiemae & Palmer, 2003). We precisely quantify 3D jaw movements and tongue

deformations using XROMM (X-ray Reconstruction of Moving Morphology), an innovative imaging workflow. We compare feeding performance, jaw and tongue kinematics, and tongue-jaw coordination before and after the tactile nerve block. Our results demonstrate the role of tactile feedback in supporting coordination and performance of a vital motor behavior.

# METHODS

## SUBJECTS

Experiments were performed on three adult male rhesus macaques (monkeys R, Y and B; *Macaca mulatta*, 9-10 kg). All protocols were approved by the University of Chicago Animal Care

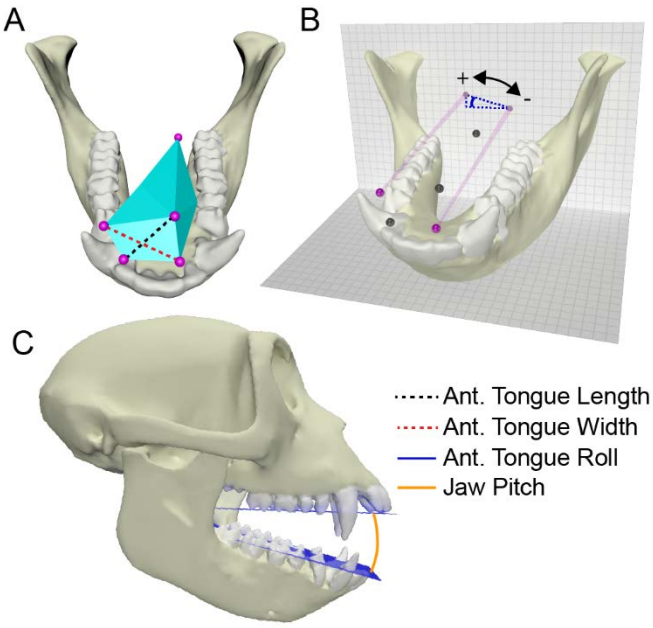


**Figure 3.1. Kinematics extracted from XROMM data.** (A) Anterior tongue length (black dashed line) and width (red dashed line) are the instantaneous Euclidean distances between anterior tongue markers. (B) Anterior tongue roll angle (blue line) was derived from the height difference of the two anterior lateral markers projected onto a coronal (frontal) plane. Positive roll is counter-clockwise when looking at the tongue from the front (thus the tongue is negatively rolled as depicted). (C) Mandible pitch (orange line) is the angle made by theoretical planes fitted to the upper and lower teeth using a joint coordinate system (see Methods).

and Use Committee and complied with the National Institutes of Health Guide for the Care and Use of Laboratory Animals.

### Behavioral Task

Subjects sat calmly and received and consumed food items while head-fixed and seated in a standard primate chair in the University of Chicago XROMM Facility. The experimental paradigm involved two feeding conditions: natural feeding and feeding after a peripheral nerve block (see below). In both conditions experimental food comprised half grapes and half gummy bears (the Haribo candy) of equal size presented directly to the monkey's mouth via a long stylus.

Table 3.1. Sample sizes

| *Individual* | *Food* | *Sequences [Fig. 3.4]* | | *Rhythmic Chews [Fig. 3.5]* | | *Rhythmic Right Chews [Fig. 3.7,8]* | | *Bouts of chews [Fig. 3.10,11]* | |
|---|---|---|---|---|---|---|---|---|---|
| | | Control | Block | Control | Block | Control | Block | Control | Block |
| *R* | Grape | 36 | 9 | 174 | 49 | 110 | 27 | 56 | 15 |
| | Gummy | 24 | 27 | 262 | 219 | 116 | 112 | 26 | 27 |
| *Y* | Grape | 24 | 6 | 219 | 51 | 0 | 7 | 66 | 12 |
| | Gummy | 9 | 8 | 255 | 90 | 40 | 76 | 28 | 16 |
| *B* | Grape | 14 | 7 | 40 | 54 | 9 | 6 | 12 | 8 |
| | Gummy | 8 | 6 | 32 | 49 | 17 | 18 | 4 | 7 |

### Tactile Nerve Block

To temporarily silence tactile signals from the mouth (while sparing efferent motor and afferent proprioceptive signals), a nerve block of sensory fibers was performed via bilateral bupivacaine (2% with 1:100,000 epinephrine) injections to multiple branches of the trigeminal nerve (lingual, inferior alveolar, buccal, palatine; see SI methods for specific details of approach.)

The nerve block was performed while the subjects were under full sedation, and all experimental data were collected within 90 minutes of the nerve block (well within the effective duration of bupivacaine). Consistent syringe placement was enabled by the creation of individual-specific, 3D-printed needle guides. Nerve block effectiveness was assessed via both behavioral observation (lack of responsiveness to touch in anesthetized areas), and a global decrease in baseline firing rates of somatosensory neurons recorded using multi-electrode arrays implanted in the primary motor and primary somatosensory areas of the orofacial cortex (Fig. 3.3).

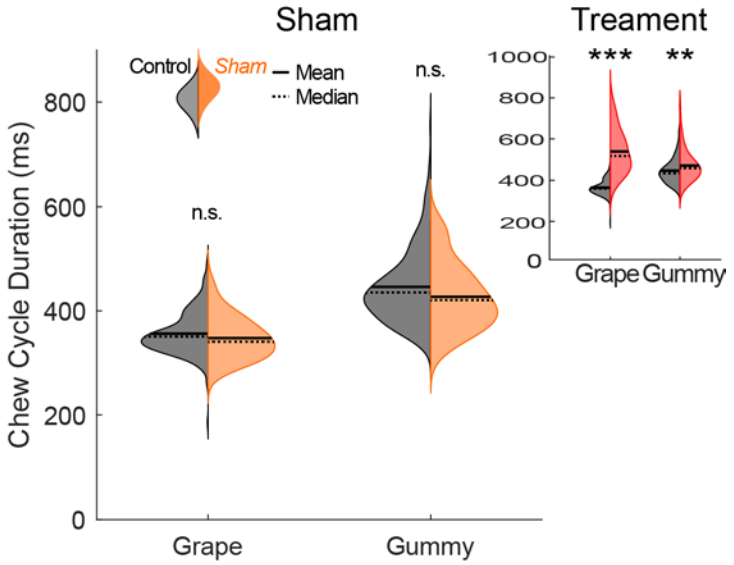


**Figure 3.2. No effect of sham nerve block on chew cycle durations in Monkey Y.** Left halves of hemi-violins (black) are control and right halves (yellow) are sham nerve block. Smaller inset plot is the same variable in the treatment (i.e. same as Fig. 3A), for reference. Sham procedure was identical to a typical nerve block, except for the substitution of saline for the anesthetic. Horizontal solid lines are means and horizontal dashed lines are medians. A significance test (two-tailed t-test) yielded no significant differences (n.s.; P>0.1).

SHAM

To rule out sedation as a possible source of confounding effects on tongue and jaw kinematics, we performed a sham nerve block. During the sham, Monkey Y was sedated and the

full nerve block procedure was performed with saline instead of bupivacaine. There were no significant changes to jaw kinematics following the sham nerve block (Fig. 3.2).

XROMM

During feeding, high-speed (200 Hz) biplanar videoradiography data were collected to visualize the movements of 24 radiopaque beads (tantalum, 1 mm diameter) that had been surgically implanted into the tongue, mandible, and cranium following previously described methods (Orsbon et al., 2018, 2020). The 3D positions of the tongue beads as well as the rigid body transformations of the cranium and mandible were reconstructed following the XROMM workflow. For kinematic data processing we employed a modification of the XROMM workflow that incorporates machine learning through DeepLabCut (Laurence-Chasen et al., 2020). This

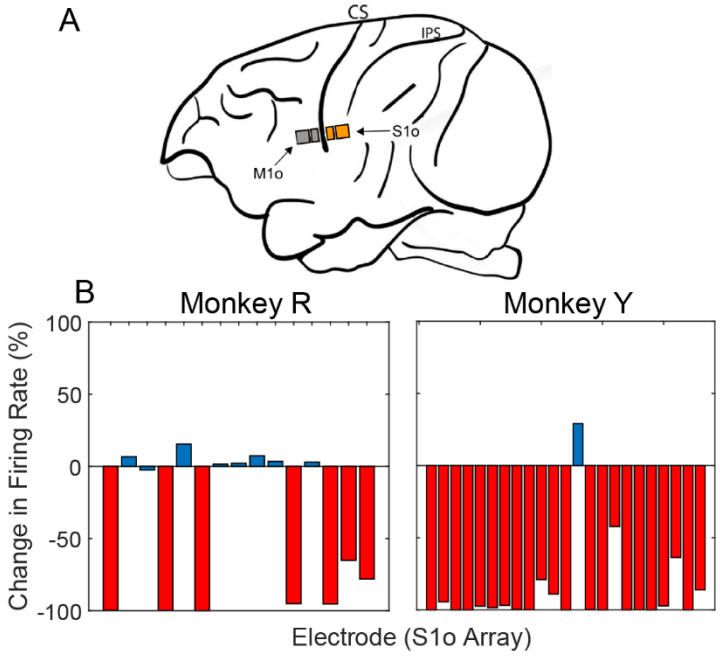


**Figure 3.3. Change in firing rates of cortical somatosensory neurons.** (A) Locations of micro-electrode arrays implanted in the primary motor (grey; M1o) and somatosensory (orange; S1o) orofacial cortex. (B) Change in multi-unit neuronal firing rates in S1o were used as one metric for determining nerve block success; specifically, a decrease in firing rate in over 50% of neurons was the criterion for a successful block. Red bars indicate a relative decrease in firing rate for a given electrode, blue bars indicate an increase. Electrodes for which the control baseline firing rate was greater than 3 spikes/s are shown.

yielded what is, to our knowledge, the largest number of frames (by a factor of 10) ever analyzed in an *in vivo* XROMM study.

### Neural data and electromyography

Jaw and tongue muscle electromyographic (EMG) activity and orofacial sensorimotor cortical neuronal activity were recorded synchronously with jaw and tongue kinematic data using chronically implanted EMG electrodes and multi-electrode arrays, respectively. EMG electrodes were bilaterally implanted into the major muscles of mastication, as well as multiple intrinsic and extrinsic tongue muscles following (Orsbon et al., 2018). Multi-electrode arrays were implanted unilaterally in the orofacial regions of the primary motor and somatosensory cortices (Arce-McShane, 2021; Arce-McShane et al., 2016). Neural data were used to confirm the success of failure of the nerve block, and EMG data was used to quantify number of gape cycles in a feeding sequence.

### Data Analysis

All analysis was performed in MATLAB 2020a. Kinematic analysis was performed at the level of individual jaw gape cycles, and gape cycle phases were calculated from mandibular pitch following previously established definitions (Ross & Iriarte-Diaz, 2014). Mandibular pitch itself was measured using a temporomandibular joint coordinate system (Grood & Suntay, 1983; Menegaz et al., 2015). Each gape cycle was individually categorized as either manipulation, stage 1 transport, left chew, right chew, chew (unknown side), stage 2 transport, intercalated swallow, or terminal swallow. Tongue shape variables (length, width, roll) and were computed from the

anterior tongue 3D marker positions (see Fig. 3.1). Length and width were the Euclidean distances of the midline or lateral markers, respectively (see Fig. 3.1 A). Roll was calculated as the angle made by the height difference of the two lateral markers, when projected onto a frontal plane (Fig. 3.1 B). To minimize the impact of differences in marker placement between animals, roll angle was zeroed based on a rest frame (after a terminal swallow) for each monkey. Cross-correlation

analysis was performed with the MATLAB function `xcorr`, with inputs being the mean-subtracted jaw pitch and tongue signals, for a given sequence.

Previous studies have found large inter-individual kinematic variation after oral nerve blocks (Montuelle et al., 2019; Montuelle, Olson, Curtis, & Williams, 2020; Schaerlaeken et al., 2007); thus all analyses were performed at the individual level. Unless otherwise noted, significant differences in magnitude and variance between conditions were assessed with a two-tailed *t*-test

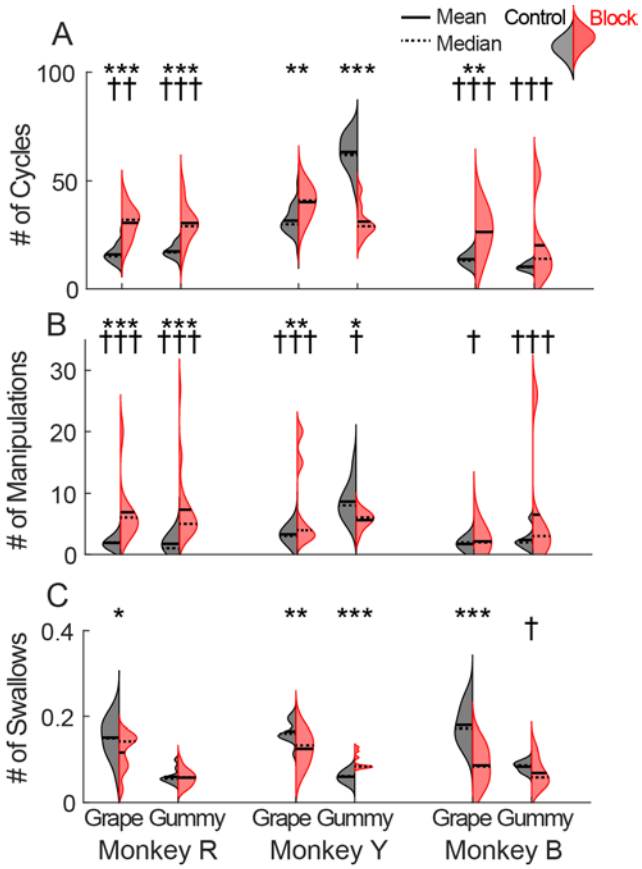


**Figure 3.4. Effect of tactile nerve block on feeding performance variables for three animals eating two food types.** Left halves of hemi-violins (black) are control and right halves (red) are nerve block for a single food type for an individual. (A) Total number of gape cycles (all cycle types) per food item, from initial ingestion of food to terminal swallow. (B) Number of gape cycles, manipulation and/or stage I transport, prior to the onset of rhythmic chewing. (C) Swallow frequency, as measured by number of swallows per 10 gape cycles. Results of a two-tailed ¬t¬-test and F-test of equality of variances are indicated by asterisks and crosses, respectively: *,†: P<0.05; **,††: P<0.01; ***,†††: P<0.001. Horizontal solid lines are means and horizontal dashed lines are medians. Sample sizes are provided in Table 1.

and *F*-test of equality of variances, respectively. Sample sizes are provided in Table S1. Data were pooled (e.g. Figs. 3.5 B and 3.6) when there was no significant effect of food types (Two-factor ANOVA, with individuals and food type as factors; $P>0.1$).

## RESULTS

We evaluated the role of oral tactile sensation by comparing 3D jaw and tongue kinematics of three monkeys as they fed with and without an oral tactile nerve block. We implanted a lattice of radio-opaque markers into the tongue and skull, then visualized the motion of those markers using biplanar videoradiography and the XROMM workflow (Brainerd et al., 2010). Using XMALab (Knörlein et al., 2016) and a novel deep learning method (Laurence-Chasen et al., 2020), we precisely reconstructed, relative to the cranium, the 3D trajectories of the jaw and tongue markers. Differences in jaw and tongue kinematics, as well as changes to jaw-tongue coordination with and without oral tactile sensation, were quantified. We validated the results through a sham nerve block procedure.

### IMPAIRED FEEDING PERFORMANCE

We first quantified the effect of loss of oral tactile sensation on overall feeding performance (Huckabee et al., 2018)—in terms of feeding sequence duration (i.e., number of gape cycles from food ingestion to terminal swallow), number of manipulation cycles, and swallow frequency. Feeding performance was adversely impacted by the loss of tactile sensation (Fig. 3.4). Across all animals, it took significantly more gape cycles to eat a grape as compared to the control condition,

resulting in a 70% average increase in sequence duration (Fig. 3.4 A, $P<0.05$, independent two-tailed *t*-tests; same for significance results that follow). Monkeys R and Y showed significant changes in sequence duration for gummy bears; Monkey R's average sequence duration increased with nerve block, and Monkey Y's decreased. A significant increase in the variance of number of gape cycles for both foods was seen in two animals (Fig. 3.4 A, $P<0.05$, *F*-test of equal variance). The increase in total number of gape cycles was driven in some cases by changes to the number of manipulation cycles before the onset of rhythmic chewing (Fig. 3.4 B). Monkeys R and Y showed significant changes to number of manipulation cycles, and, notably, there was a significant increase in variance of number of manipulation cycles for all animals for both foods. These results corresponded to qualitative observations of oral incoordination upon receiving a food item; the

animals appeared to find handling the food challenging, and took longer to position it from the ingestion point onto the post-canine teeth (stage 1 transport).

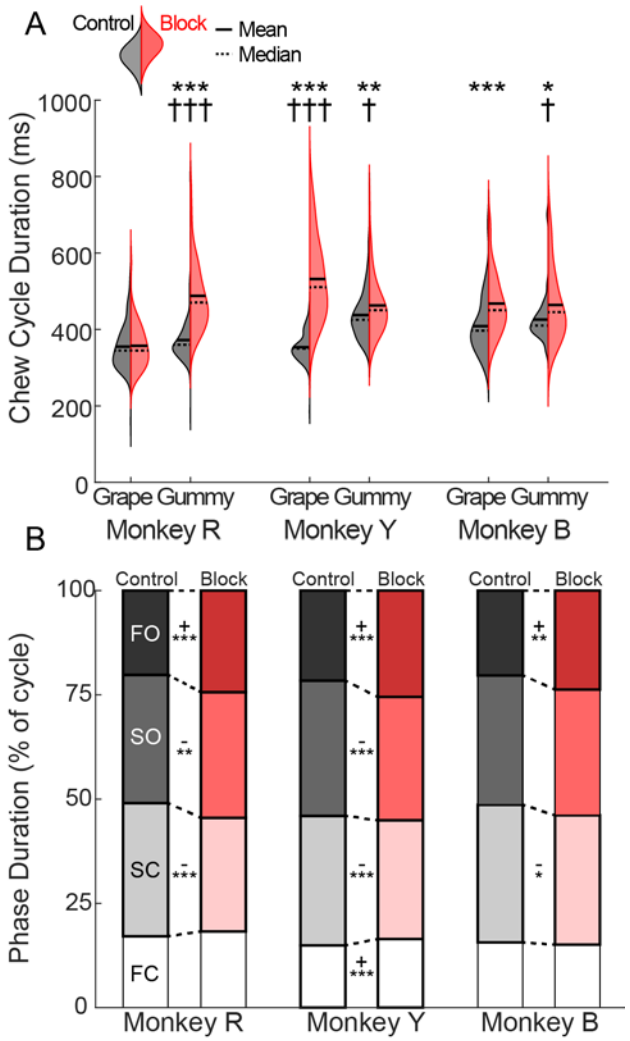


**Figure 3.5. Effect of nerve block on jaw kinematics.** (A) Chew cycle duration. Left halves of hemi-violins (black) are control and right halves (red) are nerve block for a single food type for an individual. Results of a two-tailed *t*-test and F-test of equality of variances are indicated by asterisks and crosses, respectively: *,†: P<0.05; **,††: P<0.01; ***,†††: P<0.001. Horizontal solid lines are means and horizontal dashed lines are medians. (B) Relative duration of gape cycle phases. Grey-scale bars are control durations and red-scale bars are nerve block durations. FC is fast close, SC is slow close, SO is slow open, and FO is fast open. See Methods for definitions of gape cycle phases and rhythmic chews. Asterisks and signs (+/-) indicate the significance level and the direction of a significant change, respectively. There were no significant food type effects, thus chews on both grapes and gummy bears were pooled for the phase analysis. Sample sizes are provided in Table 1.

After chewing began, there were also significant changes to the frequency of swallowing (Fig. 3.4 C). When feeding on grapes, swallows occurred significantly less frequently in all animals after the nerve block. The baseline swallow frequency for gummy bears was substantially lower in all animals, and no consistent pattern of nerve block effect was observed; Monkey Y exhibited a significantly higher swallow frequency, and Monkey B exhibited higher variance in swallow frequency.

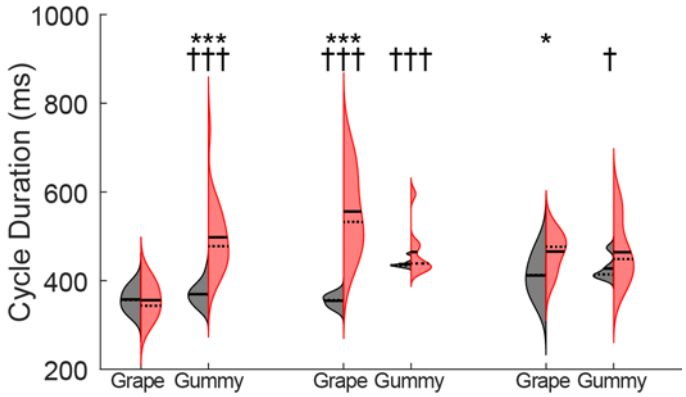


**Figure 3.6. Sequence-average chew cycle duration.** Left halves of hemi-violins (black) are control and right halves (red) are nerve block for a single food type for an individual. Results of a two-tailed *t*-test and *F*-test of equality of variances are indicated by asterisks and crosses, respectively: *,†: p<0.05; **,††: p<0.01; ***,†††: p<0.001. Horizontal solid lines are means and horizontal dashed lines are medians.

### CHANGES TO GAPE CYCLE KINEMATICS

To understand the source of the marked decrease in feeding performance we measured changes to the gape cycle, the kinematic 'framework' of mastication (Ross & Iriarte-Diaz, 2014). All animals exhibited a significant increase in chew cycle duration following the nerve block (Fig. 3.5 A). The prolonged chewing was found in all subjects when eating gummy bears and in two of three subjects when eating grapes. Moreover, feeding on gummy bears showed increased variance

following nerve block across all subjects. In four of the five cases where there was a significant change in cycle duration mean, there was also a significant increase in the cycle duration variance. Thus, not only were the animals chewing slower after the nerve block, but the variation in cycle duration was higher. This finding held both for chew cycles pooled across sequences, and for sequence-level means (Fig. S1; $P<0.05$). To ensure the increased cycle durations were not a side-

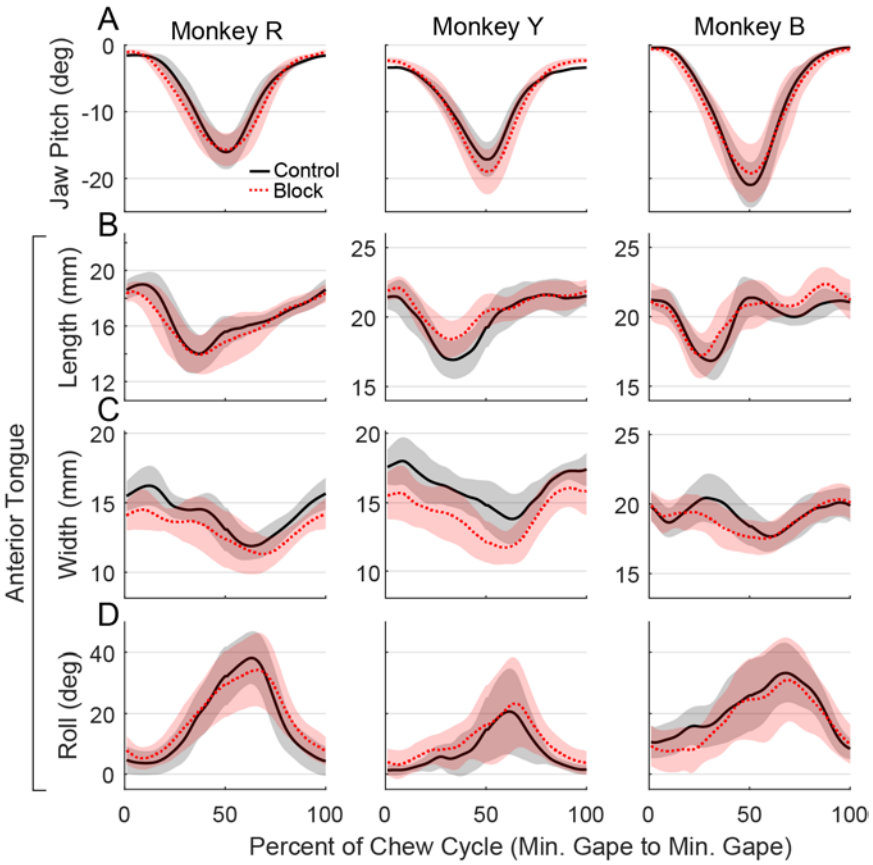


**Figure 3.7. Effect of tactile nerve block on tongue deformation trajectory during rhythmic right chews.** See Figure 3.1 for definitions of shape variables. (A) Jaw pitch, for reference. (B) Anterior tongue length. (C) Anterior tongue width. (D) Anterior tongue roll, where positive roll is the rotation of the dorsum of the tongue to the right. Lines are mean±1 s.d.; black is control and red dashed is treatment (tactile nerve block). Cycles are from minimum gape to minimum gape, and scaling was performed independently on opening and closing phases to control for shifting phase durations (see Methods section and Fig. 4); thus, 50% of cycle is always maximum gape. Sample sizes are provided in Table 1.

effect of the sedation required for the nerve block, we performed a sham procedure (see Methods) and found that cycle durations were unchanged (Fig. S2, $P>0.10$)

To assess how changes to gape cycle duration were effected at the cycle phase-level, we measured the relative duration, in terms of percent of cycle, of the four gape cycle phases (fast close, slow close, slow open, fast open; *sensu* (Ross & Iriarte-Diaz, 2014). Relative phase durations after nerve block differed significantly from their counterpart in the control (Fig. 3B); specifically, the relative duration of slow close decreased significantly and the relative duration of fast open increased significantly in all animals. The relative increase in fast open duration was the largest in magnitude of all the changes, and we noted a general pattern of increase in fast phase durations and decrease in slow phase durations.

### CHANGES TO 3D TONGUE KINEMATICS

The majority of tongue deformation during chewing occurred in the anterior portion (Pouderoux & Kahrilas, 1995), and we also noticed that most of that deformation occurred during the fast phases of the gape cycle (Feilich et al., 2021). Accordingly, we measured changes to anterior tongue length, width, and roll during right-side chews, from minimum gape to minimum gape (Fig. 3.7). Overall, the mean trajectories of three tongue kinematic variables remained consistent across the two experimental conditions (Fig. 3.7 B-D). We found no significant variation between food types in terms of mean trajectories, and thus pooled foods for this analysis. The most consistent and substantial nerve block effect was on tongue width; the tongue was narrower during jaw opening in all three animals (Fig. 3.7 C). In 8 out of 12 measured variables (jaw pitch and 3 tongue variables in 3 animals), the variance of the trajectory increased

significantly after the nerve block (Fig. 3.8). Only Monkey Y's tongue length and Monkey B's tongue width showed significant decreases in variance. In short, the tongue moved and deformed in similar ways after the nerve block, but there was increased variation in the shape trajectories.

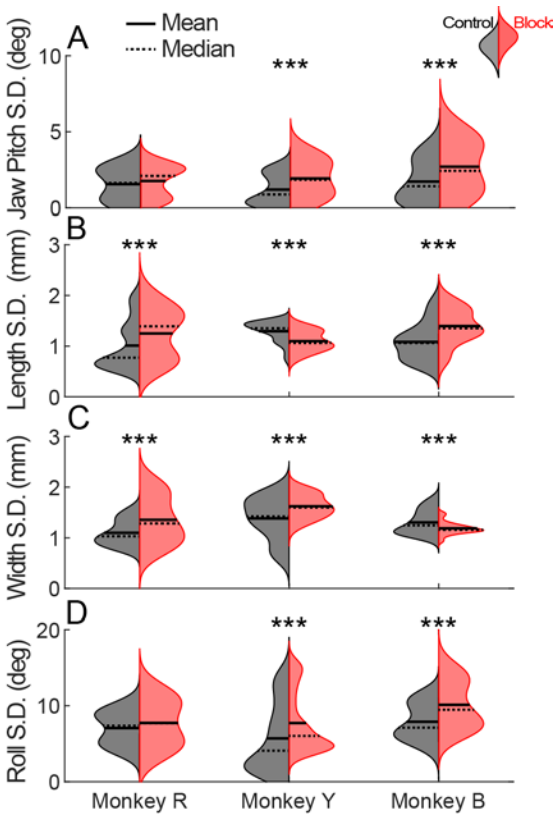


**Figure 3.8. Variance in tongue shape trajectory during chews.** Plotted values represent the mean of the standard deviation of each kinematic variable across the 100 scaled time points (i.e. mean of shaded error regions in Fig. 3.7). Thus, larger values indicate greater variance of that variable, on average, at any given time point in the chew cycle. Left halves of hemi-violins (black) are control and right halves (red) are nerve block. Results of two-tailed *t*-tests are indicated by asterisks and crosses, respectively: *: P<0.05; **: P<0.01; ***: P<0.001. Horizontal solid lines are means and horizontal dashed lines are medians.

## Strength and Consistency of Tongue-Jaw Coordination

We quantified tongue-jaw coordination with event and cross-correlation based analyses. In our event-based analysis, we used a conventional metric of tongue-jaw coordination (Hiiemae et

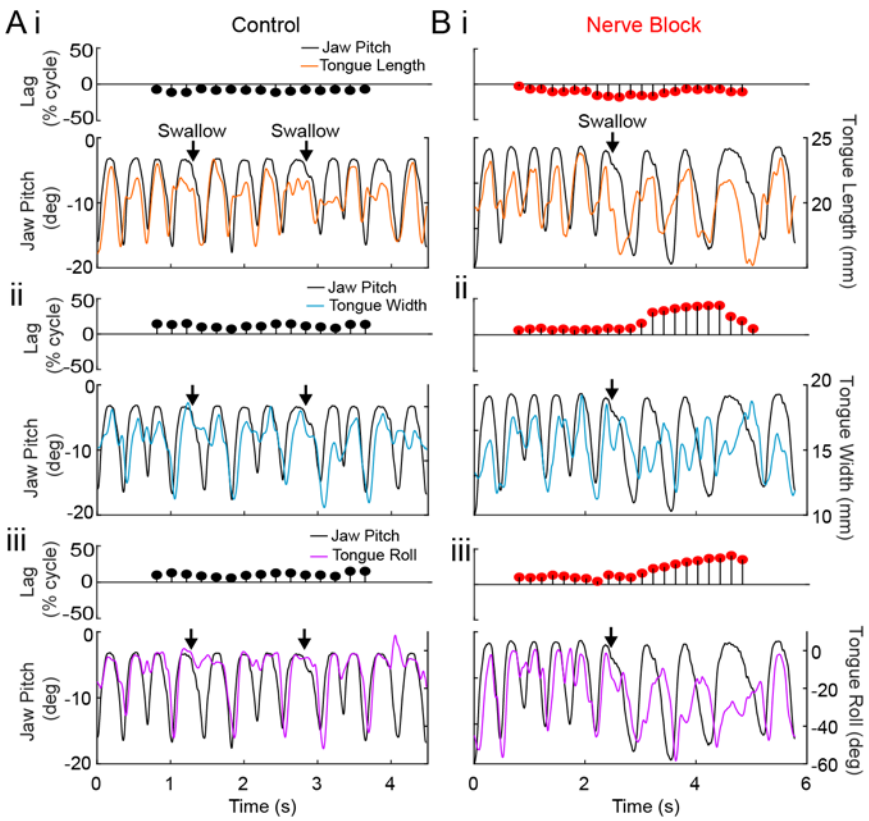


**Figure 3.9. Representative kinematic traces of tongue motion relative to jaw pitch in control (A, black) and tactile nerve block (B, red) conditions.** The upper ball-and-stick plots depict the lag of jaw pitch (black lines) and anterior tongue length (i, orange), width (ii, teal), and roll (iii, pink). Lags correspond to the maximum of the cross-correlation function of the two signals for a 300-frame range centered at that position. Note that in A, the correlation between jaw pitch and tongue width remains temporally consistent over the course of 10 chews and two intercalated swallows. In B, the initial lags are similar to A, but then shifts substantially at ~2.5 s. Swallows are indicated by black arrows.

al., 1995): the temporal lag between the anterior-to-posterior reversal of tongue tip movement and the preceding minimum gape, i.e., tongue tip reversal (Fig. S4). To account for changing gape cycle duration (Fig. 3A) we measured lags in both milliseconds (Fig. S4A) and in percent of cycle (Fig. S4B). Results were largely consistent between the two different measurement approaches;

after nerve block, tongue-tip reversal relative to minimum gape was more variable relative to the gape cycle, but the magnitude or direction of the lag was not consistent.

We used cross-correlation analysis as a second means of quantifying tongue-jaw coordination. Fig. 5 depicts representative sub-sequences from Monkey Y in which we calculated, on a rolling basis, the relative lag of jaw pitch and anterior tongue length, width, and roll (lag corresponding to maximum value of cross-correlation function). In the control condition (Fig. 5A), all dimensions of tongue motion remain consistently temporally correlated with jaw pitch over the course of 10 chews and 2 swallows. After the tactile nerve block (Fig. 5B), patterns of temporal correlation are less consistent over the duration of sequences. During the chews at the beginning of the sub-sequence, tongue-jaw lag appears to resemble the control, but then at approximately 3

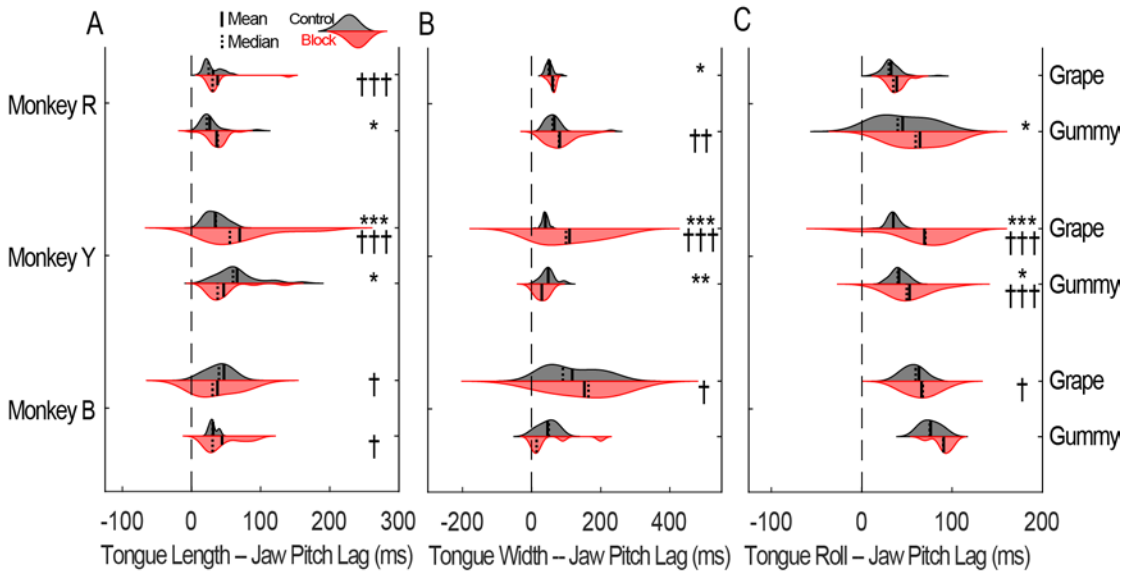


**Figure 3.10. Effect of tactile nerve block on temporal correlation of jaw pitch and anterior tongue (A) length, (B) width, and (C) roll**. Violins depict the lag (in ms) corresponding to the maximum cross-correlation coefficient for bouts of 4-10 rhythmic chews. Thus, a positive lag indicates the tongue variable follows jaw pitch when optimally correlated. Top halves of hemi-violins (black) are control and bottom halves (red) are nerve block for a single food type for an individual. Results of a two-tailed ¬t¬-test and F-test of equality of variances are indicated by asterisks and crosses, respectively: *,†: P<0.05; **,††: P<0.01; ***,†††: P<0.001. Vertical solid lines are means and vertical dashed lines. Sample sizes are provided in Table 1.

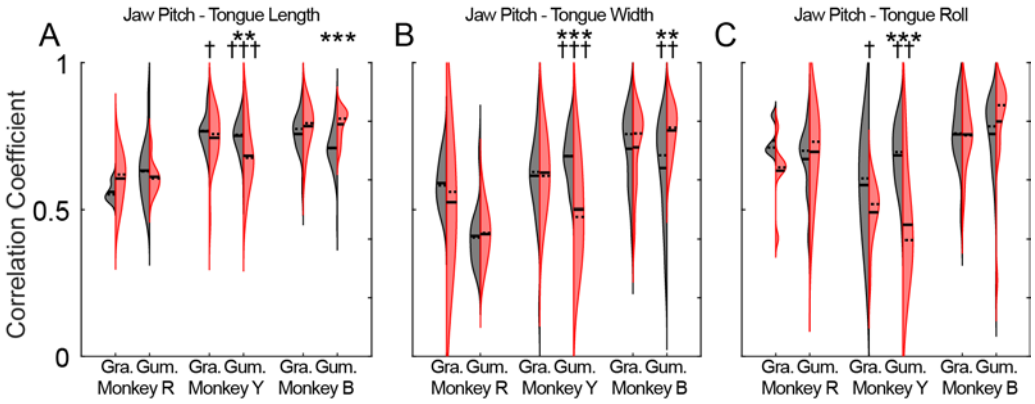


**Figure 3.11. Strength of correlation between jaw pitch and tongue shape.** Left halves of hemi-violins (black) are control and right halves (red) are nerve block for a single food type for an individual. Results of a two-tailed ¬t¬-test and F-test of equality of variances are indicated by asterisks and crosses, respectively: *,†: P<0.05; **,††: P<0.01; ***,†††: P<0.001. Horizontal solid lines are means and horizontal dashed lines are medians.

s, the lags of jaw pitch and tongue width and length change substantially. Noticing these shifting patterns of coordination, we quantified the mean tongue-jaw lag (via cross-correlation) for bouts of 3-10 rhythmic chews (Fig. 3.10). Half of the measured correlation lags showed significant shifts in magnitude, however the direction of the changes was not consistent; sometimes the tongue shifted earlier relative to the jaw after the nerve block, sometimes it shifted later. In contrast, 10 of 18 lags exhibited a significant increase in variance after the nerve block, with no significant decreases. Thus, between bouts of rhythmic chews, the pattern of tongue-jaw coordination was more variable after the nerve block.

Was this change in temporal correlation reflected in a change in strength of correlation? We took the magnitude of the maximum (absolute value) correlation coefficient for the same chewing sub-sequences (Fig. 3.11). Interestingly, there were no consistent patterns in change to correlation strength or variance in correlation strength. Of the 18 correlations, 5 exhibited a significant change after the nerve block, and the direction of the changes was not consistent. Thus,

lack of tactile sensation changes the consistency of the pattern of tongue-jaw coordination during feeding, but not the instantaneous strength of that pattern.

## DISCUSSION

The goal of this study was to address the role of oral tactile sensation in 3D tongue movement and tongue-jaw coordination during feeding. We found that, after the loss of tactile feedback, all animals exhibited impaired feeding performance and more temporal variability in the pattern of tongue deformation and tongue-jaw coordination, though the average trajectory of tongue deformation during chews remained largely unchanged.

### FEEDING PERFORMANCE

We used metrics drawn from a recently formalized feeding assessment (Huckabee et al., 2018) to quantify feeding performance. We found that feeding sequence duration increased after the tactile nerve block (Fig. 3.4 A), except in the case of one food type for one individual (Monkey Y, gummy bears), where it decreased. While an increase in sequence duration is consistent with previous findings (Inoue et al., 1989), we propose that deviation from normal values in either direction is indicative of impaired performance; more chews on a food item indicates difficultly in processing or difficultly sensing when processing is sufficient, while fewer chews on a given food item could indicate that the item is not adequately processed before swallowing. The latter presents a particular concern in regard to swallowing safety (Mayerl et al., 2021). Analysis of the material properties of the swallowed bolus would be necessary to determine whether the increased sequence durations were driven by incoordination (bolus would be under-chewed), or poor estimation of

bolus properties (bolus would be over-chewed). Given the effect of loss of tactile feedback on tongue-jaw coordination and swallowing, it seems likely that a combination of the two is responsible for the change in feeding sequence durations. The marked increase in number and variance of manipulation cycles (Fig. 3.4 B) suggests that tactile feedback plays an especially important role in the initial ingestion stages of the feeding sequence.

There was a food-dependent effect of the nerve block on swallow frequency (Fig. 3.4 C). For grapes, swallows occurred significantly less frequently after the nerve block. For gummy bears, there was no consistent change to swallow frequency. Notably, grapes had a higher baseline swallow frequency, which after the nerve block, approached that of gummy bears. A higher frequency of intercalated swallows with foods that have a liquid component has been noted previously (Hiiemae & Crompton, 1985), thus, we infer that the reduction in swallowing reflects an impaired ability to efficiently sense or handle the liquid component of the food. As many foods differ in their material properties and demand different jaw kinematics (Iriarte-Díaz et al., 2011), this result illustrates the importance of including multiple food types in future nerve block and transection feeding studies.

### JAW KINEMATICS

We found that chew cycle duration increased after the loss of tactile sensation (Fig. 3.5 A). This result is consistent with clinical findings that in neuromuscular disorders the slowing of movement can be driven by impairments to sensorimotor integration (Abbruzzese & Berardelli, 2003; Patel et al., 2014). Or, inversely, coordinated movements depend on sensory feedback for their execution at normal speeds. Relatedly, both computational and *in vivo* experiments have

demonstrated that CPGs tend to operate at lower frequencies in the absence of sensory feedback (Hatsopoulos, 1996; Huang et al., 1989; Inoue et al., 1989; Morimoto et al., 1985). Thus, our results suggest that tactile feedback is important for the maintenance of the natural chewing frequency.

Within individual gape cycles, the relative duration of the fast open phase increased after the nerve block (Fig. 3.5 B). During fast open, the tongue performs one of its principle sensorimotor tasks: the gathering of new information about bolus properties while simultaneously repositioning it onto the tooth row (Hiiemae & Palmer, 2003). An elongation of this phase after the loss of tactile feedback suggests that performance of this task depends heavily on that tactile feedback. Additionally, fast open is immediately followed by the closing phases of the gape cycle, where the risk of a tongue bite is highest. Thus, in a situation where stereognosis and manipulation of the bolus is impaired, a prolonging of the opening phase could reduce the chance of the tongue being bitten while those processes are still occurring.

### TACTILE FEEDBACK ENABLES CONSISTENT TONGUE-JAW COORDINATION

Our findings suggest that tactile feedback from the oral cavity plays a key role in regulating the pattern of tongue-jaw coordination, but not in the generation of the pattern itself. After the nerve block, there was more variation in the correlation lag between the tongue and the jaw (Fig. 3.10). This result held for multiple dimensions of tongue kinematics—both internal deformation (length and width) and positional change (roll). While the example sequence depicted in Fig. 3.9 B contains a shift in coordination corresponding to the first intercalated swallow, we did not find statistically significant ($P$>0.1) patterns in the change of temporal coordination related to swallows

or any particular time point in the feeding sequences; the increased variance in tongue-jaw temporal correlation was distributed throughout the feeding sequence. Importantly, in two of three animals this increased temporal variance was not reflected in a change to the strength of the correlations (Fig. 3.11). In other words, the tongue and jaw were not 'less' coordinated, but rather differently coordinated.

How does this difference in coordination relate to the tongue movements themselves? We found an increased variance in the trajectory of tongue deformation (Fig. 3.8), as well as some changes to the average trajectory of tongue deformation during chews—in particular anterior tongue width (Fig. 3.7). But we noted that those changes were minimal, in that that the tongue assumed approximately the same shapes at the same times in the gape cycle. This result stands in opposition to the findings of a recent study that observed differential hand postures in subjects with a chronic loss of tactile feedback (Miall et al., 2019). We believe this difference could be due to the inherent differences between chewing and grasping—both in terms of cyclicity and role of vision in the behavior. Given that cycle-to-cycle variation in tongue kinematics is expected as the tongue responds to changing bolus properties, how does the increase in variance after the loss of tactile feedback relate to impaired feeding performance? We suspect that deviations from the tongue's average kinematic trajectory in normal feeding are relatively subtle in magnitude, in part so they don't disturb the overall masticatory rhythm in which they are contextualized. Indeed, responses to perturbations or changing extrinsic factors in limbed locomotion are often rapid and result in little change to the overall gait cycle (Daley & Biewener, 2006). Thus, while some variation in kinematics is required to account for a dynamic environment (or bolus, in the case of feeding), it seems that temporal resilience of the overall motor pattern in the face of changing

external factors is a hallmark of coordinated, cyclic behaviors in mammals (Ross et al., 2010, 2013). Our results demonstrate that when the tongue and jaw are deprived of tactile feedback that consistency is impaired. That the strength of the correlations between the tongue and jaw is not degraded suggests that the generation of the pattern itself does not depend on tactile feedback. Further studies are needed to test whether proprioceptive feedback from muscle spindles is involved in the emergence of the motor pattern, as has been found in locomotion (Akay et al., 2014). Additionally, there is a non-linear relationship between the position of the tongue relative to the teeth and feeding performance; tongue close to the teeth is useful, but just a bit too close is a serious problem (it gets bitten). Thus, measurements of tongue-tooth distance before and after an oral tactile nerve block could provide an alternate means of assessing tongue coordination. Finally, our understanding of the role of the sensorimotor cortex in the control of tongue-jaw coordination is still rudimentary and constitutes an important avenue for future research (Bollu et al., 2021).

# CHAPTER 4 - DECODING TONGUE SHAPE FROM THE PRIMARY SENSORIMOTOR CORTEX[15]

## INTRODUCTION

The tongue plays a dynamic motor role in eating, drinking, and speaking (Hiiemae & Palmer, 2003). When tongue function becomes impaired—as is common in many neuromuscular disorders—quality of life can be dramatically impacted; individuals with tongue dysfunction often have difficulty swallowing solid foods, articulating speech, and, in extreme cases, breathing (Avivi-Arber & Sessle, 2018; Schimmel et al., 2017; Takizawa et al., 2016). Strategies for the restoration of lingual functionality typically involve rehabilitative exercises that target the tongue muscles (H. D. Kim et al., 2017; Robbins et al., 2007), but in situations where a partial or full glossectomy (tongue removal) is required, normal swallowing and speech are rarely restored (Dios et al., 1994; McKinstry et al., 1985).

In individuals with limb paralysis, brain-computer interfaces (BCIs) that decode intended arm movements from cortical activity have shown impressive potential for restoring lost sensorimotor function (Carmena et al., 2003; Collinger et al., 2013; Hochberg et al., 2006, 2012). The BCI approach relies on the fundamental principle that movement related information is represented in the activity of cortical neuronal populations—a well-documented finding in the arm and hand region of the primary motor cortex (Ashe & Georgopoulos, 1994; Georgopoulos et al., 1982; Hatsopoulos et al., 2007; Omrani et al., 2017; Tanji & Evarts, 1976; Thach, 1978).

[15] Author list: JD Laurence-Chasen, CF Ross, FI Arce-McShane, NG Hatsopoulos. Author contributions (following CRediT Taxonomy): Conceptualization, F.I.A-M., N.G.H., C.F.R.; Methodology, All; Analysis & Software, J.D.L-C and N.G.H.; Investigation, N.G.H., J.D.L-C. and C.F.R.; Writing – Original Draft, J.D.L-C.; Writing – Review & Editing, All; Project Administration, F.I.A-M.; Funding Acquisition, F.I.A-M. (PI), N.G.H., and C.F.R.; Supervision, F.I.A-M. and C.F.R

Preliminary studies have found that the primate orofacial sensorimotor cortex contains information about tongue protrusion direction and tongue tip position (Arce-McShane et al., 2013; S. Liu et al., 2019; Murray & Sessle, 1992b, 1992a), but it is not known whether this extends to the complex 3D postures and movements that characterize the tongue's action during feeding and speech; the tongue is hidden inside the mouth and difficult visualize in 3D.

The hand and tongue exhibit striking anatomical and functional analogy (Quinlan et al., 2015). Both rapidly change their 3D posture to deftly control food and other objects (Feix et al., 2015; Hiiemae & Palmer, 2003; Olson et al., 2021), and in both, that dexterity is enabled by rich mechanosensory innervation that provides a wealth of ongoing feedback to the brainstem and sensorimotor cortex (Haggard & de Boer, 2014; Hatanaka et al., 2005; Johansson & Vallbo, 1979). However, there is also a crucial anatomical difference between the hand and the tongue: hand posture is both constrained and facilitated by rigid internal structure of bones and joints, whereas the tongue, a muscular hydrostat (Kier & Smith, 1985), is capable of complex, non-linear deformation. The impact of this anatomical disparity on cortical encoding of motion is not known.

Here, we use X-ray Reconstruction of Moving Morphology (XROMM; (Brainerd et al., 2010) paired with intracortical microelectrode arrays to synchronously record high-resolution, 3D tongue kinematics and neuronal activity from the orofacial sensorimotor cortex (Arce-McShane, 2021; Arce-McShane et al., 2014). The goal of the present study was to decode 3D tongue posture and movement from the primary motor and somatosensory cortex in a primate for the first time.

# METHODS

## ANIMALS AND SURGERY

We recorded kinematics and neural data from two adult male rhesus macaques (monkeys R and Y; *Macaca mulatta*, 9-10 kg). Monkeys received full-time care from husbandry and veterinary staff, and all protocols were approved by the University of Chicago Animal Care and Use Committee and complied with the National Institutes of Health Guide for the Care and Use of Laboratory Animals.

Surgical procedures consisted of the implantation of radiopaque beads for marker-based XROMM and the implantation of intracortical microelectrode arrays for the recording of neural activity. In the marker implantation surgery, and angiocatheter and stylus were used to insert 15 radiopaque beads (tantalum, 1 mm diameter) into the tongue at various positions and depths (Orsbon et al., 2018). In the analysis presented here, 6 of the 15 tongue beads were used. Additional beads were implanted into the cranium and mandible (4 per bone) using a standard, drill-based technique. In the array surgery, each monkey was implanted with two Utah arrays (Blackrock Microsystems, Inc., Salt Lake City, UT), and two floating microelectrode arrays (FMA,

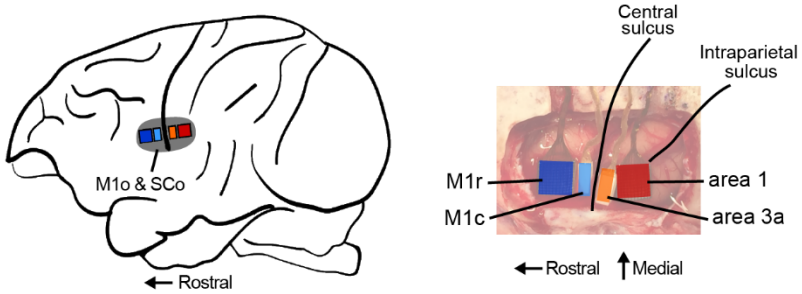


**Figure 4.1. Intracortical array locations.** Two Utah arrays (Blackrock Microsystems) were inserted into the orofacial region of the primary motor (M1o) and somatosensory cortex (SCo-area 1; dark blue and dark red, respectively). Two floating microelectrode arrays (FMAs; Microprobes for life sciences) were manually inserted adjacent to the Utah arrays, in caudal M1 and area 3a (light blue and orange, respectively).

Microprobes for Life Science, Gaithersburg, MD). Utah arrays were implanted into orofacial region of rostral M1 and area 1 of the somatosensory cortex. Floating microelectrode arrays were implanted into caudal M1 and area 3a (Arce-McShane et al., 2014, 2016).

BEHAVIORAL TASK

Subjects sat calmly and received and consumed food items while head-fixed and seated in a standard primate chair in the Universitsy of Chicago XROMM Facility. Experimental food comprised half grapes and half gummy bears of equal size presented directly to the monkey's mouth via a long stylus.

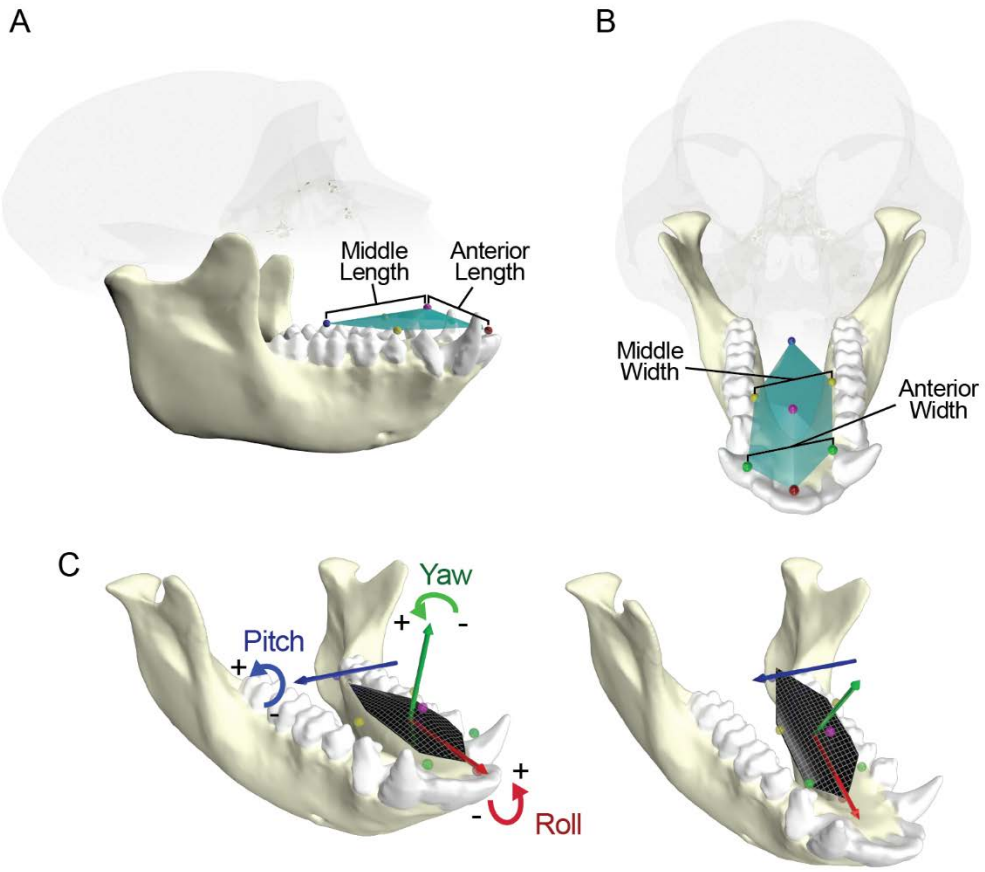


**Figure 4.2. Tongue kinematics measurements. (**A) Anterior and middle length measurements were the Euclidean distances of pairs of midline tongue markers. (B) Anterior (green) and middle (yellow) width measurements were the Euclidean distances of pairs of lateral makers. (C) Six degree of freedom pseudo-rigid body motion of the tongue was calculated by fitting a rigid body (black shape) to the marker constellation in each frame. Rotational axes about which Euler angles were measured are depicted. Translations were measured along anatomically oriented axes (i.e. anterior-posterior, medial-lateral, and superior-inferior).

KINEMATICS

We used the XROMM workflow to reconstruct the 3D rigid body transformations of the cranium and mandible, as well as the 3D positions of a constellation of small beads implanted in the tongue—from which a series of tongue kinematic variables were calculated. Data (biplanar X-ray videos to visualize radiopaque markers) were collected over multiple nerve block sessions at the University of Chicago XROMM facility. Additionally, post-surgery CT scans were taken with a Vimago Veterinary Scanner from which mesh models of the cranium and mandible were created (segmented) in the open-source software 3D Slicer (www.slicer.org). The 3D coordinates of the markers within each bone were also extracted from the CT scans. Importantly, prior to marker coordinate extraction, we digitally centered and rotated the mesh models to align with the global coordinate system, such that "CT space," for each model became identical to "anatomical space." This enabled the simple automation of the coordinate system transformations described in the following paragraph.

Videoradiographic data were processed using a recently described workflow that integrates XMALab and DeepLabCut (Laurence-Chasen et al., 2020). In short, deep neural networks were trained to track the 2D positions of the tantalum beads in both of the X-ray videos. Those 2D positions were then imported into XMALab where their 3D positions were triangulated, and the motion of the two rigid bodies (cranium and mandible) were computed. Rigid body transformation matrices and 3D points were filtered in XMALab with the built-in zero-lag, 30 Hz low-pass Butterworth filter. All subsequent data manipulation and analysis was performed in MATLAB (Mathworks) using custom scripts. Using the cranium rigid body transformation matrix, the tongue points were rotated into a cranial coordinate system, with an origin at the posterior nasal spine (following (Orsbon et al., 2018)). The coordinate system was orientated such that the anterior-

posterior axis was parallel with the maxillary post-canine tooth rows, and the medial-lateral and vertical axes were orthogonally oriented, following classic anatomical planes. Jaw pitch was measured with a temporomandibular joint coordinate system (Grood & Suntay, 1983), where the primary (i.e., first in rotation order) rotational axis passed through both mandibular condyles (Menegaz et al., 2015). The rotation was calculated by multiplying the mandible rotation matrix by the inverse of the cranium rotation matrix and decomposing the product into Tait-Bryan angles.

Tongue kinematic variables were calculated from the tongue markers, rotated into either cranial or mandibular coordinate systems. The pseudo-rigid body motion of the anterior tongue was calculated by fitting a rigid constellation of markers (taken from a frame at which the tongue was at rest), to the anterior 4 tongue markers in every frame of the video (Fig. 4.2). Actual fitting was performed using MATLAB's Procrustes function, and the resultant rotation matrix was decomposed into Tait-Bryan angles. Deformation values were the Euclidean distances of two markers –and thus invariant to coordinate system (Fig. 4.2 B).

### ELECTROPHYSIOLOGY AND NEURAL DATA PROCESSING

Neural signals were recorded with Utah arrays and FMAs using a Grapevine Neural Interface Processor (Ripple Neuro, Salt Lake City, UT). Offline spike sorting (Offline Sorter, Plexon, Dallas, TX) was performed to remove noise and to isolate individual neurons. The time-varying firing rates of neurons were computed by summing spikes in 5 ms time bins (the same resolution as kinematic data). For all decoding, a differential time lag was applied to the M1 and SC spiking data. Specifically, a -40 ms lag (neural activity leading kinematics) was applied to M1 data, and a +110 ms lag (neural activity following kinematics) was applied to SC data. Optimal

lag values were determined through the iterative test of Kalman filters with various lags. All analysis was performed at the single-unit level. Veridical locations of Monkey R array locations were confirmed through *post mortem* histology.

### DECODING

We used a Long Short-Term Memory (LSTM) network to continuously decode tongue kinematics from cortical neuronal activity (Glaser et al., 2020; Hochreiter & Schmidhuber, 1997). An LSTM network is a type of recurrent neural network where LSTM cells provide a means of mitigating the exploding/vanishing gradient problem (Pascanu et al., 2013) through the selective 'remembering' and 'forgetting' of specific information. Here, we used MATLAB's native LSTM functions found in the Deep Learning Toolbox to train a series of LSTMs for sequence-to-sequence decoding. Specific parameters used are provided in Table 4.1**.**

Table 4.1. LSTM Parameters

| **Parameter** | **Value** |
|---|---|
| Number of hidden units | 250 |
| Solver Type | Adam optimizer |
| Maximum Number of Epochs | 250 |
| Gradient Threshold | 1 |
| Initial Learning Rate | 0.005 |
| Learning Rate Schedule | Piecewise |

## RESULTS

### COMPLEXITY OF TONGUE KINEMATICS

To characterize the complexity of tongue motions during feeding, we performed a principal component analysis (PCA) on the raw XYZ marker positions (45-dimensional data). We found that the majority of the variance in tongue movement during chewing was explained by the first 6-8 components (Fig. 4.3). This result held for the motion of the tongue markers in a cranial coordinate system (Fig. 4.3 A) and in a mandibular coordinate system (Fig. 4.3 B). Subsequent analysis was performed on the computed pseudo-rigid body motion and deformation of the tongue (see Methods).

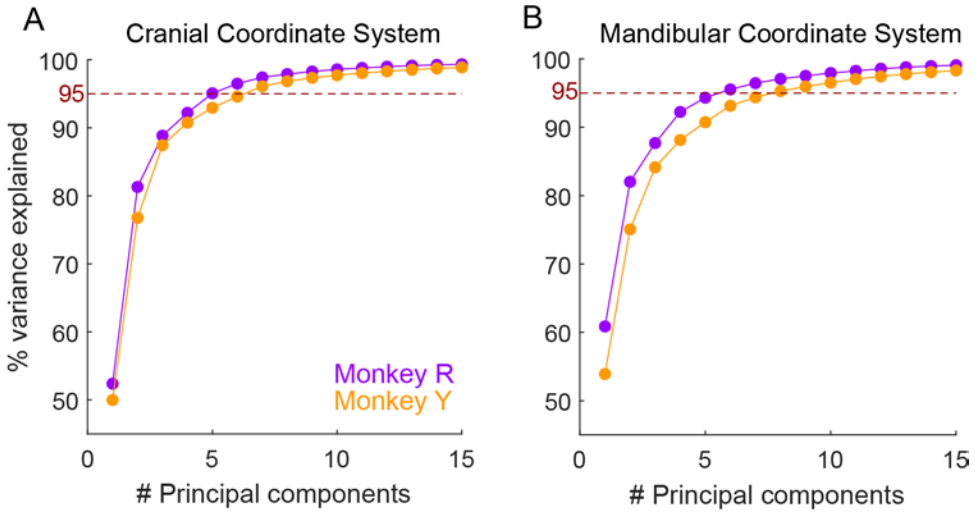


**Figure 4.3. Complexity of tongue kinematics.** Cumulative percentage of variance explained by the number of principal components of raw kinematics data. Input to the PCA was the XYZ positions of all tongue markers (45-dimensional data) in either a (A) cranial coordinate system or a (B) mandibular coordinate system.

## DECODING TONGUE KINEMATICS FROM M1 AND SC

We decoded tongue pseudo-rigid body motion (translations and rotations) and deformations (length and width) from population responses in M1 and SC. Fig. 4.4 depicts a representative feeding sequence where kinematics were decoded from M1 activity using the two different decoders. Overall, both decoders successfully predicted the various aspects of tongue kinematics, though the performance of the LSTM network was consistently better.

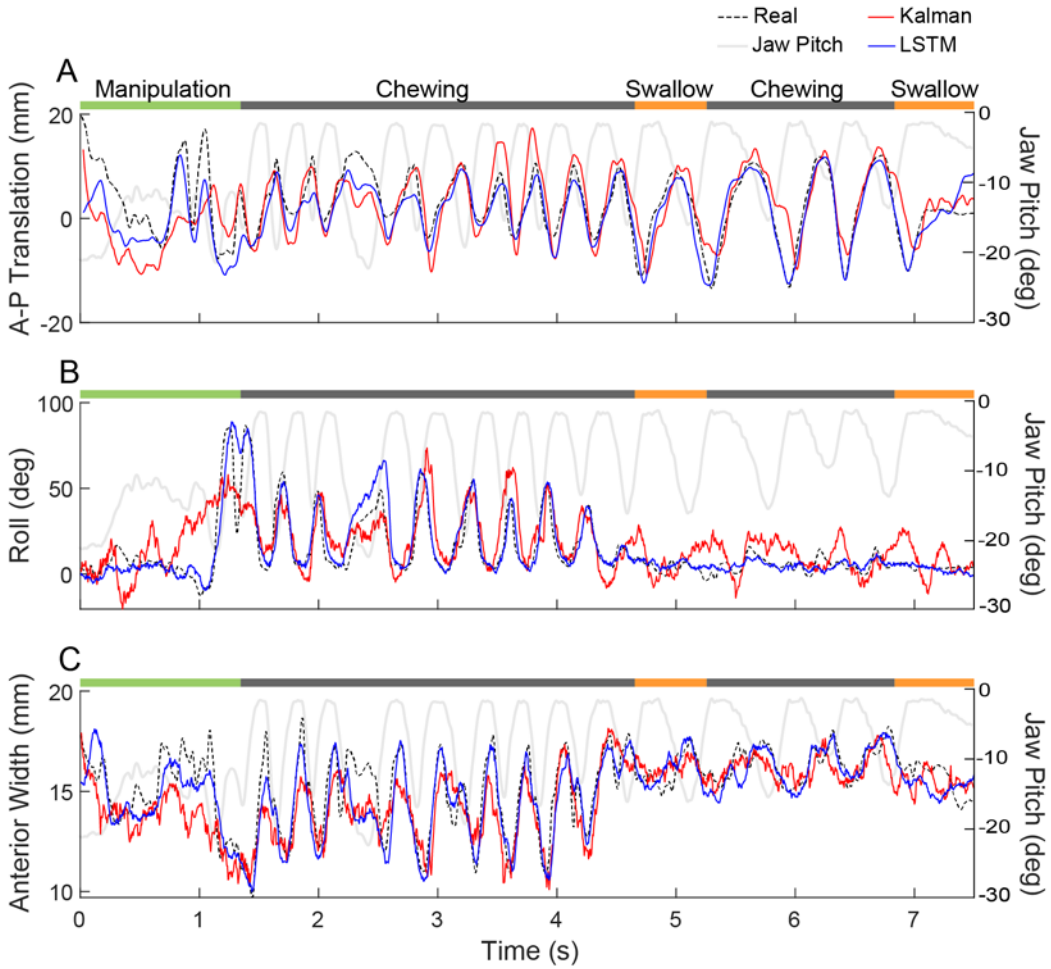


Figure 4.4. **Decoding tongue kinematics from M1 activity.** Ground-truth tongue kinematics (black dashed lines) and kinematics decoded from responses of 30 randomly selected M1 neurons (red line, Kalman filter; blue line, LSTM network) from a full feeding sequence from Monkey R. (A) Anteroposterior translation. (B) Roll. (C) Anterior Width. Jaw pitch (gape) is the light grey line, where zero is jaw closed.

CORTICAL AREA

We compared decoding performance across regions to assess how information about tongue posture is represented in different cortical areas. We iteratively drew an equal number of neurons from each cortical area and kept the train and test sets consistent. We initially compared decoding from rostral M1 and SC (area 1) responses with 30 neuron subpopulations (Fig. 4.5 A).

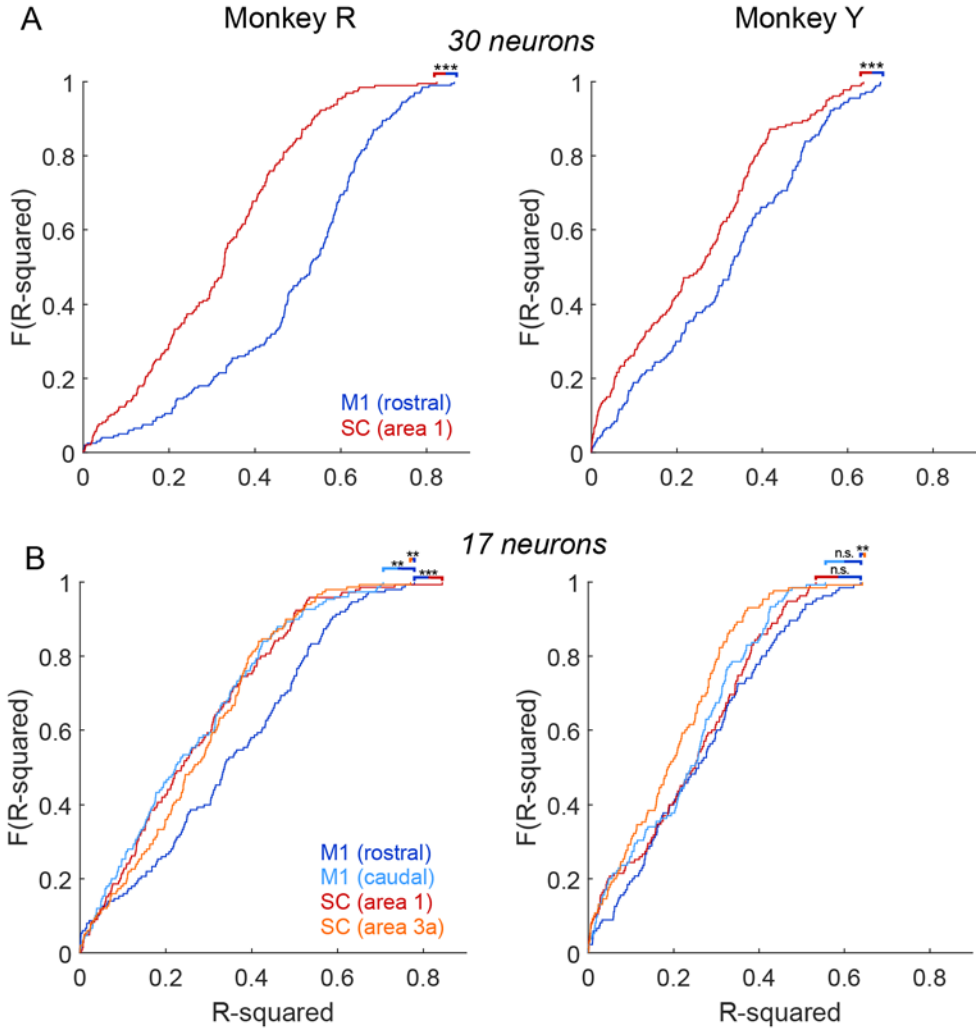


**Figure 4.5. Decoding from M1 versus SC.** Cumulative distribution functions of the accuracy ($R^2$) of tongue kinematics decoded from neural responses in multiple cortical areas in two monkeys. Data are pooled trial-level $R^2$ values for all kinematic variables for 15 held-out test trials. (A) Comparison of M1 and SC (area 1) with N=30 neurons as input to decoder. (B) Comparison of all four cortical areas (rostral M1, caudal M1, area 1, and area 3a) where the same number of neurons (N=30) was iteratively sampled from each cortical population and used as input to the decoders.

For both individuals, M1 significantly outperformed SC ($P$<0.001, two-sided Wilcoxon Rank Sum Test). The smaller FMAs in caudal M1 and area 3a recorded fewer overall neurons, so the analysis was performed again with an ensemble size of 17 neurons in each of the four areas (Fig. 4.5 B). In Monkey R, rostral M1 significantly outperformed all other regions. In Monkey Y, rostral M1 significantly outperformed area 3a, but was not significantly different than the other three regions ($P$>0.05, two-sided Wilcoxon Rank Sum Test).

## ENSEMBLE SIZE

Next, we evaluated the impact of ensemble size on decoding performance. Starting with the responses of single rostral M1 neurons, we trained and tested decoders with increasingly larger neural ensembles as input, up to 35 neurons (Fig. 4.6). We found that, for most variables, the impact of ensemble size on performance was greatest from 1 to 10 neurons. After 10 neurons, the rate of performance improvement started to gradually decrease. At an ensemble size of 35 neurons,

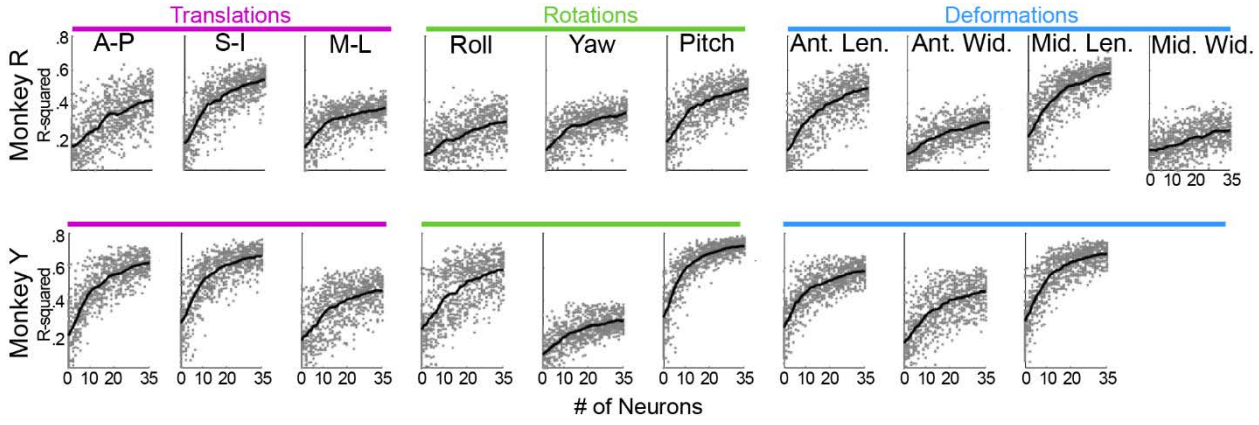


**Figure 4.6. Effect of neuronal ensemble size on decoding performance.** Black lines represent mean decoder (Kalman filter) performance across 25 iterations of random draws of an ensemble size given on the horizontal axis. Light grey dots represent the mean performance of a single neuronal ensemble / decoder across 5 test trials. Variable abbreviations: A-P, anteroposterior; S-I, superoinferior; M-L, mediolateral; Ant. Len., anterior length; Ant. Wid., anterior width; Mid. Len., middle length; Mid. Wid; middle width.

performance had not yet plateaued, but for some variables (roll, yaw) plateaus did appear imminent. Notably, for all variables there were some single neurons and pairs of neurons that performed substantially better than ensembles ten times their size.

### COMPARING TRANSLATIONS, ROTATIONS, AND DEFORMATIONS

We evaluated rostral M1 decoding performance by the type of variable (translation, rotation, deformation) and the variables' correlation with jaw pitch to assess the cortical representation of various aspect of tongue posture (Fig. 4.7). We found that, in both individuals, there were no significant effects of variable type on decoding performance (Two-way ANVOVA, $P>0.05$). We did note that for rotations and deformations, there appeared to be a relationship between a given variable's correlation with jaw pitch and decoding performance. In contrast, for the variables with the highest decoding performance (independent of variable type), there was not a relationship between performance and correlation with jaw pitch. In other words, the deformation

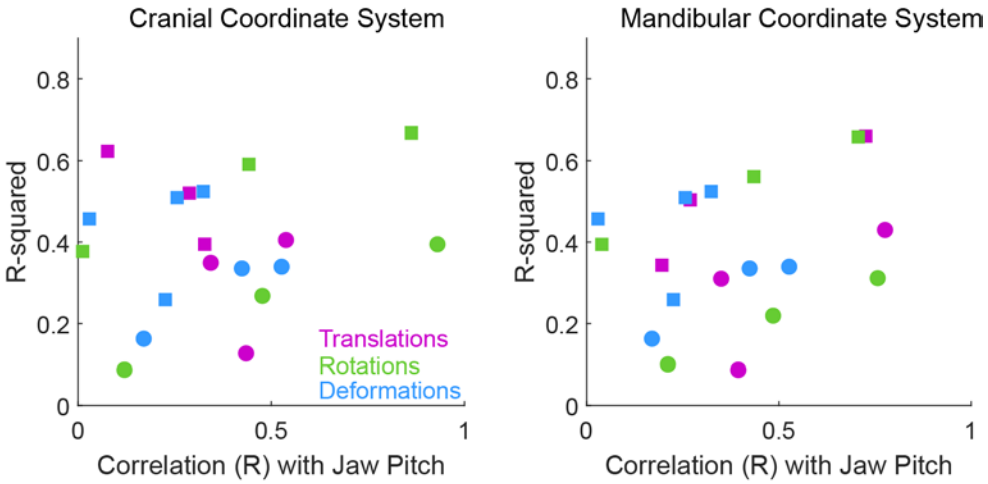


**Figure 4.7. Decoder performance by variable type and correlation with jaw pitch.** Each symbol represents the mean decoding accuracy ($R^2$) of a single variable across 3 folds of cross validation. The horizontal position indicates the variable's Pearson correlation with jaw pitch. Pseudo-rigid body motion (translations and rotations) were computed in both a cranial (left) and mandibular (right) coordinate system. Squares are Monkey R and circles are Monkey Y.

variable most correlated with jaw pitch was decoded more accurately than other deformation variables, but not necessarily more accurately than all other kinematic variables. These results held true for rotations and translations in both cranial (Fig. 7A) and mandibular (Fig. 7B) coordinate systems.

### POSITION VS. VELOCITY

In the analyses up to this point, the decoded kinematic variables have been in their 'postural' form (*sensu* Okorokova et al., 2020)—raw position values, rather than velocities or accelerations ('movement'). We assessed our ability to decode the two different variable types by training decoders on both the instantaneous translation, rotation, and deformation values, as well as their velocities (Fig. 4.8). We found that for Monkey R posture was significantly more accurately decoded than movement ($P<0.001$, two-sided Wilcoxon Rank Sum Test), but for Monkey Y there was no significant difference ($P>0.05$).

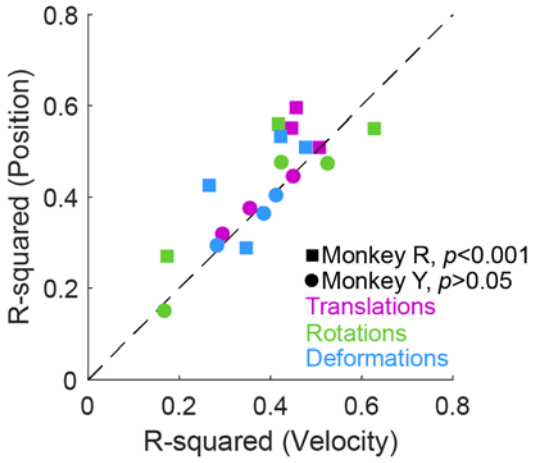


**Figure 4.8. Decoding tongue posture versus movement.** Each symbol represents the mean decoding accuracy of a variable across 3 folds of cross-validation. The horizontal axis is the performance when the variable's velocity (movement) was used, and the vertical axis is the position (posture).

# DISCUSSION

## DECODING 3D TONGUE KINEMATICS FROM THE SENSORIMOTOR CORTEX

This study is, to our knowledge, the first attempt to decode 3D tongue posture and movement beyond XYZ marker positions (see Liu et al., 2019) from the orofacial sensorimotor cortex during feeding. We found that a relatively simple linear decoder—the Kalman filter—was able to successfully predict various aspects of tongue posture with relatively high accuracy (Fig. 4.3), but a more sophisticated machine-learning algorithm— an LSTM—achieved even better performance. This finding is consistent with previous characterizations of the performance of different algorithms (Glaser et al., 2020). Notably, we found that the difference between the LSTM and Kalman was often substantial, especially in cases of subtle or atypical movements (see Fig. 4.3, end of the sequence). We expect that the non-linear nature of tongue deformation and movement may explain these performance differences, as the LSTM makes no assumption of linearity its modeling.

## CORTICAL AREAS

We achieved the highest decoding accuracy from populations of rostral M1 neurons (Fig. 4.5 A). This result is consistent with previous findings in both the hand and the arm (Hatsopoulos et al., 2004; Okorokova et al., 2020). With a smaller ensemble size (N=17, Fig. 4.5 B), performance was more similar across the different cortical areas, but greater inter-individual variation was observed. Interestingly, despite significantly different performance across all variables ($P<0.01$ two-sided Wilcoxon Rank Sum Test), the single best performances from each cortical area were approximately the same in terms of accuracy; for at least one variable,

decoding accuracy from SC was equal to that of rostral M1. This analysis pooled all of the decoded variables, so it is not necessarily the case that the same variables were decoded equally well from different cortical areas.

### TONGUE POSTURE VERSUS MOVEMENT

A recent study found that the cortical decoding of hand posture (joint angles) was more accurate than that of hand movement (joint angular velocities) (Okorokova et al., 2020). This result stands in contrast to the recurring finding that the primary motor cortex (M1) more strongly encodes 'higher-order' movement parameters like proximal limb velocity and/or trajectory (Omrani et al., 2017; Saleh et al., 2010). We found that, in this regard, the tongue is like the hand. For all variables, decoding accuracy of posture was higher than that of movement (Fig. 4.8). The anatomical and functional similarities (rich sensory innervation, dexterous manipulation), may explain the consistency of decoding results.

### NEURAL CONTROL OF A MUSCULAR HYDROSTAT

The tongue is a muscular hydrostat, unconstrained by rigid internal structure (Kier & Smith, 1985). Consequently, the theorical dimensionality, or number degrees of freedom of tongue movement, is large. We found that the majority of variance (95%) in our tongue kinematics data (45-dimensional data) was explained by the first 6-8 principle components of a PCA (Fig. 4.3). Notably, this is the same number of dimensions as reported for the hand during a reaching task (Okorokova et al., 2020). We do not find this result particularly surprising for three reasons. First, feeding is a cyclic behavior that involves repeated motions that follow fairly stereotyped

trajectories (Hiiemae et al., 1995). Second, there are a finite number of muscles (~16) and motor units within the tongue (Sanders & Mu, 2013); thus, in a realistically constrained model (even one without bones), the number of degrees of freedom is not infinite. Third, from a neuromechanical control perspective, a smaller number of functional degrees of freedom simplifies control dramatically. Overall, our results suggest that while the underlying biomechanics of the tongue are substantially different from that of the hand, the movement-related information represented in the sensorimotor cortex is similar.

### IMPLICATION FOR NEUROPROSTHETICS

Our results have significant implications for the development of lingual neuroprostheses. Currently, individuals who experience total loss of tongue function or full glossectomy have few options for regaining tongue function (Dios et al., 1994). Mandibular and palatal protheses exist, but do not offer any active aid in speaking or swallowing (Marunick & Tselios, 2004). The finding that 3D tongue posture can be accurately decoded from the sensorimotor cortex opens up a new avenue for potential BCI-based protheses for restoring orolingual function and communication (Willett et al., 2021). As the field of soft-robotics continues to flourish (S. Kim et al., 2013), the reality of such a device becomes increasingly likely.

# CHAPTER 5 - CONCLUSIONS AND PROSPECTUS

In this final chapter, I will summarize the contents of Chapters 1-4, explore the broader implications of the results reported therein, and discuss future directions.

## SUMMARY

In Chapter 1, I provided background on the neuromechanics of the primate tongue, with particular focus on the role of the tongue during feeding. I described several outstanding questions that, with new methodological developments, we can address for the first time.

In Chapter 2, I tested whether DeepLabCut, a new deep learning package built for markerless tracking, could be applied to videoradiographic data to improve data processing throughput. I propose a novel workflow that integrates XMALab, the existing XROMM marker tracking software, and DeepLabCut while retaining each program's utility. XMALab is used for generating training datasets, error correction, and 3D reconstruction, whereas the majority of marker tracking is transferred to DeepLabCut for automatic batch processing. In the two case studies that involved an *in vivo* behavior, my workflow achieved a 6 to 13-fold increase in data throughput. In the third case study, which involved an acyclic, *post mortem* manipulation, DeepLabCut struggled to generalize to the range of novel poses and did not surpass the throughput of XMALab alone. Deployed in the proper context, this new workflow facilitates large scale XROMM studies that were previously precluded by software constraints.

In Chapter 3, I used XROMM to quantify 3D tongue-jaw kinematics and coordination during feeding in three rhesus macaques (*Macaca mulatta*). I leveraged the tongue's anatomically

separate tactile and proprioceptive pathways to temporarily block oral tactile sensation while preserving motor and proprioceptive signals. I found that in the absence of tactile sensation to the tongue and other oral structures, feeding performance decreased, and the fast open phase of the gape cycle became significantly longer, relative to the other phases. I measured the temporal coordination of jaw pitch with anterior tongue length, width, and roll, using event- and correlation-based metrics. The tongue made similar shapes in both the control and nerve block conditions, but the pattern of tongue-jaw coordination became significantly more variable after the block. My results suggest that feedback from lingual proprioceptors is sufficient for the formation of standard tongue shapes and the performance of feeding, but that tactile sensation underlies the tight patterns of tongue-jaw coordination that characterize the behavior.

In Chapter 4, I used the Kalman filter and LSTM to decode 3D tongue posture and movement from the activity of neurons in the primary sensorimotor cortex. I found that tongue translation, rotation, and deformation during feeding can be decoded with equal accuracy. Overall, tongue decoding performance was similar to that of decoded hand joint angles and angular velocities during a grasping task (Okorokova et al., 2020). Of all the cortical areas from which decoding was attempted, I found that rostral M1 yielded the best results, consistent with findings from studies of cortical control of the upper limb. Despite fairly dramatic anatomical differences between the tongue and the hand (namely the presence and absence of bones), a similar amount of motion-related information appears to be present in neural population activity in the sensorimotor cortex for both effectors.

# IMPLICATIONS

## IMPLICATIONS FOR XROMM

The impact of the integration of a deep learning software package with XMALab on the XROMM workflow is profound. Since the formal definition of XROMM by Brainerd et al. (2010), tens of XROMM studies have been published—most of which have fewer than 10 trials per individual. In some cases, a small sample size can be attributed to un-cooperative animals, but more commonly it is due to the marker tracking bottleneck. The likelihood of an average XROMM user independently employing the use of DeepLabCut or a related machine learning software to alleviate this bottleneck is vanishingly small, given that XROMM already involves learning several new programs, each with their own idiosyncrasies. Thus, I view the continued development of the pipeline presented here as essential to the growth of XROMM as a method that can be applied to more than just small kinematics datasets. That datasets like those presented in Manafzadeh et al. (2021) require hundreds of hours of marker tracking (tens of thousands of mouse clicks) is unsustainable and quite literally dangerous—see Carpal Tunnel Syndrome. My hope is that this workflow culminates, eventually, in the total dissolution of the marker tracking bottleneck and its constraint on XROMM studies.

## IMPLICATIONS FOR FEEDING BIOMECHANICS

Understanding the drivers of kinematic variation—or lack thereof—is core to biomechanics. It illuminates the ways in which organisms engage with the world around them, and the role of their anatomy in mediating that engagement. Importantly, the active modulation of muscle activity has a bidirectional influence on kinematic variation; it can drive consistent

kinematics in the face of changing external conditions, or it can induce variation if external conditions are less variable than the modulation (Ross, Dharia, et al., 2007; Ross, Eckhardt, et al., 2007). In Chapter 3, I demonstrated that loss of tactile feedback from the mouth during chewing resulted in greater inconsistencies in the temporal coordination of tongue and jaw movements, which was in turn correlated with impaired feeding performance. The instantaneous strength of the correlation of the tongue and jaw was not impacted (Fig. 3.10), leading to the characterization of the effect as 'differently correlated' rather than 'less correlated'. Following the recent goal-oriented definition of coordination by Ram & Ross (2019), since the change in kinematics was associated with impaired feeding performance the effect of the nerve block is a *decrease* in coordination. From these results, I conclude that oral tactile feedback is necessary for the consistent and adaptable temporal patterns of tongue and jaw kinematics that underlie coordination and, ultimately, feeding performance.

The finding that tactile sensory feedback enables consistent patterns of tongue-jaw coordination highlights an interesting point of comparison with limbed locomotion, another cyclic, coordinated behavior (Granatosky et al., 2019; Granatosky & Ross, 2020). In locomotion, muscle spindles and Golgi tendon organs constitute the principle sources of sensory feedback that drive modulation in muscle activity (Akay et al., 2014; Höhne et al., 2009); cutaneous, tactile sensation in the foot seems to be used solely for stationary balance and posture (Wang & Lin, 2008). The proprioceptive information that spindles and tendon organs convey allows for rapid adaption of the gait cycle to external perturbations (Daley & Biewener, 2006). Thus, the mechanosensory substrates that enable consistent patterns of coordination between musculoskeletal elements (jaw and tongue, or left and right leg), appear to be different between feeding and locomotion.

More broadly, the results of Chapter 3 further emphasize the central role of dexterous tongue movements in feeding; when their execution and coordination with the jaw becomes disrupted, feeding performance suffers.

### Implications for Pathological Loss of Sensation

Disruption of oral somatosensation by iatrogenic neuropathy[16] is unfortunately common (Agbaje et al., 2016; Tay & Zuniga, 2007). The lingual and inferior alveolar nerves are the most likely to be damaged, given their close proximity to the third molar (wisdom tooth). It is well documented in the clinical literature that such damage can result in 'difficulty' performing regular orofacial behaviors like eating and speaking (Coulthard et al., 2014). However, descriptions of the impact of oral sensory impairment rarely go beyond such qualitative statements, despite that fact that a quantitative understanding of the effects of oral trigeminal neuropathy is essential for the development of effective therapeutic approaches to its treatment. In Chapter 3, I demonstrated that a loss of oral sensation induces incoordination of the tongue and jaw via alterations to inter-structure temporal correlation. This is, to my knowledge, the first quantification of the kinematic basis for the impaired oral coordination after trigeminal somatosensory disruption. My hope is that continued effort toward uncovering the specific roles of the various modes of orofacial somatosensation will help to build a foundation from which clinical approaches to oral neuropathies can be advanced.

[16] Nerve damage by medical intervention.

### Implications for Restoration of Lingual Function

In the tragic scenario of a total glossectomy—usually a consequence of cancer (Biller et al., 1983)—patients have few therapeutic options for the restoration of normal speech and swallowing. There are two main types of prostheses, mandibular and palatal, both of which are entirely passive and depend on action of extra-lingual muscles (Marunick & Tselios, 2004). In most glossectomy cases, speech and swallowing can be preserved to some extent through a laryngoplasty, but they rarely return to normal. Moreover, over a million people in the United States have a neuromuscular impairment that results in a serious verbal communication deficit (Chakrabarti et al., 2015). My hope is that the results of Chapter 4—successful decoding of 3D tongue posture and movement from cortical population activity—represents an early stage of a potential brain-computer interface revolution similar to that which has taken place with the arm and hand.

## Future Directions

### XROMM-DLC Pipeline

The integrated data processing pipeline I describe in Chapter 2 enables an enormous increase in XROMM throughput, but it is not without its limits. The pipeline in its current form performs well specifically when the behavior at hand is cyclic and experimentally constrained. When the animal is able to rotate substantially within the capture volume, DeepLabCut struggles to accurately identify specific markers. Moreover, DeepLabCut appears to identify the approximate region the marker is in, rather than the exact centroid of the marker itself. Additionally, unrelated to tracking accuracy, the workflow is simply difficult to learn—there are

many intermediate steps as data is transferred in between XMALab and DeepLabCut. Thus, I see four potential improvements that, if implemented, would greatly elevate the performance and useability of my pipeline. Notably, versions of these suggested improvements already exist in independently developed software packages, and in some cases those packages were written specifically to augment DeepLabCut.

1. *Seamless integration with XMALab*

   XMALab files are ZIP files that contain folders of CSVs. Data in the form of 2D and 3D point positions are trivial to extract once the general structure of the file is known. In an ideal scenario, a user would never have to manually export data from XMALab for conversion and import to DeepLabCut. If the programs 'talked to each other' via functions that read from and write to XMALab files directly, the pipeline could be substantially simplified.

2. *Leverage XMALab's marker centroid detection algorithm*

   XMALab has an exceptionally good marker centroid detection algorithm, designed specifically for marker-based XROMM. Currently, my pipeline only uses this tracking feature in the initial generation of a training dataset and in the final correction stage. Ideally, after initial prediction by DeepLabCut, XMALab's algorithm would be called to detect the marker centroid to refine the prediction. This would likely reduce the marker 'drift' and offset that sometimes occurs when DeepLabCut thinks a marker is in a specific area but cannot find it exactly. This improvement has been recently proposed by Philip Lai of Harvard University (unpublished).

3. *Integrate 3D camera calibration into marker prediction*

   Currently, DeepLabCut does not consider reprojection error or rigid body error when making its predictions. A recently released package that works on top of DeepLabCut, Anipose (Karashchuk et al., 2020), adds this functionality by providing a series of additional functions that enable 3D camera calibration and the filtering of predicted points based on various 3D metrics. While I see this as a great step, once again, it adds complexity to an already involved workflow. XMALab already has a robust toolkit of 3D error quantification metrics that could be integrated with the tracking process algorithm. Ideally, this would occur completely under the hood, with no additional user effort.

4. *Integrate marker position and velocity through time into prediction*

   In additional to 3D camera calibration, XMALab also uses a marker's velocity and position to refine predictions in subsequent frames. Currently, DeepLabCut evaluates frames in temporal isolation, sacrificing a large of amount of spatiotemporal data. The recently released Deep Graph Pose (Wu et al., 2020), an add-on to DeepLabCut, recognizes the importance of a landmark's spatiotemporal context and endeavors to add this functionality. And once again, I believe that an ideal implantation of this feature would involve no additional effort for the user.

## QUANTIFYING TONGUE POSTURE AND MOTION

The extent to which tongue deformation and tongue movement are related is an open question. I expect that the relative contribution of those two parameters to a given tongue posture depends on the posture in question, which itself can be broken down into the activity of the specific tongue muscles, as well as the relative position of the mandible and hyoid. In mathematic terms:

$$(Any\ Tongue\ Posture) = Deformation + Movement$$

$$= Activation_{Intrinsic\ Mm.} \times Activation_{Extrinsic\ Mm.} \times Position_{Hyoid} \times Position_{Mandible}$$

With the methods I have established for quantifying the pseudo-rigid body motion of the tongue, a next step would be to measure the correlations of those degrees of freedom with the deformation variables during different tongue behaviors. For example, I would predict that tongue protrusion is the result of both anterior translation of the tongue and anterior and middle lengthening. However, given the inherent non-linearity of tongue deformation, the existence of simple relationships between tongue shape change and overall postural change seems unlikely. Establishing clear definitions of tongue motions and clarifying the role of deformation and translation/rotation in those motions is essential—especially as more and more 3D tongue kinematics data are collected.

### ELECTROMYOGRAPHY

A missing piece of the puzzle presented in this dissertation is muscle activity; perhaps the most logical next step for both Chapters 3 and 4 is the addition of electromyography (EMG) to elucidate the role of individual muscles in generating the range of tongue motions and deformations that are documented therein. For all the individuals in this dissertation, EMG data were collected along with the XROMM data. However, *post mortem* investigation of the location of the electrodes suggested that the majority of the tongue muscle electrodes had migrated away from their intended location. I expect that this is due to a combination of the large range of motion of the tongue and the difficulty in securing (i.e., suturing) the electrodes into specific muscles. If quality EMG data are to be collected from the full array of macaque lingual muscles, it would most

likely need to occur immediately after the EMG implantation to reduce the risk of electrode migration and loss. A complete XROMM + EMG dataset from the majority of lingual muscles (especially the intrinsic muscles) would be immensely useful for addressing a range of biomechanical questions about the neuromechanics of the tongue during feeding.

### Untangling Oral Proprioception

*In vivo* studies of the role of proprioceptive feedback from jaw muscle spindles abound (Komuro et al., 2001; J. P. Lund et al., 1979; Mameli et al., 2009; Scutter & Türker, 1999; A. Tsuboi et al., 2003). Virtually none exist for the muscle spindles of the tongue; our knowledge of the contribution of muscle spindles to tongue kinematics during feeding is purely theoretical. Ideally, an identical study to that detailed in Chapter 3 would be performed, except with a tongue muscle spindle knockout (specifically Ia afferent knockout, *sensu* Akay et al., 2014) in the place of a tactile nerve block. As of now, such methods do not exist for non-human primates.

## Conclusion

The ubiquity of neuromuscular disorders that impact the tongue and jaw demands a deeper understanding of orofacial neuromechanics than has been achieved thus far. Fortunately, with innovative tools like XROMM and DeepLabCut in our arsenal, many of those questions, previously fodder for speculation, are now tractable. This is an exciting moment for mammalian feeding neuromechanics, and I feel grateful and humbled to have played a small part in it.

# REFERENCES


Abbruzzese, G., & Berardelli, A. (2003). Sensorimotor integration in movement disorders. *Mov Disord.*, *18*(3), 231–240. https://doi.org/10.1002/mds.10327

Abd-El-Malek, S. (1955). The part played by the tongue in mastication and deglutition. *Journal of Anatomy*, *89*(2), 250–254. http://www.ncbi.nlm.nih.gov/pubmed/14367222%0Ahttp://www.pubmedcentral.nih.gov/articlerender.fcgi?artid=PMC1244789

Adachi, K., Lee, J.-C., Hu, J. W., Yao, D., & Sessle, B. J. (2007). Motor cortex neuroplasticity associated with lingual nerve injury in rats. *Somatosensory & Motor Research*, *24*(3), 97–109.

Agbaje, J. O., Van de Casteele, E., Hiel, M., Verbaanderd, C., Lambrichts, I., & Politis, C. (2016). Neuropathy of Trigeminal Nerve Branches After Oral and Maxillofacial Treatment. *Journal of Maxillofacial and Oral Surgery*, *15*(3), 321–327. https://doi.org/10.1007/s12663-015-0843-9

Akay, T., Tourtellotte, W. G., Arber, S., & Jessell, T. M. (2014). Degradation of mouse locomotor pattern in the absence of proprioceptive sensory feedback. *Proceedings of the National Academy of Sciences*, *111*(47), 16877–16882. https://doi.org/10.1073/pnas.1419045111

Appenteng, K., Donga, R., & Williams, R. G. (1985). Morphological and electrophysiological determination of the projections of jaw-elevator muscle spindle afferents in rats. *The Journal of Physiology*, *369*(1), 93–113.

Arce-McShane, F. I. (2021). The association between age-related changes in oral neuromechanics and Alzheimer's disease. *Advances in Geriatric Medicine and Research*, *3*(2).

Arce-McShane, F. I., Hatsopoulos, N. G., Lee, J.-C., Ross, C. F., & Sessle, B. J. (2014). Modulation Dynamics in the Orofacial Sensorimotor Cortex during Motor Skill Acquisition. *The Journal of Neuroscience : The Official Journal of the Society for Neuroscience*, *34*(17), 5985–5997. https://doi.org/10.1523/JNEUROSCI.4367-13.2014

Arce-McShane, F. I., Lee, J.-C., Ross, C. F., Sessle, B. J., & Hatsopoulos, N. G. (2013). Directional information from neuronal ensembles in the primate orofacial sensorimotor cortex. *Journal of Neurophysiology*, *110*(6), 1357–1369. https://doi.org/10.1152/jn.00144.2013

Arce-McShane, F. I., Ross, C. F., Takahashi, K., Sessle, B. J., & Hatsopoulos, N. G. (2016). Primary motor and sensory cortical areas communicate via spatiotemporally coordinated networks at multiple frequencies. *Proceedings of the National Academy of Sciences*, *113*(18), 5083–5088. https://doi.org/10.1073/pnas.1600788113

Ashe, J., & Georgopoulos, A. P. (1994). Movement parameters and neural activity in motor cortex and area 5. *Cerebral Cortex, 4*(6), 590–600. https://doi.org/10.1093/cercor/4.6.590

Augurelle, A. S., Smith, A. M., Lejeune, T., & Thonnard, J. L. (2003). Importance of cutaneous feedback in maintaining a secure grip during manipulation of hand-held objects. *Journal of Neurophysiology*, *89*(2), 665–671. https://doi.org/10.1152/jn.00249.2002

Avivi-Arber, L., & Sessle, B. J. (2018). Jaw sensorimotor control in healthy adults and effects of ageing. *Journal of Oral Rehabilitation*, *45*(1), 50–80. https://doi.org/10.1111/joor.12554

Badin, P., Tarabalka, Y., Elisei, F., & Bailly, G. (2010). Can you "read" tongue movements? Evaluation of the contribution of tongue display to speech understanding. *Speech Communication*, *52*(6), 493–503. https://doi.org/10.1016/j.specom.2010.03.002

Bailey, E. F., Huang, Y. H., & Fregosi, R. F. (2006). Anatomic consequences of intrinsic tongue muscle activation. *Journal of Applied Physiology*, *101*(5), 1377–1385. https://doi.org/10.1152/japplphysiol.00379.2006

Bhullar, B. A. S., Manafzadeh, A. R., Miyamae, J. A., Hoffman, E. A., Brainerd, E. L., Musinsky, C., & Crompton, A. W. (2019). Rolling of the jaw is essential for mammalian chewing and tribosphenic molar function. *Nature*, *566*(7745), 528–532. https://doi.org/10.1038/s41586-019-0940-x

Biedenbach, M. A., & Chan, K. Y. (1971). Tongue mechanoreceptors: comparison of afferent fibers in the lingual nerve and chorda tympani. *Brain Research*, *35*(2), 584–588. https://doi.org/10.1016/0006-8993(71)90507-5

Biller, H. F., Lawson, W., & Baek, S. M. (1983). Total Glossectomy: A Technique of Reconstruction Eliminating Laryngectomy. *Archives of Otolaryngology*, *109*(2), 69–73. https://doi.org/10.1001/archotol.1983.00800160003001

Bollu, T., Ito, B. S., Whitehead, S. C., Kardon, B., Redd, J., Liu, M. H., & Goldberg, J. H. (2021). Cortex-dependent corrections as the tongue reaches for and misses targets. *Nature*. https://doi.org/10.1038/s41586-021-03561-9

Bowman, J. P. (1968). Muscle spindles in the intrinsic and extrinsic muscles of the rhesus monkey's (Macaca mulatta) tongue. *The Anatomical Record*, *161*(5), 483–487. https://doi.org/10.1002/ar.1091610410

Brainerd, E. L., Baier, D. B., Gatesy, S. M., Hedrick, T. L., Metzger, K. A., Gilbert, S. L., & Crisco, J. J. (2010). X-ray reconstruction of moving morphology (XROMM): precision, accuracy and applications in comparative biomechanics research. *Journal of Experimental Zoology. Part A, Ecological Genetics and Physiology*, *313*(5), 262–279. https://doi.org/10.1002/jez.589

Brannon, R. M. (2018). Rotation, Reflection, and Frame Changes. In *Orthogonal tensors in computational engineering mechanics*. IOP Publishing. https://doi.org/10.1088/978-0-7503-1454-1

Bremer, F. (1923). Physiologie nerveuse de la mastication chez le chat et le lapin. Reflexes de

mastication. Reponses masticatrices corticales et centre cortical du gout. *Archives Internationales de Physiologie*, *21*, 308–358.

Brust, C. A., Käding, C., & Denzler, J. (2019). Active learning for deep object detection. *Proceedings of the 14th International Joint Conference on Computer Vision, Imaging and Computer Graphics Theory and Applications*. https://doi.org/10.5220/0007248601810190

Carmena, J. M., Lebedev, M. A., Crist, R. E., O'Doherty, J. E., Santucci, D. M., Dimitrov, D. F., Patil, P. G., Henriquez, C. S., & Nicolelis, M. A. L. (2003). Learning to control a brain-machine interface for reaching and grasping by primates. *PLoS Biology*, *1*(2), e42. https://doi.org/10.1371/journal.pbio.0000042

Chakrabarti, S., Sandberg, H. M., Brumberg, J. S., & Krusienski, D. J. (2015). Progress in speech decoding from the electrocorticogram. *Biomedical Engineering Letters*, *5*(1), 10–21.

Cheng, S., Butler, J. E., Gandevia, S. C., & Bilston, L. E. (2008). Movement of the tongue during normal breathing in awake healthy humans. *Journal of Physiology*, *586*(17), 4283–4294. https://doi.org/10.1113/jphysiol.2008.156430

Collinger, J. L., Wodlinger, B., Downey, J. E., Wang, W., Tyler-Kabara, E. C., Weber, D. J., McMorland, A. J. C. C., Velliste, M., Boninger, M. L., & Schwartz, A. B. (2013). High-performance neuroprosthetic control by an individual with tetraplegia. *The Lancet*, *381*(9866), 557–564. https://doi.org/10.1016/S0140-6736(12)61816-9

Coulthard, P., Kushnerev, E., Yates, J. M., Walsh, T., Patel, N., Bailey, E., & Renton, T. F. (2014). Interventions for iatrogenic inferior alveolar and lingual nerve injury. *Cochrane Database of Systematic Reviews*, *2014*(4). https://doi.org/10.1002/14651858.CD005293.pub2

Daley, M. A., & Biewener, A. A. (2006). Running over rough terrain reveals limb control for intrinsic stability. *Proceedings of the National Academy of Sciences*, *103*(42), 15681–15686. https://doi.org/10.1073/pnas.0601473103

Davidson, L. (2006). Comparing tongue shapes from ultrasound imaging using smoothing spline analysis of variance. *The Journal of the Acoustical Society of America*, *120*(1), 407–415. https://doi.org/10.1121/1.2205133

Dios, P. D., Feijoo, J. F., Ferreiro, M. C., & Alvarez, J. A. (1994). Functional consequences of partial glossectomy. *Journal of Oral and Maxillofacial Surgery*, *52*(1), 12–14. https://doi.org/10.1016/0278-2391(94)90005-1

Ebied, A. M., Kemp, G. J., & Frostick, S. P. (2004). The role of cutaneous sensation in the motor function of the hand. *Journal of Orthopaedic Research*, *22*, 862–866.

Feilich, K., Laurence-Chasen, J. D., Orsbon, C. P., Gidmark, N. J., & Ross, C. F. (2021). Twist and chew: three dimensional tongue kinematics during chewing in macaque primates. *Biology Letters (Submitted)*.

Feix, T., Romero, J., Schmiedmayer, H.-B., Dollar, A. M., & Kragic, D. (2015). The grasp taxonomy of human grasp types. *IEEE Transactions on Human-Machine Systems*, *46*(1),

66–77.

Fitzgerald, M. J., & Sachithanandan, S. R. (1979). The structure and source of lingual proprioceptors in the monkey. *Journal of Anatomy*, *128*(Pt 3), 523–552. http://www.pubmedcentral.nih.gov/articlerender.fcgi?artid=1232905&tool=pmcentrez&rendertype=abstract

Franks, H. A., Crompton, A. W., & German, R. Z. (1984). Mechanism of intraoral transport in macaques. *American Journal of Physical Anthropology*, *65*(3), 275–282. https://doi.org/10.1002/ajpa.1330650307

Georgopoulos, A. P., Kalaska, J. F., Caminiti, R., & Massey, J. T. (1982). On the relations between the direction of two-dimensional arm movements and cell discharge in primate motor cortex. *Journal of Neuroscience*, *2*(11), 1527–1537. https://doi.org/10.1523/jneurosci.02-11-01527.1982

German, R. Z., Crompton, A. W., Levitch, L. C., & Thexton, A. J. (1992). The mechanism of suckling in two species of infant mammal: Miniature pigs and long-tailed macaques. *Journal of Experimental Zoology*, *261*(3), 322–330. https://doi.org/10.1002/jez.1402610311

Gintof, C., Konow, N., Ross, C. F., & Sanford, C. P. J. (2010). Rhythmic chewing with oral jaws in teleost fishes: a comparison with amniotes. *Journal of Experimental Biology*, *213*(11), 1868–1875. https://doi.org/10.1242/jeb.041012

Glaser, J. I., Chowdhury, R. H., Perich, M. G., Miller, L. E., & Kording, K. P. (2020). Machine learning for neural decoding. *ArXiv*, *7*(August).

Goldberg, L. J., Chandler, S. H., & Tal, M. (1982). Relationship between jaw movements and trigeminal motoneuron membrane-potential fluctuations during cortically induced rhythmical jaw movements in the guinea pig. *Journal of Neurophysiology*, *48*(1), 110–125. https://doi.org/10.1152/jn.1982.48.1.110

Granatosky, M. C., McElroy, E. J., Laird, M. F., Iriarte-Diaz, J., Reilly, S. M., Taylor, A. B., & Ross, C. F. (2019). Joint angular excursions during cyclical behaviors differ between tetrapod feeding and locomotor systems. *Journal of Experimental Biology*, *222*(9). https://doi.org/10.1242/jeb.200451

Granatosky, M. C., & Ross, C. F. (2020). Differences in muscle mechanics underlie divergent optimality criteria between feeding and locomotor systems. *Journal of Anatomy*, *237*(6), 1072–1086.

Granit, R. (1975). The functional role of the muscle spindles--facts and hypotheses. *Brain: A Journal of Neurology*, *98*(4), 531–556.

Graving, J. M., Chae, D., Naik, H., Li, L., Koger, B., Costelloe, B. R., & Couzin, I. D. (2019). DeepPoseKit, a software toolkit for fast and robust animal pose estimation using deep learning. *ELife*. https://doi.org/10.7554/elife.47994

Green, H. D., & Walker, A. E. (1938). The Effects of Ablation of the Cortical Motor Face Area in Monkeys. *Journal of Neurophysiology*, *1*(3), 262–280.

https://doi.org/10.1152/jn.1938.1.3.262

Grood, E. S., & Suntay, W. J. (1983). A joint coordinate system for the clinical description of three-dimensional motions: Application to the knee. *Journal of Biomechanical Engineering*, *105*(2), 136–144. https://doi.org/10.1115/1.3138397

Haggard, P., & de Boer, L. (2014). Oral somatosensory awareness. *Neuroscience and Biobehavioral Reviews*, *47*, 469–484. https://doi.org/10.1016/j.neubiorev.2014.09.015

Hatanaka, N., Tokuno, H., Nambu, A., Inoue, T., & Takada, M. (2005). Input-output organization of jaw movement-related areas in monkey frontal cortex. *Journal of Comparative Neurology*, *492*(4), 401–425. https://doi.org/10.1002/cne.20730

Hatsopoulos, N. G. (1996). Coupling the neural and physical dynamics in rhythmic movements. *Neural Computation*, *8*(3), 567–581. https://doi.org/10.1162/neco.1996.8.3.567

Hatsopoulos, N. G., Joshi, J., & O'Leary, J. G. (2004). Decoding continuous and discrete motor behaviors using motor and premotor cortical ensembles. *Journal of Neurophysiology*, *92*(2), 1165–1174. https://doi.org/10.1152/jn.01245.2003

Hatsopoulos, N. G., Xu, Q., & Amit, Y. (2007). Encoding of Movement Fragments in the Motor Cortex. *Journal of Neuroscience*, *27*(19), 5105–5114. https://doi.org/10.1523/jneurosci.3570-06.2007

Hedrick, T. L. (2008). Software techniques for two- and three-dimensional kinematic measurements of biological and biomimetic systems. *Bioinspiration and Biomimetics*, *3*(3), 1–6. https://doi.org/10.1088/1748-3182/3/3/034001

Hidaka, O., Morimoto, T., Kato, T., Masuda, Y., Inoue, T., & Takada, K. (1999). Behavior of jaw muscle spindle afferents during cortically induced rhythmic jaw movements in the anesthetized rabbit. *Journal of Neurophysiology*, *82*(5), 2633–2640.

Hiiemae, K. M., & Crompton, A. W. (1985). Mastication, food transport, and swallowing. *Functional Vertebrate Morphology*, 262–290.

Hiiemae, K. M., Hayenga, S. M., & Reese, A. (1995). Patterns of tongue and jaw movement in a cinefluorographic study of feeding in the macaque. *Archives of Oral Biology*, *40*(3), 229–246. https://doi.org/10.1016/0003-9969(95)98812-D

Hiiemae, K. M., & Palmer, J. B. (2001). Tongue-jaw linkages—mechanisms of feeding revisited. *Bull Mus Comp Zool*, *155*, 697–709.

Hiiemae, K. M., & Palmer, J. B. (2003). Tongue movements in Feeding and Speech. *Crit Rev Oral Biol Med*, *14*(6), 413–429. https://doi.org/10.1177/154411130301400604

Hochberg, L. R., Bacher, D., Jarosiewicz, B., Masse, N. Y., Simeral, J. D., Vogel, J., Haddadin, S., Liu, J., Cash, S. S., & Van Der Smagt, P. (2012). Reach and grasp by people with tetraplegia using a neurally controlled robotic arm. *Nature*, *485*(7398), 372–375.

Hochberg, L. R., Serruya, M. D., Friehs, G. M., Mukand, J. A., Saleh, M., Caplan, A. H.,

Branner, A., Chen, D., Penn, R. D., & Donoghue, J. P. (2006). Neuronal ensemble control of prosthetic devices by a human with tetraplegia. *Nature*, *442*(7099), 164–171. https://doi.org/10.1038/nature04970

Hochreiter, S., & Schmidhuber, J. (1997). Long short-term memory. *Neural Computation*, *9*(8), 1735–1780.

Hohne, A., Ali, S., Stark, C., & Bruggemann, G. P. (2012). Reduced plantar cutaneous sensation modifies gait dynamics, lower-limb kinematics and muscle activity during walking. *European Journal of Applied Physiology*, *112*(11), 3829–3838. https://doi.org/10.1007/s00421-012-2364-2

Höhne, A., Stark, C., & Brüggemann, G.-P. (2009). Plantar pressure distribution in gait is not affected by targeted reduced plantar cutaneous sensation. *Clinical Biomechanics*, *24*(3), 308–313.

Huang, C. S., Hiraba, H., Murray, G. M., & Sessle, B. J. (1989). Topographical distribution and functional properties of cortically induced rhythmical jaw movements in the monkey (*Macaca fascicularis*). *Journal of Neurophysiology*, *61*(3), 635–650.

Huckabee, M. L., McIntosh, T., Fuller, L., Curry, M., Thomas, P., Walshe, M., McCague, E., Battel, I., Nogueira, D., Frank, U., van den Engel-Hoek, L., & Sella-Weiss, O. (2018). The Test of Masticating and Swallowing Solids (TOMASS): reliability, validity and international normative data. *International Journal of Language and Communication Disorders*, *53*(1), 144–156. https://doi.org/10.1111/1460-6984.12332

Inoue, T., Kato, T., Masuda, Y., Nakamura, T., Kawamura, Y., & Morimoto, T. (1989). Modifications of masticatory behavior after trigeminal deafferentation in the rabbit. *Experimental Brain Research*, *74*(3), 579–591. https://doi.org/10.1007/BF00247360

Insafutdinov, E., Pishchulin, L., Andres, B., Andriluka, M., & Schiele, B. (2016). Deepercut: A deeper, stronger, and faster multi-person pose estimation model. *ECCV*. https://doi.org/10.1007/978-3-319-46466-4_3

Iriarte-Díaz, J., Reed, D. A., & Ross, C. F. (2011). Sources of variance in temporal and spatial aspects of jaw kinematics in two species of primates feeding on foods of different properties. *Integrative and Comparative Biology*, *51*(2), 307–319. https://doi.org/10.1093/icb/icr072

Jacobs, R., Wu, C. H., Goossens, K., Van Loven, K., Van Hees, J., & Van Steenberghe, D. (2002). Oral mucosal versus cutaneous sensory testing: A review of the literature. *Journal of Oral Rehabilitation*, *29*(10), 923–950. https://doi.org/10.1046/j.1365-2842.2002.00960.x

Johansson, R. S., & Vallbo, A. B. (1979). Tactile sensibility in the human hand: relative and absolute densities of four types of mechanoreceptive units in glabrous skin. *The Journal of Physiology*, *286*(1), 283–300.

Kaas, J. H. (2013). The evolution of brains from early mammals to humans. *Wiley Interdisciplinary Reviews: Cognitive Science*, *4*(1), 33–45. https://doi.org/10.1002/wcs.1206

Kambic, R. E., Roberts, T. J., & Gatesy, S. M. (2017). 3-D range of motion envelopes reveal interacting degrees of freedom in avian hind limb joints. *Journal of Anatomy*, *231*, 906–920. https://doi.org/10.1111/joa.12680

Karashchuk, P., Rupp, K., Dickinson, E., Sanders, E., Azim, E., Brunton, B., & Tuthill, J. (2020). Anipose: a toolkit for robust markerless 3D pose estimation. *BioRxiv*. https://doi.org/10.1101/2020.05.26.117325

Kawai, R., Markman, T., Poddar, R., Ko, R., Fantana, A. L., Dhawale, A. K., Kampff, A. R., & Ölveczky, B. P. (2015). Motor cortex is required for learning but not for executing a motor skill. *Neuron*, *86*(3), 800–812.

Kier, W. M., & Smith, K. K. (1985). Tongues, tentacles and trunks: the biomechanics of movement in muscular-hydrostats. *Zoological Journal of the Linnean Society*, *83*(4), 307–324. https://doi.org/10.1111/j.1096-3642.1985.tb01178.x

Kim, H. D., Choi, J. B., Yoo, S. J., Chang, M. Y., Lee, S. W., & Park, J. S. (2017). Tongue-to-palate resistance training improves tongue strength and oropharyngeal swallowing function in subacute stroke survivors with dysphagia. *Journal of Oral Rehabilitation*, *44*(1), 59–64. https://doi.org/10.1111/joor.12461

Kim, S., Laschi, C., & Trimmer, B. (2013). Soft robotics: A bioinspired evolution in robotics. *Trends in Biotechnology*, *31*(5), 287–294. https://doi.org/10.1016/j.tibtech.2013.03.002

Knörlein, B. J., Baier, D. B., Gatesy, S. M., Laurence-Chasen, J. D., & Brainerd, E. L. (2016). Validation of XMALab software for marker-based XROMM. *The Journal of Experimental Biology*, *219*(23), 3701–3711. https://doi.org/10.1242/jeb.145383

Komuro, A., Morimoto, T., Iwata, K., Inoue, T., Masuda, Y., Kato, T., & Hidaka, O. (2001). Putative feed-forward control of jaw-closing muscle activity during rhythmic jaw movements in the anesthetized rabbit. *Journal of Neurophysiology*, *86*(6), 2834–2844. https://doi.org/10.1152/jn.2001.86.6.2834

Kubota, K., Negishi, T., & Masegi, T. (1975). Topological distribution of muscle spindles in the human tongue and its significance in proprioception. *The Bulletin of Tokyo Medical and Dental University*, *22*(3), 235–242. http://europepmc.org/abstract/MED/132308

Labuguen, R., Bardeloza, D. K., Negrete, S. B., Matsumoto, J., Inoue, K., & Shibata, T. (2019). *Primate Markerless Pose Estimation and Movement Analysis Using DeepLabCut*. https://doi.org/10.1109/iciev.2019.8858533

Larson, C. R., Byrd, K. E., Garthwaite, C. R., & Luschei, E. S. (1980). Alterations in the pattern of mastication after ablations of the lateral precentral cortex in rhesus macaques. *Experimental Neurology*, *70*(3), 638–651. https://doi.org/10.1016/0014-4886(80)90189-2

Laurence-Chasen, J. D., Manafzadeh, A. R., Hatsopoulos, N. G., Ross, C. F., & Arce-McShane, F. F. I. (2020). Integrating XMALab and DeepLabCut for high-throughput XROMM. *The Journal of Experimental Biology*, *223*(17), jeb226720. https://doi.org/10.1242/jeb.226720

Liu, S., Iriarte-Diaz, J., Hatsopoulos, N. G., Ross, C. F., Takahashi, K., & Chen, Z. (2019).

Dynamics of motor cortical activity during naturalistic feeding behavior. *Journal of Neural Engineering*, *16*(2), 026038. https://doi.org/10.1088/1741-2552/ab0474

Liu, Z. J., Shcherbatyy, V., Kayalioglu, M., & Seifi, A. (2009). Internal kinematics of the tongue in relation to muscle activity and jaw movement in the pig. *Journal of Oral Rehabilitation*, *36*(9), 660–674. https://doi.org/10.1111/j.1365-2842.2009.01981.x

Lowe, A. A. (1980). The neural regulation of tongue movements. *Progress in Neurobiology*, *15*(4), 295–344. https://doi.org/10.1016/0301-0082(80)90008-8

Lucas, P. W., Prinz, J. F., Agrawal, K. R., & Bruce, I. C. (2002). Food physics and oral physiology. In *Food Quality and Preference*. https://doi.org/10.1016/S0950-3293(00)00036-7

Lund, J. P., Smith, A. M., Sessle, B. J., & Murakami, T. (1979). Activity of trigeminal α- and γ-motoneurons and muscle afferents during performance of a biting task. *Journal of Neurophysiology*, *42*(3), 710–725. https://doi.org/10.1152/jn.1979.42.3.710

Lund, James P. (1991). Mastication and its Control by the Brain Stem. *Critical Reviews in Oral Biology & Medicine*, *2*(1), 33–64. https://doi.org/10.1177/10454411910020010401

Lund, James P., & Kolta, A. (2006). Generation of the central masticatory pattern and its modification by sensory feedback. *Dysphagia*, *21*(3), 167–174. https://doi.org/10.1007/s00455-006-9027-6

Lund, James P., Sasamoto, K., Murakami, T., & Olsson, K. A. (1984). Analysis of rhythmical jaw movements produced by electrical stimulation of motor-sensory cortex of rabbits. *Journal of Neurophysiology*, *52*(6), 1014. http://www.ncbi.nlm.nih.gov/pubmed/6520627%5Cnhttp://jn.physiology.org/content/52/6/1014.abstract

Macefield, V. G. (2021). The roles of mechanoreceptors in muscle and skin in human proprioception. *Current Opinion in Physiology*, *21*, 48–56. https://doi.org/10.1016/j.cophys.2021.03.003

Mameli, O., Stanzani, S., Russo, A., Pellitteri, R., Spatuzza, M., Caria, M. A., Mulliri, G., & De Riu, P. L. (2009). Hypoglossal nucleus projections to the rat masseter muscle. *Brain Research*, *1283*, 34–40. https://doi.org/10.1016/j.brainres.2009.06.004

Manafzadeh, A. R., Kambic, R. E., & Gatesy, S. M. (2021). A new role for joint mobility in reconstructing vertebrate locomotor evolution. *Proceedings of the National Academy of Sciences*, *118*(7). https://doi.org/10.1073/pnas.2023513118

Manafzadeh, A. R., & Padian, K. (2018). ROM mapping of ligamentous constraints on avian hip mobility: implications for extinct ornithodirans. *Proc. R. Soc. B*, *285*(1879).

Marder, E., & Bucher, D. (2001). Central pattern generators and the control of rythmic movements. *Current Biology*, *11*, R986–R996. https://doi.org/10.1016/S0960-9822(01)00581-4

Martinez, C. M., McGee, M. D., Borstein, S. R., & Wainwright, P. C. (2018). Feeding ecology underlies the evolution of cichlid jaw mobility. *Evolution*, *72*(8), 1645–1655. https://doi.org/10.1111/evo.13518

Marunick, M., & Tselios, N. (2004). The efficacy of palatal augmentation prostheses for speech and swallowing in patients undergoing glossectomy: A review of the literature. *Journal of Prosthetic Dentistry*, *91*(1), 67–74. https://doi.org/10.1016/j.prosdent.2003.10.012

Mathis, A., Mamidanna, P., Cury, K. M., Abe, T., Murthy, V. N., Mathis, M. W., & Bethge, M. (2018). DeepLabCut: markerless pose estimation of user-defined body parts with deep learning. *Nature Neuroscience*, *21*(9), 1281–1289. https://doi.org/10.1038/s41593-018-0209-y

Mathis, M. W., & Mathis, A. (2019). *Deep learning tools for the measurement of animal behavior in neuroscience*. *60*(60), 1–11. http://arxiv.org/abs/1909.13868

Mayerl, C. J., Myrla, A. M., Gould, F. D. H., Bond, L. E., Stricklen, B. M., & German, R. Z. (2021). Swallow safety is determined by bolus volume during infant feeding in an animal model. *Dysphagia*, *36*(1), 120–129. https://doi.org/10.1007/s00455-020-10118-x

McKinstry, R. E., Aramany, M. A., Beery, Q. C., & Sansone, F. (1985). Speech considerations in prosthodontic rehabilitation of the glossectomy patient. *The Journal of Prosthetic Dentistry*, *53*(3), 384–387. https://doi.org/10.1016/0022-3913(85)90518-9

Ménard, L., Aubin, J., Thibeault, M., & Richard, G. (2012). Measuring tongue shapes and positions with ultrasound imaging: A validation experiment using an articulatory model. *Folia Phoniatrica et Logopaedica*, *64*(2), 64–72. https://doi.org/10.1159/000331997

Menegaz, R. A., Baier, D. B., Metzger, K. A., Herring, S. W., & Brainerd, E. L. (2015). XROMM analysis of tooth occlusion and temporomandibular joint kinematics during feeding in juvenile miniature pigs. *Journal of Experimental Biology*, *218*(16), 2573–2584. https://doi.org/10.1242/jeb.119438

Miall, R. C., Rosenthal, O., Ørstavik, K., Cole, J. D., & Sarlegna, F. R. (2019). Loss of haptic feedback impairs control of hand posture: a study in chronically deafferented individuals when grasping and lifting objects. *Experimental Brain Research*, *237*(9), 2167–2184. https://doi.org/10.1007/s00221-019-05583-2

Mioche, L., Hiiemae, K. M., & Palmer, J. B. (2002). A postero-anterior videofluorographic study of the intra-oral management of food in man. *Archives of Oral Biology*, *47*(4), 267–280. https://doi.org/10.1016/S0003-9969(02)00007-9

Molina-Luna, K., Pekanovic, A., Röhrich, S., Hertler, B., Schubring-Giese, M., Rioult-Pedotti, M. S., & Luft, A. R. (2009). Dopamine in motor cortex is necessary for skill learning and synaptic plasticity. *PLoS ONE*, *4*(9). https://doi.org/10.1371/journal.pone.0007082

Montuelle, S. J., Olson, R. A., Curtis, H., Beery, S., & Williams, S. H. (2020). Effects of food properties on chewing in pigs: Flexibility and stereotypy of jaw movements in a mammalian omnivore. *PLoS ONE*, *15*(2), 1–20. https://doi.org/10.1371/journal.pone.0228619

Montuelle, S. J., Olson, R. A., Curtis, H., Sidote, J. A. V., & Williams, S. H. (2019). The effect of unilateral lingual nerve injury on the kinematics of mastication in pigs. *Archives of Oral Biology*, *98*, 226–237. https://doi.org/10.1016/j.archoralbio.2018.11.024

Montuelle, S. J., Olson, R. A., Curtis, H., & Williams, S. H. (2020). Unilateral lingual nerve transection alters jaw-tongue coordination during mastication in pigs. *Journal of Applied Physiology*, *128*(4), 941–951. https://doi.org/10.1152/JAPPLPHYSIOL.00398.2019

Morimoto, T., Inoue, T., Nakamura, T., & Kawamura, Y. (1985). Characteristics of rhythmic jaw movements of the rabbit. *Archives of Oral Biology*, *30*(9), 673–677. https://doi.org/10.1016/0003-9969(85)90154-2

Morquette, P., Lavoie, R., Fhima, M. D., Lamoureux, X., Verdier, D., & Kolta, A. (2012). Generation of the masticatory central pattern and its modulation by sensory feedback. *Progress in Neurobiology*, *96*(3), 340–355. https://doi.org/10.1016/j.pneurobio.2012.01.011

Murray, G. M., & Sessle, B. J. (1992a). Functional properties of single neurons in the face primary motor cortex of the primate. II. Relations with trained orofacial motor behavior. *Journal of Neurophysiology*, *67*(3), 759–774.

Murray, G. M., & Sessle, B. J. (1992b). Functional properties of single neurons in the face primary motor cortex of the primate. III. Relations with different directions of trained tongue protrusion. *Journal of Neurophysiology*, *67*(3), 775–785.

Nakamura, Y., Iriarte-Diaz, J., Arce-McShane, F. I., Orsbon, C. P., Brown, K. A., Eastment, M. K., Avivi-Arber, L., Sessle, B. J., Inoue, M., Hatsopoulos, N. G., Ross, C. F., & Takahashi, K. (2017). Sagittal plane kinematics of the jaw and hyolingual apparatus during swallowing in *Macaca mulatta*. *Dysphagia*, *32*(5), 663–677. https://doi.org/10.1007/s00455-017-9812-4

Nath, T., Mathis, A., Chen, A. C., Patel, A., Bethge, M., & Mathis, M. W. (2018). Using DeepLabCut for 3D markerless pose estimation across species and behaviors. *BioRxiv*, *14*(July), 476531. https://doi.org/10.1101/476531

Nazruddin, Suemune, S., Shirana, Y., Yamauchi, K., & Shigenaga, Y. (1989). The cells of origin of the hypoglossal afferent nerves and central projections in the cat. *Brain Research*, *490*(2), 219–235. https://doi.org/10.1016/0006-8993(89)90240-0

Okorokova, E. V., Goodman, J. M., Hatsopoulos, N. G., & Bensmaia, S. J. (2020). Decoding hand kinematics from population responses in sensorimotor cortex during grasping. *Journal of Neural Engineering*.

Olson, R. A., Montuelle, S. J., Curtis, H., & Williams, S. H. (2021). Regional tongue deformations during chewing and drinking in the pig. *Integrative Organismal Biology*. https://doi.org/10.1093/iob/obab012

Omrani, M., Kaufman, M. T., Hatsopoulos, N. G., & Cheney, P. D. (2017). Perspectives on classical controversies about the motor cortex. *Journal of Neurophysiology*, *1982*, jn.00795.2016. https://doi.org/10.1152/jn.00795.2016

Orsbon, C. P. (2018). *Swallowing Biomechanics of the* Macaca mulatta *Hyolingual Apparatus*

[ProQuest Dissertations & Theses]. https://books.google.com/books?id=nsmJwgEACAAJ

Orsbon, C. P., Gidmark, N. J., Gao, T., & Ross, C. F. (2020). XROMM and diceCT reveal a hydraulic mechanism of tongue base retraction in swallowing. *Scientific Reports*, *10*(1), 1–16. https://doi.org/10.1038/s41598-020-64935-z

Orsbon, C. P., Gidmark, N. J., & Ross, C. F. (2018). Dynamic Musculoskeletal Functional Morphology: Integrating diceCT and XROMM. *The Anatomical Record*, *301*(2), 378–406. https://doi.org/10.1002/ar.23714

Orsbon, C. P., & Nabavizadeh, A. (2015). New Insights into Macaque Hyolingual Anatomy: A Preliminary microCT Study. *The FASEB Journal*, *29*(1_supplement), LB4.

Owen, S. F., Liu, M. H., & Kreitzer, A. C. (2019). Thermal constraints on in vivo optogenetic manipulations. *Nature Neuroscience*. https://doi.org/10.1038/s41593-019-0422-3

Palmer, J. B., Hiiemae, K. M., & Liu, J. (1997). Tongue-jaw linkages in human feeding: A preliminary videofluorographic study. *Archives of Oral Biology*, *42*(6), 429–441. https://doi.org/10.1016/S0003-9969(97)00020-4

Parmiani, P., Lucchetti, C., Bonifazzi, C., & Franchi, G. (2019). A kinematic study of skilled reaching movement in rat. *Journal of Neuroscience Methods*. https://doi.org/10.1016/j.jneumeth.2019.108404

Pascanu, R., Mikolov, T., & Bengio, Y. (2013). On the difficulty of training recurrent neural networks. *International Conference on Machine Learning*, 1310–1318.

Patel, N., Jankovic, J., & Hallett, M. (2014). Sensory aspects of movement disorders. *The Lancet Neurology*, *13*(1), 100–112. https://doi.org/10.1016/S1474-4422(13)70213-8

Pereira, T. D., Aldarondo, D. E., Willmore, L., Kislin, M., Wang, S. S. H., Murthy, M., & Shaevitz, J. W. (2019). Fast animal pose estimation using deep neural networks. *Nature Methods*, *16*, 117–125. https://doi.org/10.1038/s41592-018-0234-5

Perkell, J. S. (1969). *Physiology of speech production: Results and implications of a quantitative cineradiographic study. MIT research monograph, No 53.*

Pouderoux, P., & Kahrilas, P. J. (1995). Deglutitive tongue force modulation by volition, volume, and viscosity in humans. *Gastroenterology*, *108*(5), 1418–1426.

Quinlan, D. J., Culham, J. C., Buckingham, G., Mary, C., & Hughes, L. (2015). Direct comparisons of hand and mouth kinematics during grasping, feeding and fork-feeding actions. *Frontiers in Human Neuroscience*, *9*(October), 1–13. https://doi.org/10.3389/fnhum.2015.00580

Ram, Y., & Ross, C. F. (2019). *Jaw Elevator Muscle Coordination during Rhythmic Mastication in Primates : Are Triplets Units of Motor Control ?* 1–14. https://doi.org/10.1159/000503890

Robbins, J., Kays, S. A., Gangnon, R. E., Hind, J. A., Hewitt, A. L., Gentry, L. R., & Taylor, A.

J. (2007). The effects of lingual exercise in stroke patients with dysphagia. *Archives of Physical Medicine and Rehabilitation*, *88*(2), 150–158.

Robles-De-La-Torre, G. (2006). The importance of the sense of touch in virtual and real environments. *IEEE Multimedia*, *13*(3), 24–30. https://doi.org/10.1109/MMUL.2006.69

Ross, C. F., Baden, A. L., Georgi, J., Herrel, A., Metzger, K. A., Reed, D. A., Schaerlaeken, V., & Wolff, M. S. (2010). Chewing variation in lepidosaurs and primates. *Journal of Experimental Biology*, *213*(4), 572–584. https://doi.org/10.1242/jeb.036822

Ross, C. F., Blob, R. W., Carrier, D. R., Daley, M. A., Deban, S. M., Demes, B., Gripper, J. L., Iriarte-Diaz, J., Kilbourne, B. M., Landberg, T., Polk, J. D., Schilling, N., & Vanhooydonck, B. (2013). The evolution of locomotor rhythmicity in tetrapods. *Evolution*, *67*(4), 1209–1217. https://doi.org/10.1111/evo.12015

Ross, C. F., Dharia, R., Herring, S. W., Hylander, W. L., Liu, Z. J., Rafferty, K. L., Ravosa, M. J., & Williams, S. H. (2007). Modulation of mandibular loading and bite force in mammals during mastication. *Journal of Experimental Biology*, *210*(6), 1046–1063. https://doi.org/10.1242/jeb.02733

Ross, C. F., Eckhardt, A., Herrel, A., Hylander, W. L., Metzger, K. A., Schaerlaeken, V., Washington, R. L., & Williams, S. H. (2007). Modulation of intra-oral processing in mammals and lepidosaurs. *Integrative and Comparative Biology*, *47*(1), 118–136. https://doi.org/10.1093/icb/icm044

Ross, C. F., & Iriarte-Diaz, J. (2014). What does feeding system morphology tell us about feeding? *Evolutionary Anthropology*, *23*(3), 105–120. https://doi.org/10.1002/evan.21410

Rowlerson, A., Mascarello, F., Barker, D., & Saed, H. (1988). Muscle-spindle distribution in relation to the fibre-type composition of masseter in mammals. *Journal of Anatomy*, *161*, 37.

Saleh, M., Takahashi, K., Amit, Y., & Hatsopoulos, N. G. (2010). Encoding of Coordinated Grasp Trajectories in Primary Motor Cortex. *Journal of Neuroscience*, *30*(50), 17079–17090. https://doi.org/10.1523/JNEUROSCI.2558-10.2010

Sanders, I., & Mu, L. (2013). A three-dimensional atlas of human tongue muscles. *Anatomical Record*, *296*(7), 1102–1114. https://doi.org/10.1002/ar.22711

Sasamoto, K., Zhang, G., & Iwasaki, M. (1990). Two types of rhythmical jaw movements evoked by stimulation of the rat cortex. *Japanese Journal of Oral Biology*, *32*(1), 57–68. https://doi.org/10.2330/joralbiosci1965.32.57

Schaerlaeken, V., Meyers, J. J., & Herrel, A. (2007). Modulation of prey capture kinematics and the role of lingual sensory feedback in the lizard *Pogona vitticeps*. *Zoology*, *110*(2), 127–138. https://doi.org/10.1016/j.zool.2006.09.002

Schimmel, M., Ono, T., Lam, O. L. T., & Müller, F. (2017). Oro-facial impairment in stroke patients. *Journal of Oral Rehabilitation*, *44*(4), 313–326.

Schultz, S. (2007). Signal-to-noise ratio in neuroscience. *Scholarpedia*, *2*(6), 2046. https://doi.org/10.4249/scholarpedia.2046

Schwenk, H., & Bengio, Y. (2000). Boosting neural networks. *Neural Computation*, *12*(8), 1869–1887. https://doi.org/10.1162/089976600300015178

Scutter, S. D., & Türker, K. S. (1999). Muscle spindle afferent input to motoneurons in human masseter. *Journal of Neurophysiology*, *82*(1), 505–507.

Seagard, J. L., Van Brederode, J. F., Dean, C., Hopp, F. A., Gallenberg, L. A., & Kampine, J. P. (1990). Firing characteristics of single-fiber carotid sinus baroreceptors. *Circulation Research*, *66*(6), 1499–1509.

Sessle, B. J. (2011). Face sensorimotor cortex. Its role and neuroplasticity in the control of orofacial movements. *Progress in Brain Research*, *188*, 71–82. https://doi.org/10.1016/B978-0-444-53825-3.00010-3

Splaingard, M. L., Hutchins, B., Sulton, L. D., & Chaudhuri, G. (1988). Aspiration in rehabilitation patients: Videofluoroscopy vs bedside clinical assessment. *Archives of Physical Medicine and Rehabilitation*, *69*(8), 637–640.

Stone, M., & Lundberg, A. (1996). Three-dimensional tongue surface shapes of English consonants and vowels. *The Journal of the Acoustical Society of America*, *99*(6), 3728–3737. https://doi.org/10.1121/1.414969

Stringer, C., Pachitariu, M., Steinmetz, N., Reddy, C. B., Carandini, M., & Harris, K. D. (2019). Spontaneous behaviors drive multidimensional, brainwide activity. *Science*, *346*. https://doi.org/10.1126/science.aav7893

Takizawa, C., Gemmell, E., Kenworthy, J., & Speyer, R. (2016). A Systematic Review of the Prevalence of Oropharyngeal Dysphagia in Stroke, Parkinson's Disease, Alzheimer's Disease, Head Injury, and Pneumonia. *Dysphagia*, *31*(3), 434–441. https://doi.org/10.1007/s00455-016-9695-9

Tanji, J. U. N., & Evarts, E. V. (1976). Anticipatory activity of motor cortex neurons in relation to direction of an intended movement. *Journal of Neurophysiology*, *39*(5), 1062–1068.

Tay, A. B. G., & Zuniga, J. R. (2007). Clinical characteristics of trigeminal nerve injury referrals to a university centre. *International Journal of Oral and Maxillofacial Surgery*, *36*(10), 922–927. https://doi.org/10.1016/j.ijom.2007.03.012

Thach, W. T. (1978). Correlation of neural discharge with pattern and force of muscular activity, joint position, and direction of intended next movement in motor cortex and cerebellum. *Journal of Neurophysiology*, *41*(3), 654–676. https://doi.org/10.1152/jn.1978.41.3.654

Thexton, A. J. (1992). Mastication and swallowing: An overview. *British Dental Journal*, *173*(6), 197–206. https://doi.org/10.1038/sj.bdj.4808002

Trulsson, M. (2006). Sensory-motor function of human periodontal mechanoreceptors. *Journal of Oral Rehabilitation*, 262–273. https://doi.org/10.1111/j.1365-2842.2006.01629.x

Trulsson, M., & Essick, G. K. (1997). Low-threshold mechanoreceptive afferents in the human lingual nerve. *Journal of Neurophysiology*, *77*(2), 737–748. https://doi.org/10.1152/jn.1997.77.2.737

Trulsson, M., & Essick, G. K. (2010). Sensations Evoked by Microstimulation of Single Mechanoreceptive Afferents Innervating the Human Face and Mouth. *Journal of Neurophysiology*, 1741–1747. https://doi.org/10.1152/jn.01146.2009.

Trulsson, M., & Johansson, R. S. (2002). Orofacial mechanoreceptors in humans: Encoding characteristics and responses during natural orofacial behaviors. *Behavioural Brain Research*, *135*(1–2), 27–33. https://doi.org/10.1016/S0166-4328(02)00151-1

Trulsson, M., Johansson, R. S., & Olsson, K. A. (1992). Directional Sensitivity of Human Periodontal Mechanoreceptive Afferents to Forces Applied to the Teeth. *Journal of Physiology*, *447*, 373–389.

Tsuboi, A., Kolta, A., Chen, C. C., & Lund, J. P. (2003). Neurons of the trigeminal main sensory nucleus participate in the generation of rhythmic motor patterns. *European Journal of Neuroscience*, *17*(2), 229–238. https://doi.org/10.1046/j.1460-9568.2003.02450.x

Tsuboi, Akito, Takafuji, Y., Itoh, S., Nagata, K., Tabata, T., & Watanabe, M. (2009). Response properties of trigeminal ganglion mechanosensitive neurons innervating the temporomandibular joint of the rabbit. *Experimental Brain Research*, *199*(2), 107–116.

Wainwright, P. C., Mehta, R. S., & Higham, T. E. (2008). Stereotypy, flexibility and coordination: key concepts in behavioral functional morphology. In *Journal of Experimental Biology* (Vol. 211, Issue 22, pp. 3523–3528). https://doi.org/10.1242/jeb.007187

Wang, T.-Y., & Lin, S.-I. (2008). Sensitivity of plantar cutaneous sensation and postural stability. *Clinical Biomechanics*, *23*(4), 493–499.

Willett, F. R., Avansino, D. T., Hochberg, L. R., Henderson, J. M., & Shenoy, K. V. (2021). High-performance brain-to-text communication via handwriting. *Nature*, *593*(7858), 249–254. https://doi.org/10.1038/s41586-021-03506-2

Wu, A., Buchanan, E. K., Whiteway, M., Schartner, M., Meijer, G., Norovich, A., Noel, J. P., Schaffer, E., Rodriguez, E., Mishra, N., Everett, C., Salzman, C. D., Angelaki, D., Bendesky, A., Cunningham, J., & Paninski, L. (2020). Deep Graph Pose: A semi-supervised deep graphical model for improved animal pose tracking. *BioRxiv*, 259705. https://doi.org/10.1101/2020.08.20.259705

Yoshida, A., Moritani, M., Nagase, Y., & Bae, Y. C. (2017). Projection and synaptic connectivity of trigeminal mesencephalic nucleus neurons controlling jaw reflexes. *Journal of Oral Science*, *59*(2), 177–182. https://doi.org/10.2334/josnusd.16-0845

Zelditch, M., Swiderski, D., & Sheets, H. (2012). Geometric Morphometrics for Biologists. In *Geometric Morphometrics for Biologists*. academic press. https://doi.org/10.1016/C2010-0-66209-2